# AN INVESTIGATION INTO THE PROPERTIES OF FERRO CEMENT AND A METHOD OF STRESS ANALYSIS

David R. Turner

A Thesis
in
The Faculty
of
Engineering

Presented in Partial Fulfillment of the Requirements for
the Degree of Doctor of Engineering at
Concordia University
Montréal, Canada

June, 1977

ABSTRACT

# ABSTRACT

DAVID R. TURNER

## AN INVESTIGATION INTO THE PROPERTIES OF FERRO CEMENT AND A METHOD OF STRESS ANALYSIS

The investigations which form the subject of this thesis commence by identifying the constituent materials of ferro cement together with their physical and mechanical properties. It is then postulated that ferro cement is a subcategory of reinforced concrete which may be defined as a lamina composite material comprising a dense sand cement mortar matrix containing fine steel wire reinforcements which are sufficiently spread to inhibit cracking of the matrix.

The governing equations for the stress analysis of ferro cement are derived and it is demonstrated that these may be used to predict the failing strength of both tensile and bending specimens.

During the course of these investigations the Department of Civil Engineering agreed to participate in a concrete canoe race. A description of the design and construction of these canoes, as well as an analysis of their hydrodynamic performance is presented.

ACKNOWLEDGEMENTS

## ACKNOWLEDGEMENTS

The work presented in this thesis was carried out under the direct supervision of Dr. M.S. Troitsky, Professor of Engineering, Department of Civil Engineering, to whom the author is deeply indebted for his valuable advice, suggestions and constant guidance throughout the course of this study.

The author also expresses his gratitude to all the Faculty members of the Civil Engineering Department who sponsored the canoe project, and in particular to Dr. P.Fazio.

Thanks are also extended to Mr. Louis Stankevicius, Structural Laboratory Technician, who assisted in conducting the experiments; to the Engineering students of Sir George Williams campus who built and manned the canoe, and to Miss M. Stredder, who typed the manuscript.

TABLE OF CONTENTS

# TABLE OF CONTENTS


| | PAGE |
|---|---|
| ABSTRACT | i |
| ACKNOWLEDGEMENTS | ii |
| LIST OF TABLES | vi |
| LIST OF FIGURES | vii |
| NOTATIONS | x |
| 1 INTRODUCTION | 1 |
| 1.1 A Historical Review | 1 |
| 2 THE COMPOSITION OF FERRO-CEMENT | 12 |
| 2.1 Ferro Cement | 12 |
| 2.2 Portland Cement | 14 |
| 2.3 Sand | 17 |
| 2.4 Water | 17 |
| 2.5 Water/Cement Ratio | 19 |
| 2.6 Reinforcing | 21 |
| 2.7 Shear Strength | 28 |
| 2.8 Bond Strength | 30 |
| 2.9 Galvanic Action | 30 |
| 3. THE STRESS ANALYSIS OF FERRO CEMENT | 32 |
| 3.1 Strain of an Orthotropic Lamina | 32 |
| 3.2 Laminate Stiffness Matrix | 36 |
| 3.3 Transformation Matrices | 37 |
| 3.4 Lamina Constitutive Equations | 46 |
| 3.5 Failure Criterion | 49 |
| 4 ANALYSIS OF FERRO CEMENT IN TENSION | 50 |
| 4.1 The Tensile Specimen | 50 |
| 4.2 Strength of the Reinforcing Wire | 53 |
| 4.3 Strain of the Diagonal Wires | 54 |
| 4.4 Predicted Failing Load | 57 |
| 4.5 Modulus of Elasticity | 58 |
| 4.6 Predicted Failing Load Using Lamina Analysis | 64 |

PAGE

5 ANALYSIS OF FERRO CEMENT IN BENDING . . . . . 70

5.1 The Bending Specimen . . . . . 70
5.2 Method of Loading . . . . . 74
5.3 Test Results . . . . . 74
5.4 Curvature of the Specimen . . . . . 79
5.5 Initial Analysis . . . . . 82
5.6 Lamina Constitutive Equations and the Governing Differential Equations . . . . . 87
5.7 Modulus of Elasticity . . . . . 90
5.8 Predicted Stress Levels Using Lamina Analysis. 92

6 FRACTURE TOUGHNESS OF FERRO CEMENT . . . . . 101

6.1 Crack Propagation . . . . . 101
6.2 Method of Testing . . . . . 104
6.3 Evaluation of Fracture Toughness . . . . . 105
6.4 Reinforcing Wire Spacing . . . . . 113

7 CONSTRUCTION OF FERRO CEMENT CANOES . . . . . 114

7.1 The Concrete Canoe Race . . . . . 114
7.2 The Reinforcing Mesh . . . . . 115
7.3 Design Stress Levels . . . . . 115
7.4 Method of Construction . . . . . 120

8 HYDRODYNAMIC CHARACTERISTICS OF THE CANOES . . . . . 126

8.1 General . . . . . 126
8.2 Buoyancy . . . . . 126
8.3 Wetted Surface . . . . . 127
8.4 Frictional Resistance . . . . . 134
8.5 Wave Making Resistance . . . . . 137
8.6 Prismatic Coefficient . . . . . 140
8.7 Eddy Making Resistance . . . . . 141
8.8 Propulsion . . . . . 143
8.9 Metacentric Height . . . . . 144
8.10 The Measured Resistance . . . . . 145
8.11 Stability Curve . . . . . 146

9 SUMMARY AND CONCLUSIONS . . . . . 152

9.1 Summary . . . . . 152
9.2 Conclusions . . . . . 153

PAGE

REFERENCES . . . . . 156

APPENDIX "A" - SECTION PROPERTIES . . . . . 160

A.1.1 Program to Derive Sectional Properties . . . . . 161

A.1.2 Input and Output Data - Canoe No. 1 . . . . 163

A.1.3 Input and Output Data - Canoe No. 2 . . . . 166

LIST OF TABLES

# LIST OF TABLES


| NUMBER | DESCRIPTION | PAGE |
|---|---|---|
| 2.1. | The Strength of Cement . . . . . | 16 |
| 2.2 | Average Mechanical Properties of Various Steels . . . . . | 23 |
| 2.3 | Strength of Reinforcing Bar . . . . . | 26 |
| 2.4 | Bond Strength of Typical Reinforcing Rods . . . | 31 |
| 4.1 | Breaking Load of Reinforcing Wire . . . . . | 53 |
| 4.2 | Statistical Evaluation of Wire Strength . . . . | 54 |
| 5.1 | Test Results, Deflection vs Load . . . . . | 76 |
| 5.2 | Transverse Curvature . . . . . | 81 |
| 5.3 | Initial Estimates of Elastic Modulus and Stress Level . . . . . | 86 |
| 5.4 | Elastic Modulus Obtained From the Composite Section . . . . . | 94 |
| 5.5 | Stress Levels in the Outer Laminate . . . . . | 98 |
| 6.1 | The Fracture Toughness of Ferro Cement . . . . | 109 |
| 6.2 | Fracture Toughness of Ferro Cement With Diagonal Reinforcing . . . . . | 112 |
| 8.1 | Cross-Sectional Area vs Depth of Immersion, Canoe No. 1 . . . . . | 129 |
| 8.2 | Cross-Sectional Area vs Depth of Immersion, Canoe No. 2 . . . . . | 129 |
| 8.3 | Displacement vs Depth of Immersion . . . . . | 132 |
| 8.4 | Perimeter of Immersed Sections . . . . . | 132 |
| 8.5 | Frictional Resistance . . . . . | 136 |
| 8.6 | Froude Number and Speed Length Ratio . . . . . | 139 |

# LIST OF FIGURES

# LIST OF FIGURES


| FIGURE | | PAGE |
|---|---|---|
| 1.1 | Ferro Cement Cruising Yachts Under Construction | 11 |
| 2.1 | Grading Curves for Sand Aggregate | 18 |
| 2.2 | Porosity of Cement | 20 |
| 2.3 | Mesh Factor and Specific Reinforcing Surface | 22 |
| 2.4 | Typical Stress Strain Curves for Steel | 25 |
| 2.5 | A Typical Stress Strain Curve for Cement | 29 |
| 3.1 | Laminate Orientation | 33 |
| 3.2 | Strain of an Orthotropic Element | 34 |
| 3.3 | Equilibrium of a Triangular Element | 38 |
| 3.4 | Transformation of the Strain Axes | 42 |
| 3.5 | Lamina and Laminate Axes | 44 |
| 3.6 | Cross-Section of a Laminate | 47 |
| 4.1 | The Wire Fabric in the Tensile Specimen Mold Prior to Cementing | 51 |
| 4.2 | A Cross-Section of the Specimen | 52 |
| 4.3 | An Element of Mesh | 55 |
| 4.4 | A Specimen Showing Typical Transverse Crack Pattern Which Occurs at Yield Load, and Also the Ultimate Failure | 59 |
| 4.5 | Stress-Strain Curves for the Component Materials of Ferro Cement | 61 |
| 4.6 | A Strip of Ferro Cement | 63 |
| 4.7 | Secant Modulus of Ferro Cement Reinforced With Quarter-Inch Mesh and Loaded Longitudinally | 65 |

FIGURE PAGE


| | | |
|---|---|---|
| 5.1 | Four Point Loading | 71 |
| 5.2 | The Mold for the Bending Specimen With the Wire in Place | 72 |
| 5.3 | Cross-Section of the Bending Specimen | 73 |
| 5.4 | The Specimen Showing the Method of Loading and the Position of the Dial Gauges | 75 |
| 5.5 | The Specimen Under Load | 77 |
| 5.6 | Deflection of the Bending Specimen | 78 |
| 5.7 | Radius of Curvature of Loaded Beam | 80 |
| 5.8 | The Crack Pattern on the Tension Face of the Bending Specimen | 83 |
| 5.9 | Simple Beam Deflection | 84 |
| 5.10 | Longitudinal and Transverse Curvature of the Specimen Under Load | 93 |
| 5.11 | Bending Cross-Section of the Specimen | 95 |
| 5.12 | Secant Modulus of Ferro Cement in Bending | 96 |
| 6.1 | Fracture Toughness Specimens | 106 |
| 6.2 | Dimensions of the Test Specimens | 108 |
| 6.3 | Stress Strain Curves for Various Reinforcings | 111 |
| 7.1 | Profile and Water Lines of the Canoes | 116 |
| 7.2 | Lines of Canoe No. 1, to-scale | 117 |
| 7.3 | Lines of Canoe No. 2, to-scale | 118 |
| 7.4 | Moments of Inertia of the Canoe Sections | 119 |
| 7.5 | Moments of Inertia of the Canoes | 121 |
| 7.6 | A Finished Reinforcing on the Wooden Mold | 124 |
| 7.7 | A Canoe With the Cement Mortar in Place | 124 |

| FIGURE | | PAGE |
|---|---|---|
| 7.8 | A Canoe in the Water Prior to a Race . . . . . | 125 |
| 7.9 | A Canoe During a Race . . . . . | 125 |
| 8.1 | Immersed Area . . . . . | 128 |
| 8.2 | Cross-Sectional Areas vs Water-Line Length . . . . . | 130 |
| 8.3 | Depth of Immersion vs Displacement . . . . . | 131 |
| 8.4 | Wetted Surface . . . . . | 133 |
| 8.5 | Variation of Kinematic Viscosity of Water With Temperature . . . . . | 135 |
| 8.6 | Optimum Prismatic Coefficient . . . . . | 142 |
| 8.7 | The Variation of Total Resistance With Speed . . . . . | 147 |
| 8.8 | Canoe No. 2 Floating Empty . . . . . | 148 |
| 8.9 | The Canoe Being Towed at 2.8 ft/sec, Balasted to Simulate Crew Weight . . . . . | 148 |
| 8.10 | The Canoe at 4.2 ft/sec, the Bow Wave is Distinctly Visible . . . . . | 149 |
| 8.11 | The Canoe at 6.25 ft/sec, the Stern Wave and Transverse Wave Pattern May be Seen . . . . . | 149 |
| 8.12 | The Canoe at 8.3 ft/sec, Settling into the Trough Between Bow and Stern Waves . . . . . | 150 |
| 8.13 | Stability Curve for Canoe No. 2 . . . . . | 151 |

# NOTATIONS

# NOTATIONS

The symbols used are identified in the text where they occur, the sign ~ denotes a matrix and a - indicates a vector.

| | |
|---|---|
| A | Area |
| a | Intense energy region at the tip of a crack |
| E | Young's Modulus |
| $E_s$ | Secant Modulus |
| G | Shear Modulus |
| g | Acceleration due to gravity |
| h | Laminate thickness |
| I | Moment of inertia |
| K | Strain at failure |
| L | Length |
| r | Radius of curvature |
| t | Lamina thickness |
| w | Plate deflection |
| z | Distance to centre of lamina |
| $\delta$ | Deflection |
| $\varepsilon$ | Strain |
| $\gamma$ | Shear strain |
| $\sigma$ | Stress |
| $\nu$ | Poisson's ratio |
| $\theta$ | Angle between lamina and laminate axes |

| | |
|---|---|
| $\chi$ | Curvature |
| $\tau$ | Shear stress |
| $\underset{\sim}{A}$, $\underset{\sim}{B}$, $\underset{\sim}{D}$ | Sub-matrices of the constitutive equation of laminated plates |
| $\underset{\sim}{C}$ | Stiffness matrix |
| $\underset{\sim}{S}$ | Moduli of compliance |
| $\underset{\sim}{T}$ | Transformation matrix |
| $\underline{N}$ | Vector of direct loads |
| $\underline{M}$ | Vector of bending moments |

Subscripts

| | |
|---|---|
| X, Y | Laminate axes |
| 1, 2 | Lamina natural axes |

# CHAPTER - 1

# INTRODUCTION

# CHAPTER 1

# INTRODUCTION

## 1.1 A HISTORICAL REVIEW

The invention of reinforced concrete is attributed to Joseph Lambot, of Miraval in France, who started to develop the material in 1840. His patent for Ferciment was awarded in 1858 and the specification reads as follows:

> "My invention shows a new product which helps replace timber where it is endangered by wetness, as in wood flooring, water containers, plant pots, etc. The substance consists of a metal net of wire or sticks which are connected or formed like a flexible woven mat. I give this net a form which looks similar to the article I want to create, then I put hydraulic cement, or similar bitumen tar or mix, to fill up the joints."

Lambot's system of using a single mesh reinforcement for the mortar would not have the same characteristics as ferro cement. It was however, used to produce a number of boats. Two of his rowing boats are still in existence and capable of floating, one of them is in the museum at Brignoles, France. A similar boat was built in Holland in 1887 and is still afloat on the Pelican pond in Amsterdam Zoo. [1,2,3]

An Italian engineer, Gabellini, built numerous small concrete ships and pontoons around the turn of the century and one of his vessels, the '*Ligura*' of 150 tons, completed a voyage from Rome to Genoa. [1] Two German companies, one

in Frankfort and one in Hanover, began to produce reinforced concrete barges at this time and at least one vessel is known to have been made in the United States.

Britain launched her first concrete ship in 1910 and two years later a Norwegian engineer, Fougner, took out several patents and was associated with the construction of a ferro concrete lighter in Manila. He then designed and built a motor ship, the '*Namsenfjord*', of 356 tons which was launched in 1917, her success led to the construction of two larger vessels.

The shortage of steel during the First World War made reinforced concrete an attractive alternative for ship building and over 150,000 tons of such ships were constructed between the years 1917 and 1922. [4] These ships ranged in size from 6,000 ton steamers to small tugs and lighters. One of the most successful was the '*Armistice*' of 2,500 tons, launched in 1918 by the Yorkshire Hennebique Contracting Co. She traded between Liverpool and Lagos for over twenty-five years without mishap. [1] Fourteen ocean going ships, including six tankers, were built in the United States at this time. The first of these was the '*Faith*' of 3,427 tons, which made her maiden voyage in 1918 and went out of service in 1922, owing to a slump in shipping. [5]

Although there were no structural problems with these ships, efforts to overcome corrosion resulted in too great a thickness of cement and consequently too much weight to be

commercially viable. However, operators noted that concrete ships exhibit a marked lack of both vibration and condensation as compared to steel ships. Examples of these early vessels can still be seen in many parts of the world, some in perfect condition, while others are rusty and crumbling.[2,4,6] Nine concrete ships are being used as a floating breakwater at Powell River, B.C., Canada. The oldest of these is the '*Peralta*' of 6,065 tons, launched in San Francisco in 1920 by the builders of the '*Faith*'. [1,3]

In the period after the First World War, some fifteen concrete ships were constructed in France and most of these were built to the designs of Freyssinet, the pioneer of prestressed concrete. These vessels were 180 feet long and their dead weight was 37 percent of their fully loaded displacement. This was within 6 percent of an equivalent steel ship. Freyssinet observed that a rationally built concrete hull should comprise a skeleton of numerous steel wires of very small diameter holding the principal strains. He was convinced that hulls could be built by the reinforced concrete technique which would be as light or lighter than ordinary steel hulls. [1]

During the Second World War only two self-propelled concrete ships were built in Britain whereas twenty-four were built in the United States by McCloskey & Co. of Philadelphia. These vessels were entirely seaworthy and handled well, at least three of them passed through hurricanes

without appreciable damage. The reports of several collisions and one or two strandings indicate that they were stronger than their predecessors of the First World War.

The most important British application of reinforced concrete in marine use during the Second World War was for the construction of a great floating harbour (Mulberry) at Arromanches. The concrete caissons used were 204 feet long and in depth, varied from twenty-five to sixty feet. Floating concrete pontoons were also used in the harbour to support flexible steel piers. [1] Germany at this time produced a number of concrete barges and pontoons, some built in Norway.

In 1943, Nervi carried out experiments using many layers of fine wire mesh impregnated with a rich mortar. In so doing, he took advantage of the fact that the strain which cement is able to withstand is greatly increased in the presence of a highly subdivided reinforcement. This enables thin slabs to be made which exhibit a load-carrying capacity and a flexibility not previously obtainable without destructive cracking of the cement mortar. Nervi called this material 'ferro cement' and noted that, as a result of the subdivision of the reinforcement, forms could be eliminated and the mortar applied direct to the mesh which would act as a lathe to retain it. He considered that an important application of ferro cement would be in the field of naval construction for boats of a limited tonnage.

Impact tests showed not only the high strength of the medium but also that a failure, when it did occur, appeared as a relatively wide area of shattered mortar. The material remained in a cohesive state and still offered a good resistance to the passage of water. In the spring of 1943 work started on three 150 ton motor ships for the Italian Navy and also a 400 ton freighter, all of ferro cement. After six months this project had to be abandoned because of the war situation.

Two years later, the firm of Nervi and Bartoli launched the first ferro cement vessel, a motor sailer '*Irene*' of 165 tons. Her hull was 1.4 inches thick and the reinforcing comprised three layers of .23 inch diameter bars at four inch centres covered by four layers of mesh inside and out. She weighed 5 percent less than an equivalent wooden hull and cost 40 percent less.

The '*Irene*' saw hard service in the Mediterranean and at least three times was involved in accidents, on two occasions striking the bottom and on another occasion her side struck a harbour mole. In each case, damage was limited to local cracks which allowed slight seepage of water but were easily repairable. She was subsequently wrecked in 1957.

Nervi built for his own use a 38 foot cruising ketch which was launched in 1948. Of this ship, he wrote '*Nennele*' is a real skin structure of half-inch thickness.

She represents some outstanding advantages over similar wooden hulls. She is inexpensive to build and her inside room is efficiently used because of the very thin partitions required. The first of the small ferro cement cruising yachts, she performed well and was still in excellent condition and giving good service in 1968.

Ferro cement was used in a number of civil engineering projects at this time, probably the most notable of these being the roof of the Turin Exhibition Hall. Other projects include roofs for an Ocean Terminal building and for an enclosed swimming pool. Another interesting use of ferro cement is in a high diving complex for a swimming pool. Nervi proposed the material for the construction of railway sleepers, prefabricated tunnel sections and a roof structure spanning three hundred meters. He also built a motor fishing vessel of 165 tons which is still in operation. [7]

The first Russian ferro cement yacht was launched on the Volga River in 1957. In the fall of that year, she broke her anchor cable during a severe storm and was thrown onto the rocks on the opposite shore. She remained on the rocks through the fall and was frozen into the ice all winter. The following spring, it was found that although the sides were badly crumpled, the reinforcing mesh was undamaged. Four men with a bag of cement and river sand repaired the hull in one day.

The yacht '*Tsemental*' was the first example of a ferro cement boat built on a mold. The hull of an old wooden boat was turned keel upward and used as the mold over which five layers of mesh were laid. Cementing was carried out continuously from the keel downwards and, when cured, the hull was removed from the mold and turned over ready for finishing. She was successfully cruised for more than 2,500 miles through varied conditions on the Dnieper River and the Black Sea. Several other yachts built and launched in Russia have accomplished notable voyages and have proven to be both comfortable and seaworthy.

The first prefabricated ferro cement vessel was a floating crane of 10 tons lifting capacity. The hull was assembled from forty-five plane and two curved ribbed sections, the largest of which measured thirty-six by seven feet and weighed two-and-a-half tons. The superstructure comprised fifteen plane sections, and the components were joined together by welding the reinforcement and covering the joint with mortar. This vessel was operating on the lower reaches of the Volga. [8]

In 1961, an English firm, Windboats Ltd., developed a 34-foot cabin cruiser which was intended for charter work. The design proved successful and was put into production, ten vessels being completed in the first eighteen months of operation. In service, the hulls were found to be both economical to maintain and easy to repair, some having

suffered damage from collision, fire or explosion. [2,3] This company has also used prestressing in conjunction with the ferro cement technique for flat bottomed houseboat hulls. [1]

In the same year, ferro cement was introduced into New Zealand by Manning, who built a 24-foot yacht, and by Sutherland, of Ferro Cement Ltd. A large number of boats have been built by amateurs in that country and it is interesting to note that even the worst of these, with extra thick hulls, badly designed shapes, and rough exteriors still function satisfactorily. [3,6] The practice of using hexagonal mesh chicken wire for ferro cement originated in New Zealand where it was used as a substitute for square mesh screens which could not be obtained at that time. The first 'round-the-world voyage by a ferro cement yacht was accomplished by Griffiths in the '*Awahanee*', a 53 foot cutter which he built in New Zealand. Starting in 1965, she sailed first to Australia and then across the Indian Ocean to South Africa. Taking the South Atlantic route around Cape Horn, she then sailed to Hawaii. Several other ferro cement vessels have since completed circumnavigations. [2,9]

The art of ferro cement boat-building was introduced into Canada and the United States from New Zealand, along with the use of chicken wire reinforcement. Plans currently available to amateur builders range from a 17-foot catboat to a 60-foot schooner or ketch, as well as fishing or house-

boats.

There is now a number of commercial firms on the Pacific coast of Canada and in Montreal, which are engaged in the construction of ferro cement hulls, as well as firms in the United States, mainly in California or Florida. In addition, many craft are being built by amateurs, there being some forty hulls in various stages of completion in the Montreal area during 1975. Of special interest, is a 38-foot motor sailer built in Quebec City, in which steel cable of the type used in prestressed concrete was used, the cement mortar being applied by the shotcrete method. [10]

During the last decade, a large ferro cement buoy was built in the United States and now operates as an ocean data station, the cost being half that of an equivalent steel structure. The material would also be suitable for many types of zero displacement or submarine structures which could be used to explore, occupy and develop the continental shelf and associated banks, an area comprising 10 to 15 percent of the ocean floor. [11]

Canals played an important part in the transportation systems of many countries until the middle of the nineteenth century when railways were developed. With growing demands for economical transport and the increasing cost of fuel, it is likely that inland waterways will resume their importance. The river systems of North and South America, Africa, India

and China would be ideal for ferro cement craft. A plant near Shanghai has been producing ferro cement sampans since 1963, these range in size from three to five tons cargo capacity and are used to haul freight on a network of waterways. [1,2]

The rising cost of steel and wood make ferro cement increasingly attractive from the economic viewpoint and its resistance to attack by organic and chemical agents make it particularly suitable for use in tropical countries.

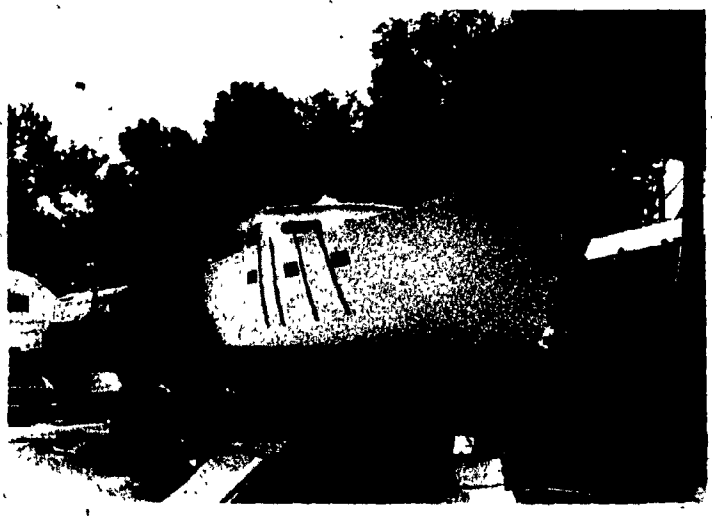

FIG. 1.1 FERRO CEMENT CRUISING YACHTS UNDER CONSTRUCTION

# CHAPTER 2

## THE COMPOSITION OF FERRO CEMENT

# CHAPTER 2

# THE COMPOSITION OF FERRO CEMENT

## 2.1 FERRO CEMENT

Ferro cement is a type of reinforced concrete in which the reinforcing comprises a large number of fine wires, usually in the form of a mesh or screen. A specified number of meshes are fastened together with wire ties in the shape of the structure being constructed. This form comprising the reinforcing mesh is then impregnated with a rich mortar of cement and fine sand and smoothed to a high surface finish. The thickness of cement should be sufficient to cover the layers of reinforcing by not more than 1/16 inch because the resistance to cracking of the surface mortar decreases rapidly as this dimension increases.

Thicker shells may be produced without an excessive number of layers of mesh by using steel rods of up to 3/8 inch diameter to provide one or more of the central layers.

Thus ferro cement is a composite material in which the steel wire provides the load-carrying capacity whilst the cement acts as a bonding agent and carries shear load between the wires. It differs from the majority of composite materials in that it has a greater proportion of matrix to filament than is usual. Consequently, the physical properties of the cement matrix are of major importance.

Cement becomes a bonding agent by virtue of the hydration of its component silicates and aluminates in the presence of water. At any stage in the process of hydration the hardening cement paste consists of various compounds referred to as gel. Also present are crystals of calcium hydroxide, unhydrated lime and water-filled spaces. These spaces are called capillary pores and they form an interconnecting network through the cement. At the optimum water/cement ratio these pores will completely fill with gel which can only form in the presence of water. If the water/cement ratio exceeds this optimum then the volume of gel is not sufficient to fill the water spaces available and some capillary pores will be left open. [12,13] There will also be interstitial voids in the gel, itself.

Griffith [14] postulated that a material will fail at a mean stress below its theoretical cohesive strength because it is only necessary to exceed that stress locally in the material. The sharp edges of the voids and unfilled capillary pores which are present in the cement provide the stress concentration sufficient to cause the cohesive strength to be exceeded at comparatively low mean tensile stress levels.

If a sufficient quantity of fine steel wire is spread throughout a wet cement mortar and this composite is subsequently cured and loaded in tension, it is found that the cement will sustain a much higher strain without cracking than would unreinforced cement. The presence of the wire in

the cement causes an increase in the stress required for unstable crack propagation by reducing the stress concentration at the pores and voids, thus effectively increasing the fracture toughness of the cement. [12,15] It is this capacity of fine wire reinforcement to increase the strain which cement mortar is capable of withstanding without cracking that distinguishes ferro cement from reinforced concrete.

Ferro cement may therefore be defined as a lamina composite material comprising a dense sand cement mortar matrix containing steel wire reinforcements which are sufficiently spread to inhibit cracking in the matrix.

The constituents of ferro cement are cement, sand, water and reinforcing steel. Each of these materials is discussed in the following paragraphs, as well as the parameters which influence the strength and porosity of the cement matrix.

## 2.2 PORTLAND CEMENT

Portland cement is produced by calcining in a furnace a mixture of clay, limestone, shale, silica, alumina and iron components in the appropriate proportions. The resulting clinker is then ground to a fine powder and mixed with a small quantity of gypsum. The properties of the resulting cement may be varied by changing the relative proportions

of the ingredients. In this way, five basic types of Portland cement are produced.

| | |
|---|---|
| Type I | For use in general concrete construction |
| Type II | For use in general concrete construction exposed to mild sulfate action or where moderate heat of hydration is required. |
| Type III | For use where high early strength is required. |
| Type IV | For use when low heat of hydration is required. |
| Type V | For use when high sulfate resistance is required. |

Variations of the five primary types are IA, IIA and IIIA, air entraining Portland cements, Type IP Portland pozzolan cement and Type IPA, Portland pozzolan cement with air entraining.

Comparative strength of these cements based upon a sample cured for one day in moist air and twenty-seven days in water is shown in Table 1. [16]

TABLE 2.1 THE STRENGTH OF CEMENT

| Type | I | II | III | IV | V | IA | IIA | IP | IPA |
|---|---|---|---|---|---|---|---|---|---|
| Compressive Strength psi | 3500 | 3500 | - | 2000 | 3000 | 2800 | 2800 | 3000 | 2500 |
| Tensile Strength psi | 350 | 325 | - | 300 | 325 | - | - | - | - |

The cements most commonly used for boat building are types I and V. Type I has been used extensively in New Zealand although type V affords better resistance to the corrosive action of sea water and is slower setting which allows more time for finishing the wet mortar.

## 2.3 SAND

The aggregate used should be a clean sharp igneous sand which meets the requirements of ASTM C33. It should be free from organic matter or chemical salts which may react detrimentally with the cement, and also from dust which may prevent a good bond from forming with the cement. Weak friable or laminated aggregate should be rejected.

The sand aggregate should be graded so as to fall within the limits shown in Figure 2.1. It will then have a modulus of fineness of between 2.0 and 2.5. Grains which will not pass a #8 ASTM sieve should be screened out. [1,2,12]

## 2.4 WATER

Almost any water that is drinkable and has no pronounced taste or odour is satisfactory as a mixing water for making concrete. Salts of manganese, tin, zinc, copper and lead in mixing water may cause significant reduction in strength and a large variation in setting time when present in concentrations of a few tenths per cent by weight of cement.

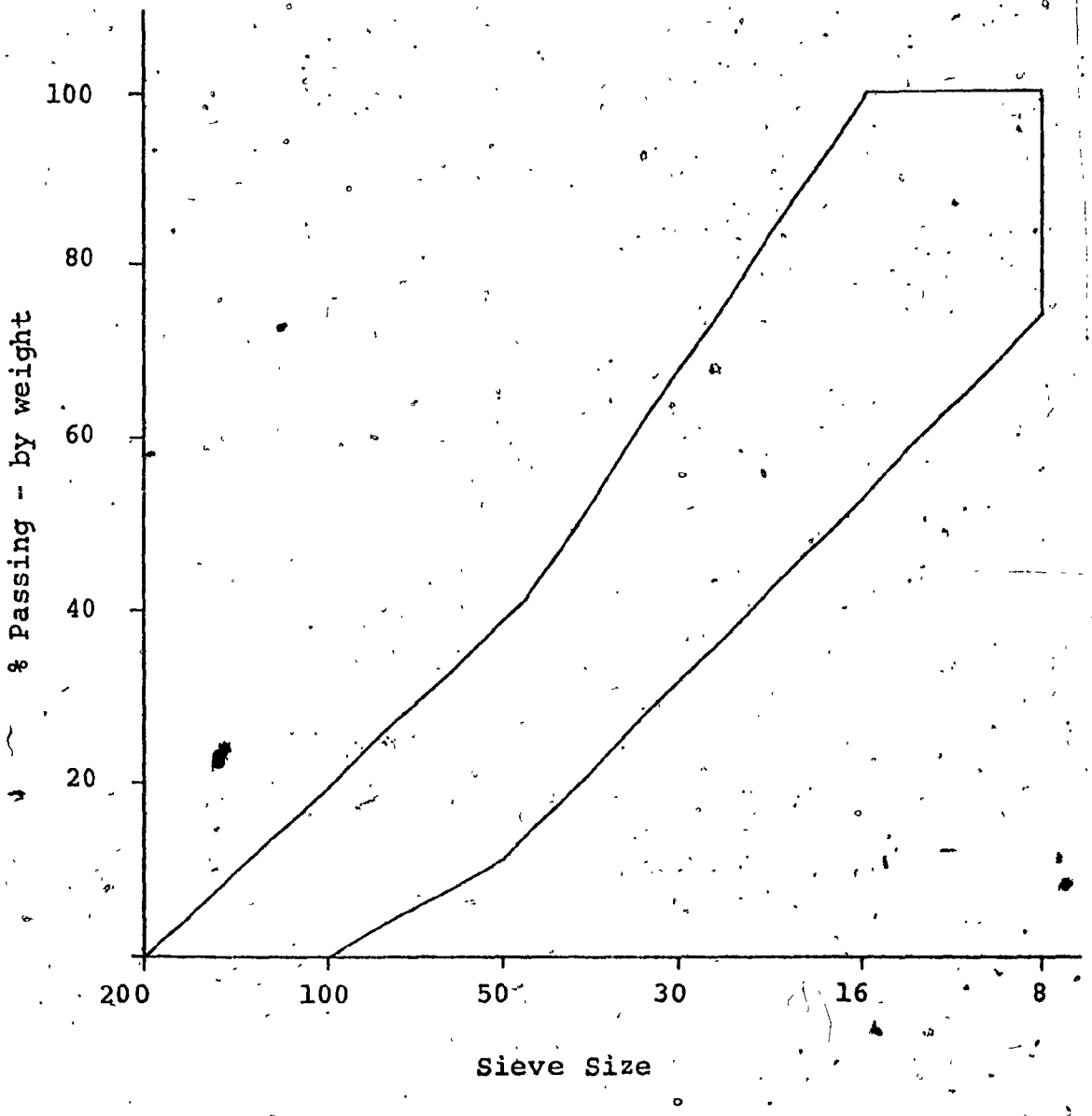


FIG. 2.1 GRADING CURVES FOR SAND AGGREGATE

Algae present in the mixing water may cause excessive reduction in strength either by combining with the cement to reduce bond, or by causing a large amount of air to be entrained in the cement. Mineral oil in concentrations of greater than two percent by weight of cement may reduce the strength of the concrete by twenty percent. Water containing organic solids, clay or fine rock particles in suspension should be avoided. [17]

## 2.5 WATER/CEMENT RATIO

The permeability of a mortar is measured by the rate at which water under a given pressure will pass through the material. The water passes through the cement via voids left by the evaporation of the free water present in the mix. The longer the mortar is cured in a damp condition the greater will be the amount of water in permanent combination with the cement and consequently there will be fewer voids. [2]

In addition to low water content and prolonged curing, as dense a mixture as possible should be used to reduce permeability. The mix used for boat-building comprises 1½ to 2 parts of sand to 1 part of cement by weight with a water/cement ratio of 0.4 to 0.45, as shown in Figure 2.2.

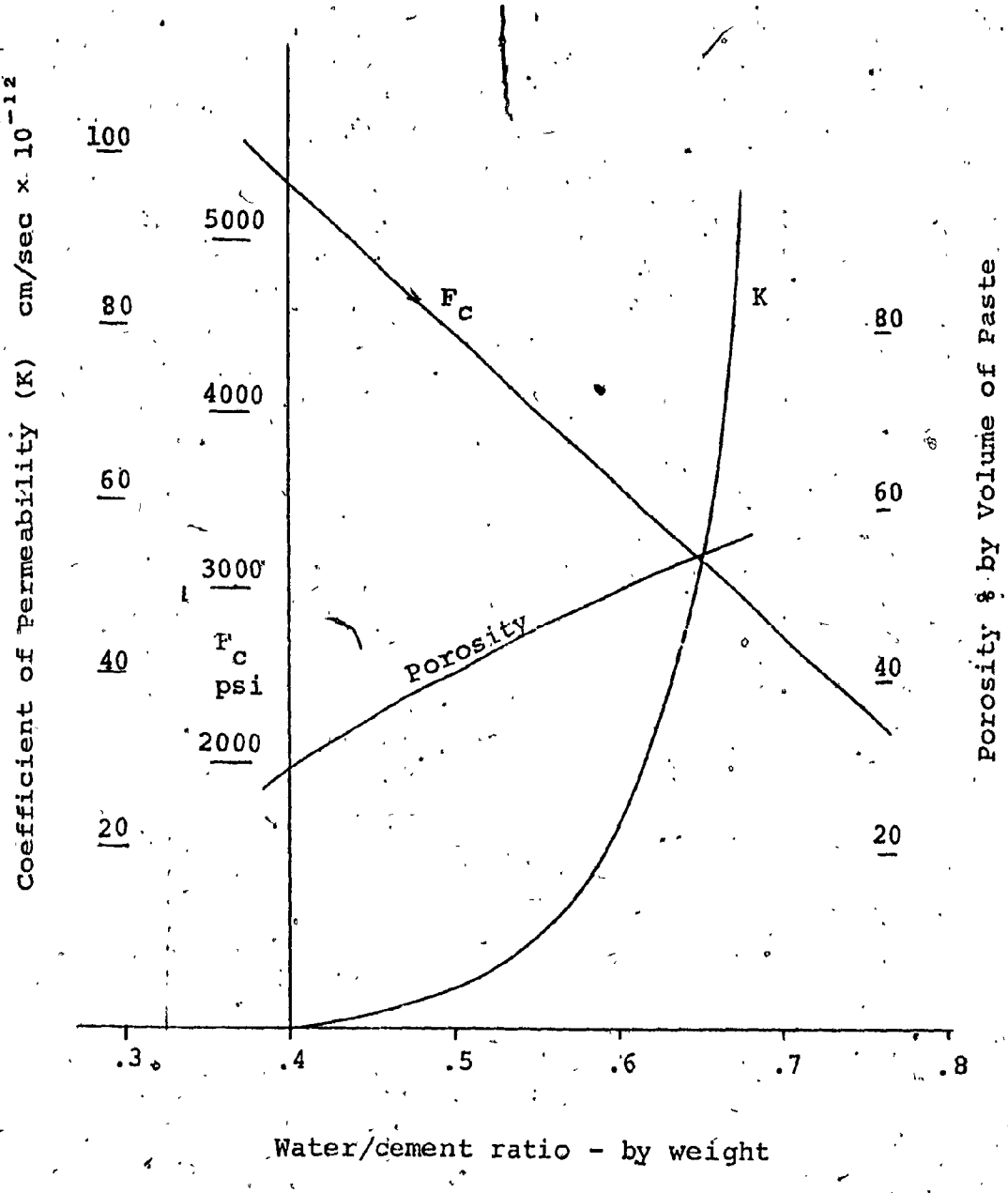


FIG. 2.2 POROSITY OF CEMENT [2]

## 2.6 REINFORCING

The reinforcing used in ferro cement consists of steel bars, wire or mesh at the rate of 25 to 40 lb/cu.ft of cement mortar. This reinforcing must be dispersed through the mortar in such a way that ratio of surface area of the reinforcing to the volume of cement is not less than 5.0 $in^2/in^3$. This ratio is known as the Specific Reinforcing Surface. [8]

The objective in dispersing the reinforcing is to delay the cracking of the mortar and tests have shown that another important parameter in achieving this result is the ratio of the reinforcing wire diameter to the area enclosed within a mesh, known as Mesh Factor. [12] It is concluded that there exists a relationship between the cracking strain of the mortar, the Specific Reinforcing Surface and the Mesh Factor such as is shown in Figure 2.3.

The reinforcing bars will be between 1/8 and 3/8 in. diameter and in these sizes, a wide variety of steels are available. Typical strength values for commercial steels are given in Table 2.2. The last two digits of the specification number refer to the carbon content, and both ultimate and yield strength increase with increasing carbon. [18]

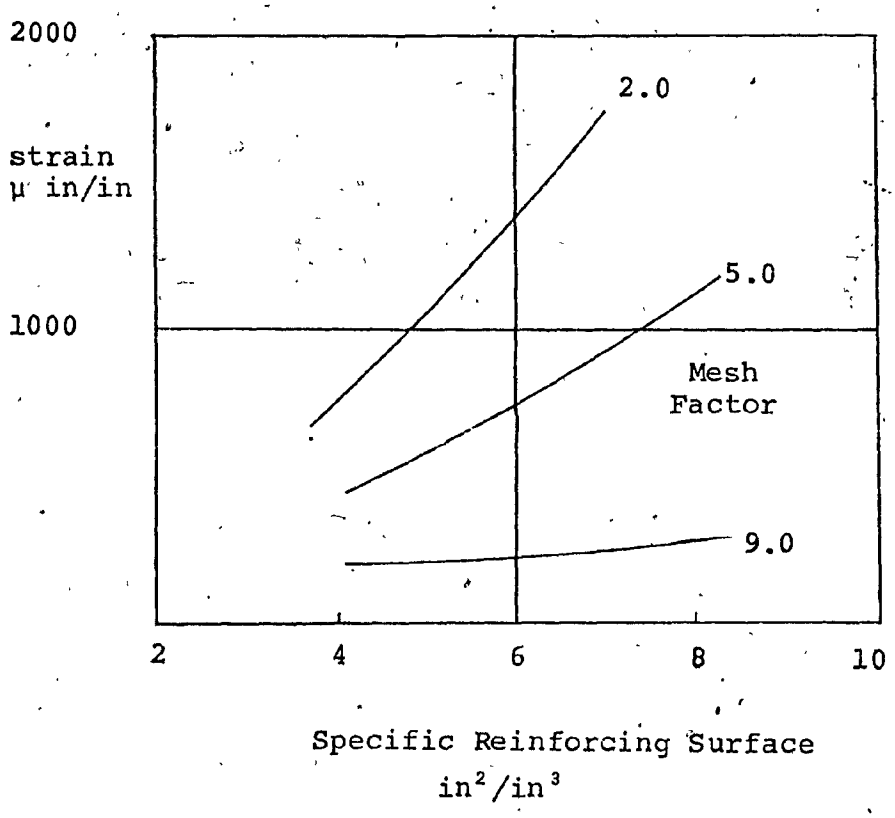


FIG. 2.3 MESH FACTOR AND SPECIFIC REINFORCING SURFACE

TABLE 2.2 AVERAGE MECHANICAL PROPERTIES OF VARIOUS STEELS

| SAE Specification | Condition | Tensile Strength KSI | Yield Point KSI |
|---|---|---|---|
| 1010 | | | |
| 1020 | Hot Rolled | 67 | 43 |
| | Cold Drawn | 74 | 47 |
| 1025 | H R | 70 | 42 |
| | C D | 79 | 66 |
| 1035 | H R | 87 | 54 |
| | C D | 93 | 67 |
| 1040 | H R | 91 | 57 |
| | C D | 98 | 69 |
| | Heat Treated | 110 | 84 |
| 1045 | H R | 97 | 59 |
| | C D | 106 | 79 |
| | H T | 120 | 93 |
| 3130 | H R | 100 | 72 |
| | C D | 105 | 85 |
| | H T | 126 | 108 |
| 3140 | H R | 97 | 64 |
| | C D | 115 | 98 |
| | H T | 142 | 125 |
| 3240 | H R | 97 | 72 |
| | C D | 112 | 92 |
| | H T | 165 | 148 |

The increase in strength of the cold drawn steels is due to a refinement of the grain structure induced by cold working. These steels do not exhibit the pronounced yield point that is apparent in hot rolled steels. However, the mechanical properties of a cold drawn steel that has been welded will revert to those of a hot rolled steel in the vicinity of the weld. [19]

Standard axle steel bars for concrete reinforcing are supplied in three grades, structural, intermediate and hard. Deformed bar is also available in a fourth grade known as 60,000 psi. The mechanical properties of these steels are shown in Table 2.3.

Welded steel wire fabric is a material composed of cold drawn steel wires, as drawn or galvanised, fabricated into a sheet or mesh formed by electric welding. The finished material comprises a series of longitudinal and transverse wires arranged at right angles and welded together at all points of intersection. The tension strength of the wire is 70 ksi ultimate and 56 ksi yield for wires finer than 0.12 in. diameter, and 75 ksi ultimate and 65 ksi yield for thicker wires.

Uncoated stress relieved wire for prestressed concrete has an ultimate strength of 250 ksi and a yield strength of 200 ksi in 3/16 in. diameter stock. There is a reduction in strength in the larger diameters.

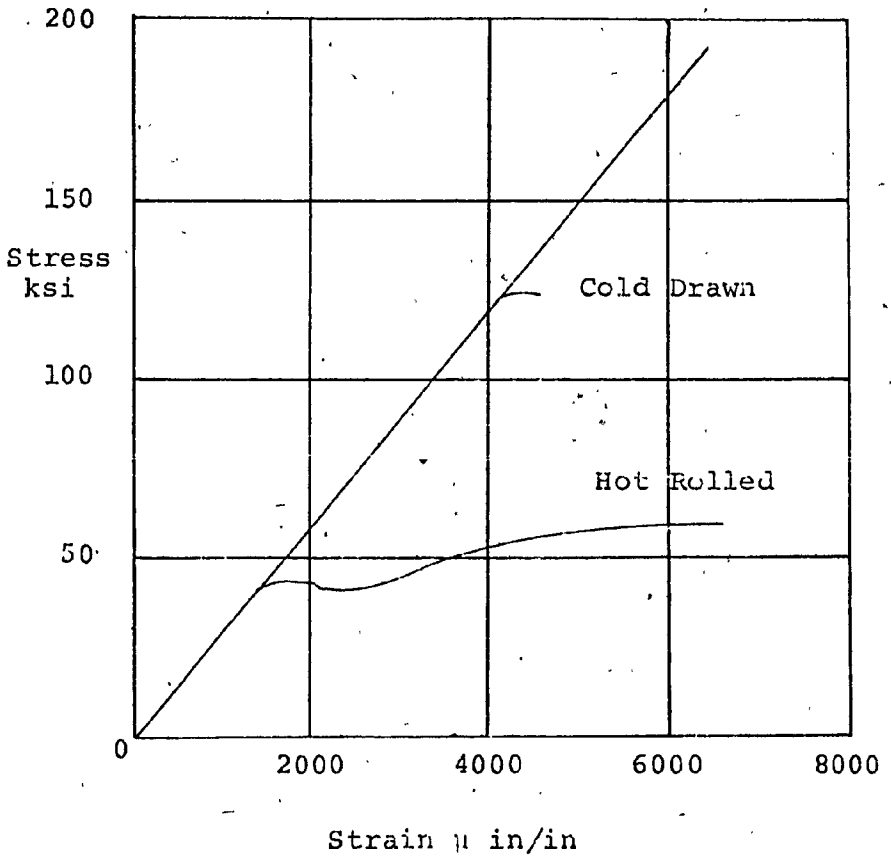


FIG. 2.4 TYPICAL STRESS-STRAIN CURVES FOR STEEL

TABLE 2.3 STRENGTH OF REINFORCING BAR

| | Structural | Intermediate | Hard | 60,000 psi |
|---|---|---|---|---|
| Tension Strength KSI | 55-75 | 70-90 | 80 | 90 |
| Yield Point KSI | 33 | 40 | 50 | 60 |

Seven-strand wire, having a central wire tightly enclosed by six helically wound outer wires is also used for prestressed concrete and has an ultimate strength of 250 ksi, and a yield of 212.5 ksi. [20]

Expanded metal has been used for ferro cement reinforcement, but it has been observed that the change of shape of the diamond mesh when under load causes a scissoring action which causes the mortar to split in the plane of the mesh. [15]

Hexagonal chicken wire is made from a low grade of steel having a yield strength of 33 ksi and an ultimate of 44 ksi. The geometry of this material precludes it from being oriented in the direction of the principal strains so that it will contribute little to the composite strength. It serves primarily as a lathe onto which the mortar is placed. The strength in this type of construction is obtained from the reinforcing bars. [12]

Expanded metal is made by feeding a sheet of metal into a machine in which diamond-shaped cutters expand one row of strands at a time. The resulting material may then be flattened by passing it through heavy rollers. It is usually supplied in sheets 4 x 8 ft and with open diamond sizes ranging from 3/4 to 1 in, being most suitable for ferro cement. The strand of metal remaining would be approximately .05 x .1 in, and a low strength steel would be used. [21]

Perforated metal having round, square, or other shaped holes may also be suitable for some special applications.

Although expanded metal is less expensive than welded or woven mesh, as far as can be ascertained, no boats have yet been built using this material.

## 2.7 SHEAR STRENGTH

The direct shear strength of mortar is difficult to determine as it is almost impossible to eliminate the effect of bearing, diagonal tension, and other stresses. For most cement, the shearing stress is at least sixty percent of the compression strength.

Mortar is not a perfectly elastic material, but exhibits a decrease in the stress-strain ratio as stress increases. Within normal working limits there is a fairly constant relation between stress and strain which may be considered as the elastic modulus. There is a relation between this modulus and the compressive strength of mortar which may be expressed as

$$E = 33{,}000\ F_c^{5/8}$$

Tests show that the modulus increases with age, richness of mix, and is less for a wet than a dry mix. [21]

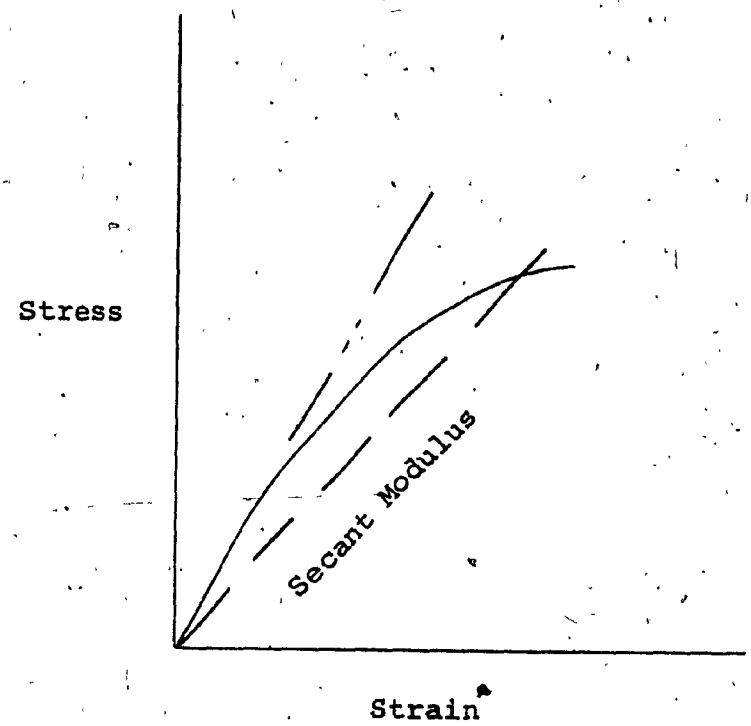


FIG. 2,5 A TYPICAL STRESS STRAIN CURVE FOR CEMENT [22]

## 2.8 BOND STRENGTH

There must be sufficient bond between the steel and the cement to transmit load. The bond stress, or tendency for steel to slide through the cement, per square inch of reinforcing surface is given a maximum value in the ACI Code of .045 times the compressive strength of the mortar. Tests carried out by the British Columbia Research Council gave the values for bond strength shown in Table 2.4. [2]

## 2.9 GALVANIC ACTION

The combination of galvanised and plain steel reinforcement produces a galvanic action in the presence of wet cement paste, and hydrogen gas is produced which interferes with the bond of the cement to the wire. This may be overcome by the addition of chromium trioxide, $CrO_3$, [2] to the mortar at the rate of 5.5 grams for each 100 lbs of cement.

TABLE 2.4 BOND STRENGTH OF TYPICAL REINFORCING RODS

| Type of Reinforcing | Bond Strength lb/sq. in of Embedded Rod Surface | |
|---|---|---|
| | 28 Days | 4½ Months |
| Hot rolled rod 1020 scale intact | 406 | 580 |
| Hot rolled rod 1020 picked | 300 | 555 |
| Double drawn rod as received | 135 | 280 |
| Double drawn rod drawing lubricant removed | 188 | 330 |
| Double drawn rod lightly rusted | 286 | 518 |
| Deformed double drawn rod clean | 651 | 660 |
| Galvanised 1020 rod | 33 | 57 |
| Reclaimed rod badly corroded | 480 | 700 |

# CHAPTER 3

# THE STRESS ANALYSIS OF FERRO CEMENT

# CHAPTER 3

# THE STRESS ANALYSIS OF FERRO CEMENT

## 3.1 STRAIN OF AN ORTHOTROPIC LAMINA

Ferro cement may be considered as a lamina material comprising a number of laminates, each consisting of a separate layer of reinforcing wire and cement. Such a laminate is shown in Fig. 3.1 lying in the X,Y plane, and with major and minor axes in the 1,2 plane.

Since the laminates are thin in the Z-direction, they may be considered to be in a state of plane stress when under load, from which it follows that the normal and the associated shear stresses will be zero.

$$\sigma_3 = 0$$
$$\tau_{13} = \tau_{23} = 0 \qquad (3.1)$$

The strains due to the tensile stresses in the 1 and 2 directions may be deduced from Fig. 3.2.

$$\varepsilon_1 = \frac{\sigma_1}{E_1} - \frac{\sigma_2 \nu_{21}}{E_2}$$
$$\varepsilon_2 = \frac{\sigma_2}{E_2} - \frac{\sigma_1 \nu_{12}}{E_1} \qquad (3.2)$$

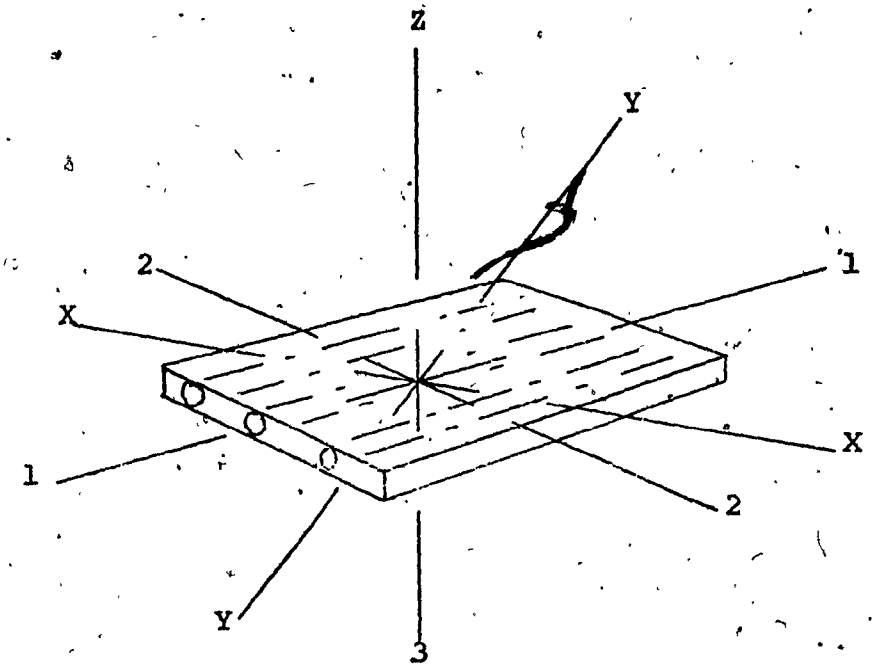


FIG. 3.1 LAMINATE ORIENTATION

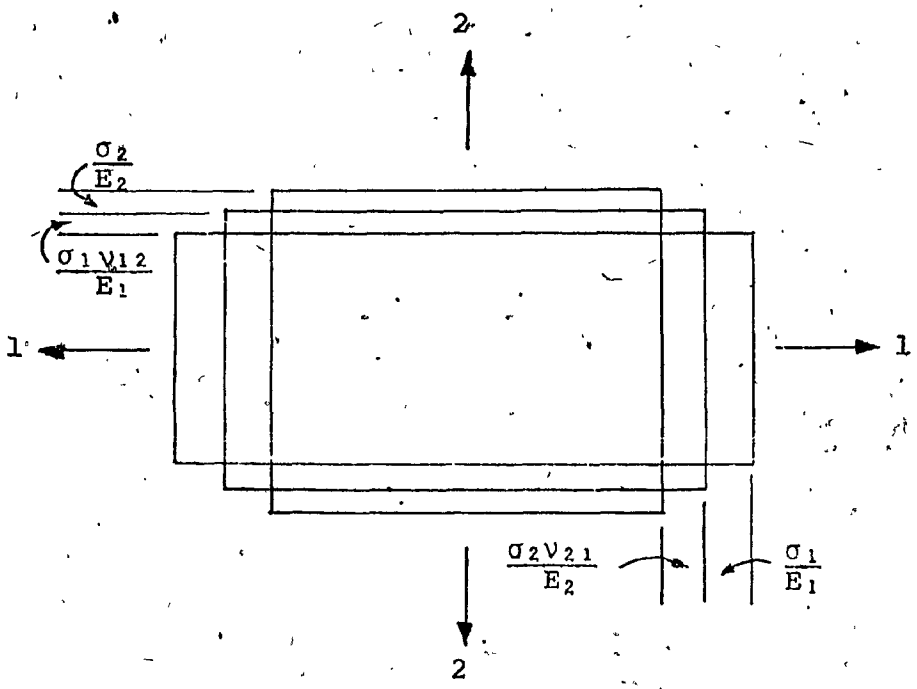


FIG. 3.2 STRAIN OF AN ORTHOTROPIC ELEMENT

The shear strain in the 1,2 plane is given by

$$\gamma_{12} = \frac{\tau_{12}}{G_{12}} \tag{3.3}$$

This may be written in matrix form.

$$\begin{bmatrix} \varepsilon_1 \\ \varepsilon_2 \\ \gamma_{12} \end{bmatrix} = \begin{bmatrix} \frac{1}{E_1} & -\frac{\nu_{21}}{E_2} & 0 \\ -\frac{\nu_{12}}{E_1} & \frac{1}{E_2} & 0 \\ 0 & 0 & \frac{1}{G_{12}} \end{bmatrix} \begin{bmatrix} \sigma_1 \\ \sigma_2 \\ \tau_{12} \end{bmatrix} \tag{3.4}$$

or
$$\underset{\sim}{\varepsilon} = \underset{\sim}{S}\ \underline{\sigma} \tag{3.5}$$

The terms of the S matrix which correspond to the inverse stress strain relations are known as the *"moduli of compliance"*.

Inverting the compliance matrix yields

$$\underline{\sigma} = \underset{\sim}{S}^{-1}\ \underline{\varepsilon}$$

or
$$\underline{\sigma} = \underset{\sim}{C}\ \underline{\varepsilon} \tag{3.6}$$

where C is the matrix of the moduli of elasticity, or the plane stress Hooke's Law matrix for an orthotropic laminate

and
$$\underset{\sim}{C} = \underset{\sim}{S}^{-1} \tag{3.7}$$

## 3.2 LAMINATE STIFFNESS MATRIX

The inversion of the S matrix proceeds by evaluating the determinant and the transpose of the signed minors, so that:

$$\underset{\sim}{S}^{-1} = \frac{E_1 E_2 G_{12}}{1-\nu_{21}\nu_{12}} \begin{bmatrix} \frac{1}{E_2 G_{12}} & \frac{\nu_{21}}{E_2 G_{12}} & 0 \\ \frac{\nu_{12}}{E_1 G_{12}} & \frac{1}{E_1 G_{12}} & 0 \\ 0 & 0 & \frac{1-\nu_{12}\nu_{21}}{E_1 E_2} \end{bmatrix} \tag{3.8}$$

and

$$\begin{bmatrix} \sigma_1 \\ \sigma_2 \\ \tau_{12} \end{bmatrix} = \begin{bmatrix} \frac{E_1}{1-\nu_{21}\nu_{12}} & \frac{E_1 \nu_{21}}{1-\nu_{21}\nu_{12}} & 0 \\ \frac{E_2 \nu_{12}}{1-\nu_{21}\nu_{12}} & \frac{E_2}{1-\nu_{21}\nu_{12}} & 0 \\ 0 & 0 & G_{12} \end{bmatrix} \begin{bmatrix} \varepsilon_1 \\ \varepsilon_2 \\ \gamma_{12} \end{bmatrix} \tag{3.9}$$

or $$\underline{\sigma} = \underset{\sim}{C}\,\underline{\varepsilon}$$

Where C is the Hooke's Law or stiffness matrix and the reciprocality relation requires that it be symmetrical about the main diagonal so that

$$E_1 \nu_{21} = E_2 \nu_{12} \qquad (3.10)$$

The determination of the stiffness matrix for a thin orthotropic laminate therefore requires the determination of four independent elastic constants, $E_1, E_2, \nu_{12}$, and $G_{12}$.

## 3.3 THE TRANSFORMATION MATRICES

The stiffness matrix obtained in this manner relates to the laminate axes 1,2 which will not always coincide with the lamina axes X,Y. It is necessary therefore, to transform the laminate stiffness matrix onto the lamina axes.

The required transformation matrix may be derived by considering the equilibrium of a triangular element, Fig. 3.3.

$$\sigma_x da - \sigma_1 da \cos\theta \cos\theta - \sigma_2 da \sin\theta \sin\theta - \tau_{12} da \cos\theta \sin\theta - \tau_{12} da \sin\theta \cos\theta = 0$$

$$\sigma_x = \sigma_1 \cos^2\theta + \sigma_2 \sin^2\theta + 2\tau_{12} \sin\theta \cos\theta$$

Similarly

$$\sigma_y = \sigma_1 \sin^2\theta + \sigma_2 \cos^2\theta + 2\tau_{12} \sin\theta \cos\theta \qquad (3.11)$$

and

$$\tau_{xy} = -\sigma_1 \cos\theta \sin\theta + \sigma_2 \sin\theta \cos\theta + \tau_{12}(\cos^2\theta - \sin^2\theta)$$

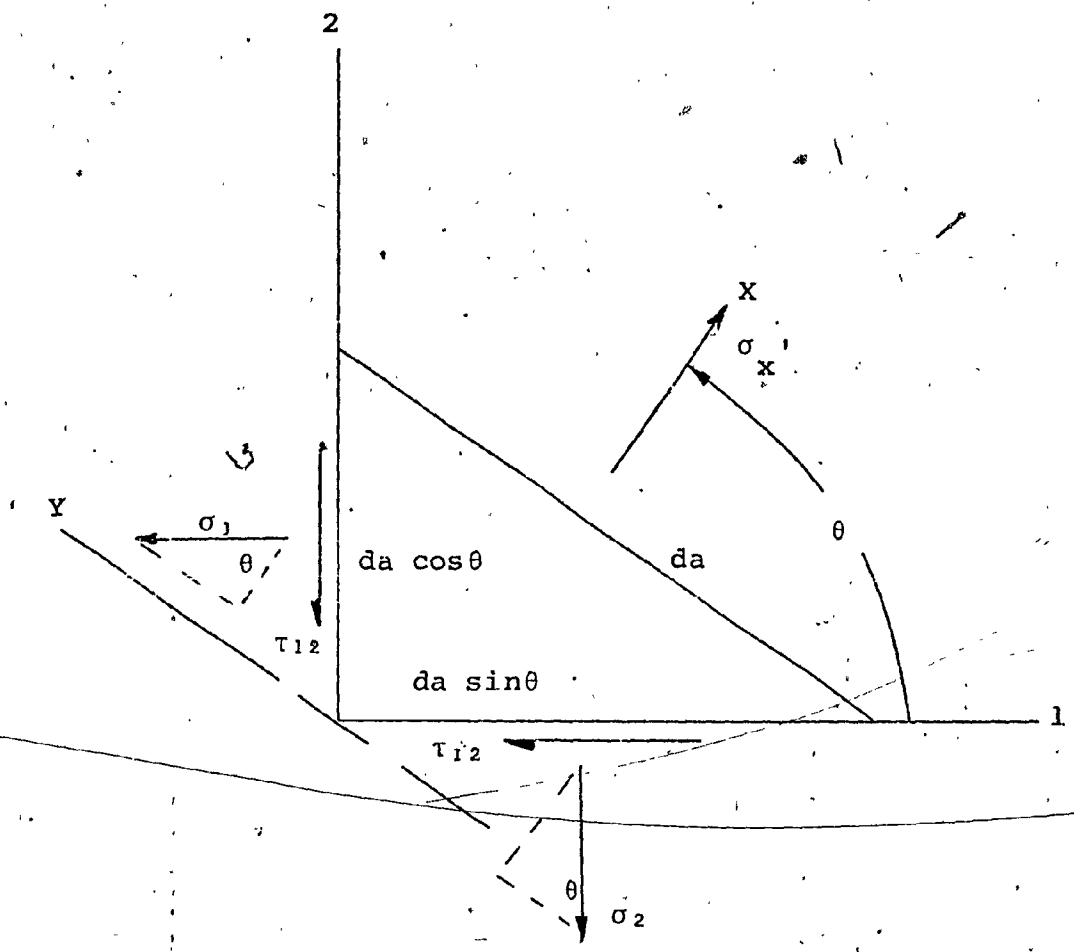


FIG. 3.3 EQUILIBRIUM OF A TRIANGULAR ELEMENT

Writing these equations in matrix form yields the required transformation

$$\begin{bmatrix} \sigma_x \\ \sigma_y \\ \tau_{xy} \end{bmatrix} = \begin{bmatrix} \cos^2\theta & \sin^2\theta & 2\sin\theta\cos\theta \\ \sin^2\theta & \cos^2\theta & -2\sin\theta\cos\theta \\ -\sin\theta\cos\theta & \sin\theta\cos\theta & (\cos^2\theta-\sin^2\theta) \end{bmatrix} \begin{bmatrix} \sigma_1 \\ \sigma_2 \\ \tau_{12} \end{bmatrix} \quad (3.12)$$

Noting that

$$\begin{aligned} \sin 2\theta &= 2\sin\theta\cos\theta \\ \sin^2\theta &= \tfrac{1}{2}(1-\cos 2\theta) \\ \cos^2\theta &= \tfrac{1}{2}(1+\cos 2\theta) \end{aligned} \quad (3.13)$$

and substituting into the transformation matrix yields the familiar Mohr's circle equations

$$\begin{aligned} \sigma_x &= \frac{\sigma_1+\sigma_2}{2} + \frac{\sigma_1-\sigma_2}{2}\cos 2\theta + \tau_{12}\sin 2\theta \\ \sigma_y &= \frac{\sigma_1+\sigma_2}{2} - \frac{\sigma_1-\sigma_2}{2}\cos 2\theta - \tau_{12}\sin 2\theta \\ \tau_{xy} &= \frac{\sigma_2-\sigma_1}{2}\sin 2\theta - \tau_{12}\cos 2\theta \end{aligned} \quad (3.14)$$

If the transformation matrix is designated $\underset{\sim}{T}$, and letting $\cos\theta = m$ and $\sin\theta = n$, then

$$\underset{\sim}{T} = \begin{bmatrix} m^2 & n^2 & 2mn \\ n^2 & m^2 & -2mn \\ -mn & mn & m^2-n^2 \end{bmatrix} \tag{3.15}$$

and

$$\underline{\sigma}_x = \underset{\sim}{T}\,\underline{\sigma}_1 \tag{3.16}$$

premultiplying by $\underset{\sim}{T}^{-1}$ yields

$$\underset{\sim}{T}^{-1}\,\underline{\sigma}_x = \underset{\sim}{T}^{-1}\,\underset{\sim}{T}\,\underline{\sigma}_1 \tag{3.17}$$

or

$$\underset{\sim}{T}^{-1}\,\underline{\sigma}_x = \underline{\sigma}_1$$

It is therefore evident from a consideration of the Mohr's circle transformation that

$$\underset{\sim}{T}^{-1} = \underset{\sim}{T}(-\theta) \tag{3.18}$$

and hence

$$\underset{\sim}{T}^{-1} = \begin{bmatrix} m^2 & n^2 & -2mn \\ n^2 & m^2 & 2mn \\ mn & -mn & m^2-n^2 \end{bmatrix} \tag{3.19}$$

A transformation of the strain on the laminate from the 1,2 axes to the X,Y axes is also required and may be derived by considering the strains on the 1,2 axes which have the values

$$\varepsilon_1 = \frac{\partial U_1}{\partial 1}$$

$$\varepsilon_2 = \frac{\partial V_2}{\partial 2} \qquad (3.20)$$

$$\gamma_{12} = \frac{\partial V_2}{\partial 1} + \frac{\partial U_1}{\partial 2}$$

The axes 1,2 are rotated through an angle $\theta$ onto the X,Y axes. The angle $\alpha$ and the distances $U_1$ and $V_2$ are infinitely small, as shown in Figure 3.4. Q' has the components $U_1$ and $V_2$ from Q.

$$Q\,Q_1 = \frac{\partial U_1}{\partial 1} d_1 + \frac{\partial U_1}{\partial 2} d_2$$

$$Q_1Q' = \frac{\partial V_2}{\partial 2} d_2 + \frac{\partial V_2}{\partial 1} d_1$$

and

$$\varepsilon_x = \frac{Q''Q' \cos\alpha}{PQ}$$

$$PQ = ds$$

$$Q''Q'\cos\alpha = Q\,Q_1\cos\theta + Q_1Q'\sin\theta$$

Dividing through by ds and noting that with $\alpha$ small $\cos\alpha = 1$

$$\frac{Q''Q'}{ds} = \left(\frac{\partial U_1}{\partial 1}\frac{d_1}{ds} + \frac{\partial U_1}{\partial 2}\frac{d_2}{ds}\right)\cos\theta + \left(\frac{\partial V_2}{\partial 2}\frac{d_2}{ds} + \frac{\partial V_2}{\partial 1}\frac{d_1}{ds}\right)\sin\theta$$

or

$$\varepsilon_x = \varepsilon_1 \cos^2\theta + \varepsilon_2 \sin^2\theta + \gamma_{12} \sin\theta \cos\theta \qquad (3.21)$$

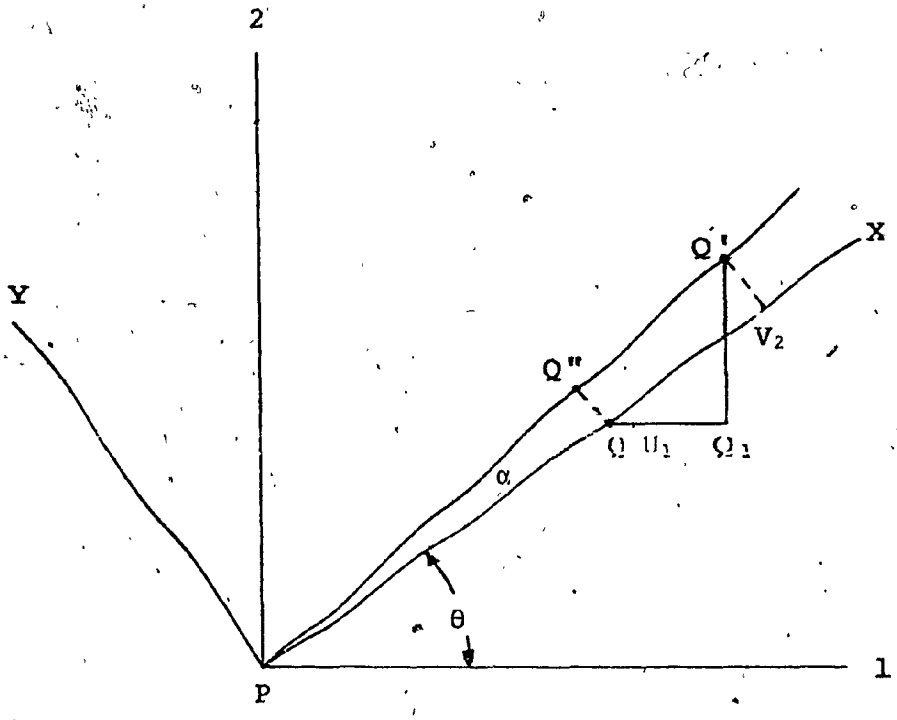


FIG. 3.4 TRANSFORMATION OF THE STRAIN AXES.

The remaining strains may be derived in a similar manner to yield the transformation matrix

$$\begin{bmatrix} \varepsilon_x \\ \varepsilon_y \\ \gamma_{xy} \end{bmatrix} = \begin{bmatrix} m^2 & n^2 & mn \\ n^2 & m^2 & -mn \\ -2mn & 2mn & m^2-n^2 \end{bmatrix} \begin{bmatrix} \varepsilon_1 \\ \varepsilon_2 \\ \gamma_{12} \end{bmatrix} \qquad (3.22)$$

If half the values of shear strain are used, then the strain transformation matrix becomes identical to the stress transformation matrix. The equations may then be reduced to the Mohr's circle transformation in terms of strain

$$\begin{bmatrix} \varepsilon_x \\ \varepsilon_y \\ \tfrac{1}{2}\gamma_{xy} \end{bmatrix} = \begin{bmatrix} m^2 & n^2 & 2mn \\ n^2 & m^2 & -2mn \\ -mn & mn & n^2-n^2 \end{bmatrix} \begin{bmatrix} \varepsilon_1 \\ \varepsilon_2 \\ \tfrac{1}{2}\gamma_{12} \end{bmatrix} \qquad (3.23)$$

The transformation of both stress and strain may now be written thus

$$\begin{bmatrix} \sigma_x \\ \sigma_y \\ \tau_{xy} \end{bmatrix} = \underline{T} \begin{bmatrix} \sigma_1 \\ \sigma_2 \\ \tau_{12} \end{bmatrix} \qquad (3.24)$$

and

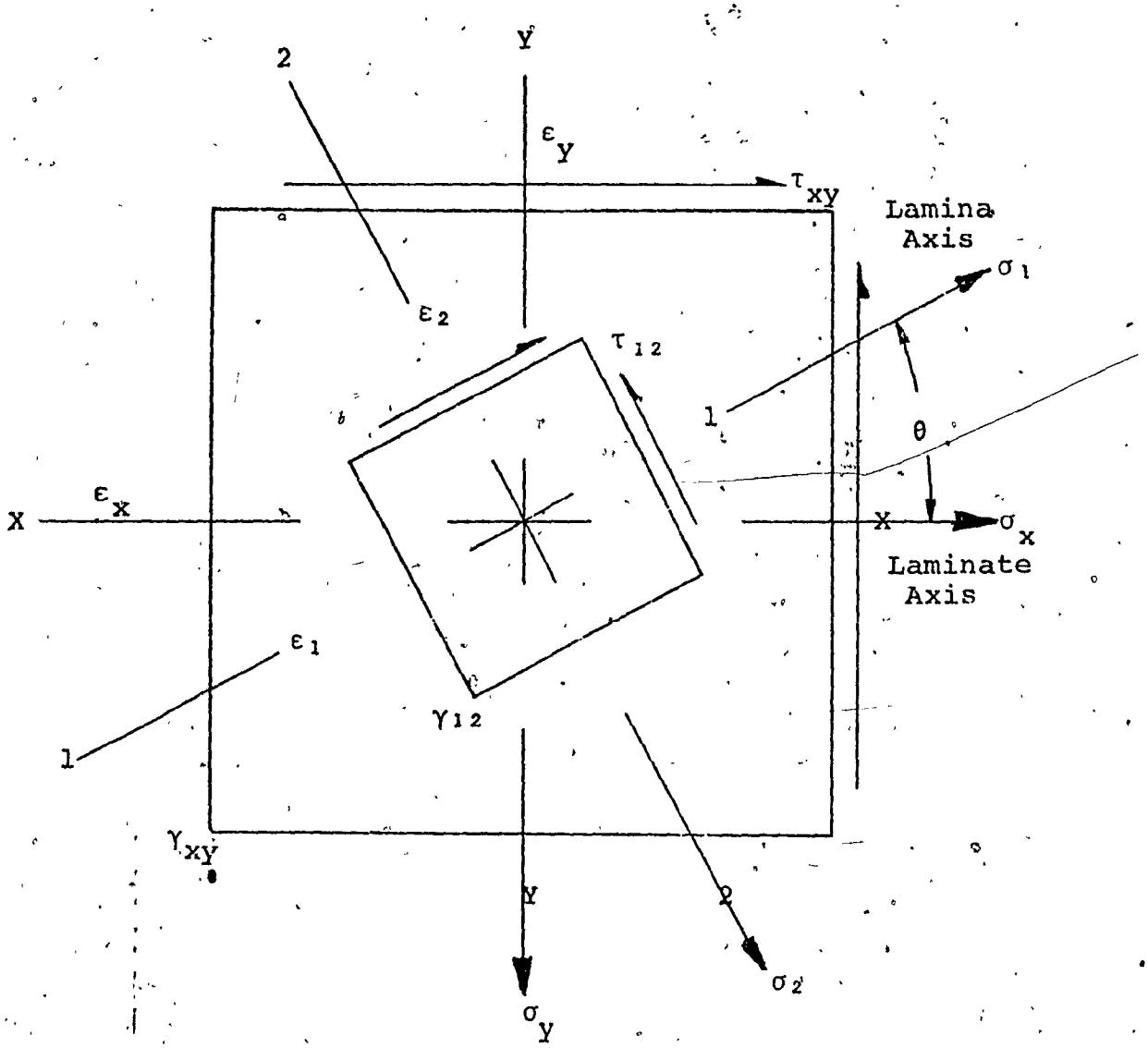


FIG. 3.5 LAMINA AND LAMINATE AXES

and

$$\begin{bmatrix} \varepsilon_x \\ \varepsilon_y \\ \frac{1}{2}\gamma_{xy} \end{bmatrix} = \underline{T} \begin{bmatrix} \varepsilon_1 \\ \varepsilon_2 \\ \frac{1}{2}\gamma_{12} \end{bmatrix} \tag{3.25}$$

From the stress strain relationship for an orthotropic lamina in the lamina axes

$$\begin{bmatrix} \sigma_1 \\ \sigma_2 \\ \tau_{12} \end{bmatrix} = \begin{bmatrix} C_{11} & C_{12} & 0 \\ C_{21} & C_{22} & 0 \\ 0 & 0 & C_{33} \end{bmatrix} \begin{bmatrix} \varepsilon_1 \\ \varepsilon_2 \\ \varepsilon_3 \end{bmatrix} \tag{3.26}$$

The corresponding relationship in the laminate axes shows the compliance matrix to be fully populated, thus

$$\begin{bmatrix} \sigma_x \\ \sigma_y \\ \tau_{xy} \end{bmatrix} = \begin{bmatrix} C_{11} & C_{12} & C_{13} \\ C_{21} & C_{22} & C_{23} \\ C_{31} & C_{32} & C_{33} \end{bmatrix} \begin{bmatrix} \varepsilon_x \\ \varepsilon_y \\ \frac{1}{2}\gamma_{xy} \end{bmatrix} \tag{3.27}$$

Rearranging Equations (3.24) to (3.27) to find the stress and strain in the laminate axes in terms of the orthotropic compliance matrix and the appropriate transformations yields

$$\underline{T}^{-1} \begin{bmatrix} \sigma_x \\ \sigma_y \\ \tau_{xy} \end{bmatrix} = \underline{C}\,\underline{T}^{-1} \begin{bmatrix} \varepsilon_x \\ \varepsilon_y \\ \frac{1}{2}\gamma_{xy} \end{bmatrix} \tag{3.28}$$

or

$$\begin{bmatrix} \sigma_x \\ \sigma_y \\ \tau_{xy} \end{bmatrix} = \underline{T}\,\underline{C}\,\underline{T}^{-1} \begin{bmatrix} \varepsilon_x \\ \varepsilon_y \\ \frac{1}{2}\gamma_{xy} \end{bmatrix} \tag{3.29}$$

## 3.4 THE LAMINA CONSTITUTIVE EQUATIONS

Now that the stress in terms of strain is determined in the laminate axes for any orthotropic lamina, it is possible to derive the constitutive equations for laminated materials by making the assumption that the stress across any lamina is constant.

Let N and M be the direct load and the bending moment respectively, acting on a plate comprising I lamina.

$$\text{End load} \quad N = \Sigma_1^I \sigma_i t_i$$

$$\text{Moment} \quad M = \Sigma_1^I \sigma_i z_i t_i \tag{3.30}$$

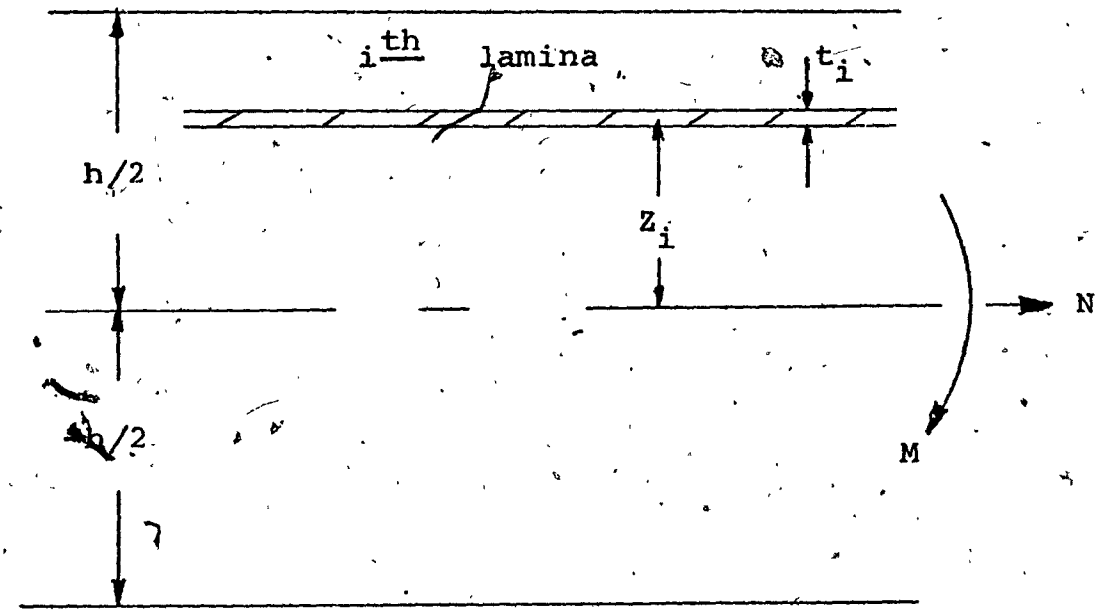


FIG. 3.6 CROSS-SECTION OF A LAMINA

The total strain on the element is the sum of the direct strain and the bending strain. The implicit assumption of a uniform temperature field providing no thermal strain is introduced at this point, but the equations derived may be expanded to include thermal strain.

$$\varepsilon = \varepsilon_0 + Z\chi \tag{3.31}$$

where

$\varepsilon_0$ is the in-plane strain

$\chi$ is the bending curvature

$Z$ is the distance to the neutral axis

Substituting the compliance matrix post-multiplied by the strain in place of stress into the end load and moment equilibrium equations gives the constitutive equations for lamina anisotropic materials [23,24].

$$\left[\begin{array}{c} N_x \\ N_y \\ N_{xy} \\ \hline M_x \\ M_y \\ M_{xy} \end{array}\right] = \left[\begin{array}{c|c} A & B \\ \hline B & D \end{array}\right] \left[\begin{array}{c} \varepsilon_x \\ \varepsilon_y \\ \frac{1}{2}\gamma_{xy} \\ \hline \chi_x \\ \chi_y \\ \frac{1}{2}\chi_{xy} \end{array}\right] \tag{3.32}$$

where,

$$\underset{\sim}{A} = \Sigma_1^I \underset{\sim}{C}_i \, t_i$$

$$\underset{\sim}{B} = \Sigma_1^I Z_i \, \underset{\sim}{C}_i \, t_i \qquad (3.33)$$

$$\underset{\sim}{D} = \Sigma_1^I Z_i^2 \, \underset{\sim}{C}_i \, t_i$$

## 3.5 FAILURE CRITERION

It is postulated that failure occurs when the strain on the cement in the material axes reaches the value at which cracking occurs.

$$\varepsilon_1 = K_1$$

$$\varepsilon_2 = K_2 \qquad (3.34)$$

$$\gamma_{12} = K_{12}$$

Where $K_1$ and $K_2$ are the tensile ultimate strains and $K_{12}$ is the shear ultimate strain. The failure envelope can be found in terms of stress by means of the Hooke's Law relationship [25]

$$\begin{bmatrix} \varepsilon_1 \\ \varepsilon_2 \\ \gamma_{12} \end{bmatrix} = \begin{bmatrix} S_{11} & S_{12} & 0 \\ S_{21} & S_{22} & 0 \\ 0 & 0 & S_{33} \end{bmatrix} \begin{bmatrix} \sigma_1 \\ \sigma_2 \\ \tau_{12} \end{bmatrix} \qquad (3.35)$$

# CHAPTER 4

# ANALYSIS OF FERRO CEMENT IN TENSION

# CHAPTER 4

# ANALYSIS OF FERRO CEMENT IN TENSION

## 4.1 THE TENSILE SPECIMEN

A tensile test specimen containing three layers of welded steel wire fabric was made and tested in the manner previously developed. [12] The centre layer had the wire in the axis of the tensile loading whilst each outer layer was oriented at 45°, as shown in Fig. 4.1. The wire diameter was .025 inch at a spacing of 1/4 inch and the mortar was made from one part of ordinary Portland cement to one and a half parts of sand, by weight. The water/cement ratio was 0.4.

The failing load of the specimen was 1,250 lbs.

The specimen comprised three layers of .0245 inch diameter wire.

Wire area = .000471 sq.in.

Circumference = .07697 in

The wire surface area per cubic inch of material

$$(.07696 \times 8 + .07697 \times 8.3 \times 2)4 = 7.5 \text{ sq.in/cu.in}$$

The weight of reinforcing

$$24.6 \times .000471 \times 144 \times 12 \times 4 \times .3 = 48 \text{ lb/cu.ft.}$$

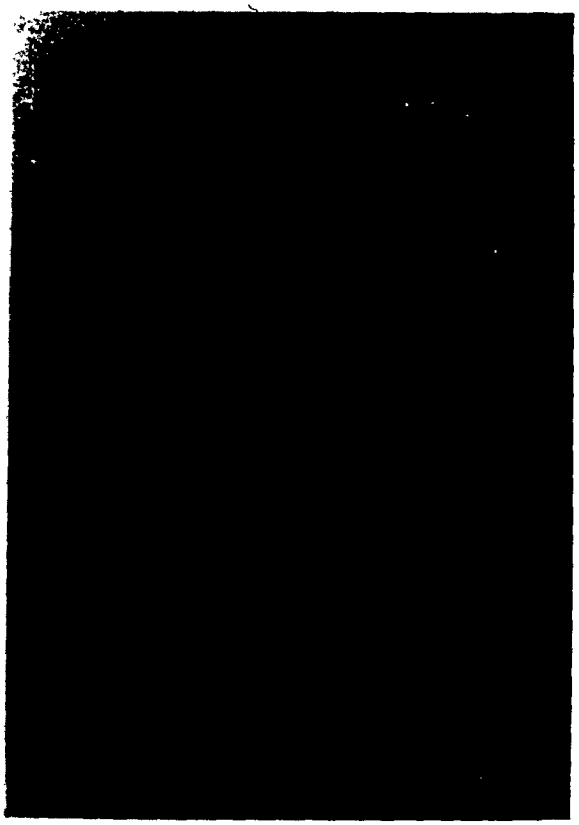

FIG. 4.1 THE WIRE FABRIC IN THE TENSILE SPECIMEN PRIOR TO CEMENTING

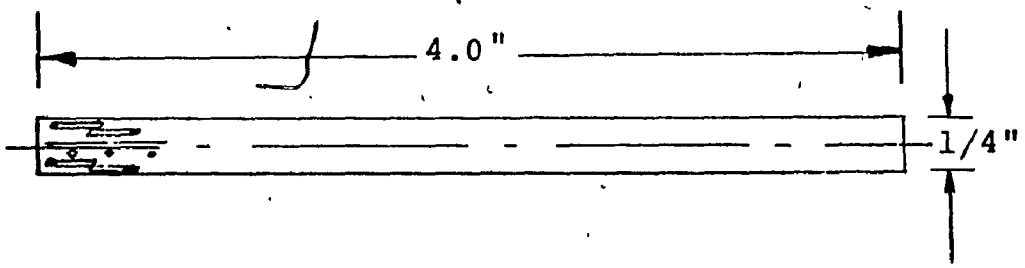


Cross-sectional area = 4 × ¼ = 1.0 sq.in.
Failing stress = 1,250 psi
Failing load = 1,250 lbs

FIG. 4.2 A CROSS-SECTION OF THE SPECIMEN

The mesh factor, being the ratio of the area, of space enclosed by the wires to the wire diameter is given by [12] :

$$\frac{.25 \times .25}{.0245} = 2.55$$

## 4.2 STRENGTH OF THE REINFORCING WIRE

Six individual strands of wire were broken in tension with the following results.

TABLE 4.1 BREAKING LOAD OF REINFORCING WIRE

| Specimen | Diameter | Breaking Load | Wire Area | Ultimate Stress |
|---|---|---|---|---|
| 1 | .024 in | 27.5 lb | $.452 \times 10^{-3}$ | 60840 psi |
| 2 | .024 | 29.0 | .452 sq.in | 64159 |
| 3 | .025 | 34.0 | .491 | 69243 |
| 4 | .0245 | 32.0 | .471 | 67940 |
| 5 | .0238 | 25.0 | .445 | 56179 |
| 6 | .0238 | 25.0 | .445 | 56179 |

Range = 69243 - 56179 = 13064 psi

Taking four class intervals:

width = 3266 psi

TABLE 4.2 STATISTICAL EVALUATION OF WIRE STRENGTH

| Interval | Boundaries | Mid | $f_i$ | $x_i - W$ | $x_i$ | $f_i x_i$ | $(f_i x_i)^2$ |
|---|---|---|---|---|---|---|---|
| 1 | 56179 - 59445 | 57812 | 2 | -3266 | -1 | -2 | 4 |
| 2 | 59446 - 62711 | 61078 | 1 | 0 | 0 | 0 | 0 |
| 3 | 62712 - 65997 | 64344 | 1 | 3266 | 1 | 1 | 1 |
| 4 | 65978 - 69243 | 67610 | 2 | 6532 | 2 | 4 | 16 |
| | | | | | | 3 | 21 |

$$\text{Variance } S^2 = \frac{21(3266)^2}{6} = 3.5 \times 3266^2$$

$$\bar{x} = \frac{3(3266)}{6} + 61078 = 62686 \text{ psi}$$

Mean failing load of each wire

$$62686 \times .000471 = 29.5 \text{ lb}$$

## 4.3 STRAIN OF THE DIAGONAL WIRES

Consider the tension load to be carried by the reinforcing wire, then the proportion of this load which is carried by the longitudinal and diagonal wires respectively may be obtained by considering the strain energy of an element of mesh.

Apply a load of 10 lbs to the conjunction point, A, of the mesh and let P be carried by the diagonals. For compatability the wires must strain together at the conjunction points, each diagonal wire will therefore carry .7071 P lbs

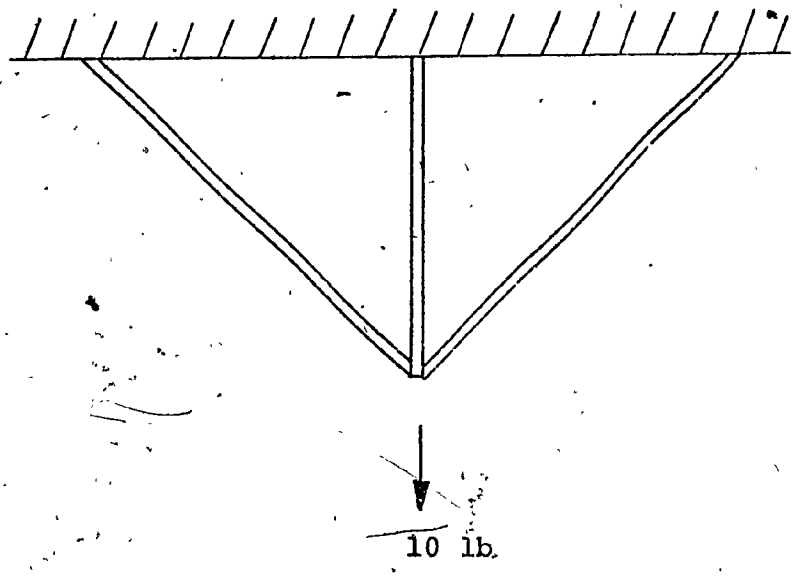


FIG. 4.3 AN ELEMENT OF MESH

and the longitudinal wire will carry 10 P lbs.

The total strain energy is given by

$$U = \frac{P^2 L}{2AE}$$

whence

$$\frac{\partial U}{\partial P} = \frac{P \partial P L}{AE}$$

and AE is constant.

So that

$$\text{Longitudinally } \frac{\partial U}{\partial P} = (10-P) \times -1 \times L$$

$$= PL - 10L$$

$$\text{Diagonally } \frac{\partial U}{\partial P} = 2(.7071P \times .7071 \times 1.414L)$$

$$= 1.414PL$$

Summing the partials and eliminating 'L yields

$$2.414P = 10$$

$$P = 4.14 \text{ lb}$$

so that the load in the longitudinal wire

$$= 10-4.14 = 5.86 \text{ lbs}$$

and the load in each diagonal

$$= \frac{4.14}{2 \times .7071} = 2.93 \text{ lbs}$$

## 4.4 PREDICTED FAILING LOAD

The steel wire fabric is made from cold drawn wire which has a yield strength of 56,000 psi, hence the yield load for the wire

$$P_y = 56{,}000 \times .000471 = 26.4 \text{ lbs}$$

and the ultimate load, as already determined

$$P_u = 29.5 \text{ lbs}$$

Now the specimen comprised sixteen longitudinal wires and forty-four diagonal wires, twenty-two on each face. The load carried by these wires at yield

$$P_y = 26.4 \times 16 + 2.93 \times \frac{26.4}{5.86} \times .7071 \times 44$$

$$= 422 + 410$$

$$= 832 \text{ lbs}$$

The proportion of the load carried by the cement in tension may be obtained from the net cross-section of the specimen which is the gross area less that part which is traversed by wires. [12]

$$= 1.0 - 4(.0245 + .5 \times .0245 \times 4)$$

$$= 0.706 \text{ sq. in.}$$

With cement of 6,000 psi crushing strength the tensile strength will be 600 psi so that the tension load carried by the cement will be

$$600 \times .706 = 420 \text{ lbs}$$

The total load carried by the specimen at yield of the wire reinforcing is then

$$832 + 420 = 1252 \text{ lbs}$$

At this load, the cement cracks along the lines which represent the least cross-section of cement which are coincident with the transverse wires, (see Figure 4.4). The whole load is now carried by the wire reinforcing, the longitudinal wires will yield so that the diagonal wires may take up the load and failure will occur when all the wires reach ultimate load.

$$P_{ult} = 29.5 \times 16 + 29.5 \times .7071 \times 44$$
$$= 472 + 917 = 1389 \text{ lbs}$$

## 4.5 MODULUS OF ELASTICITY

In order to evaluate the strength of the tensile specimen using composite theory it is necessary to establish the value of E to be used in the stiffness matrix. The required value will be a function of the constituent materials, steel and mortar, and

FIG. 4.4 THE SPECIMEN SHOWING TYPICAL TRANSVERSE CRACK PATTERN WHICH OCCURS AT YIELD LOAD, AND ALSO THE ULTIMATE FAILURE

will be dependant upon their relative proportions in the lamina. The modulus at low stress levels may be obtained by the rule of mixtures.

$$E = E_{steel} \frac{A_s}{A} + E_{mortar} \frac{A_m}{A}$$

where $A_s$ = cross-sectional area of steel fibre

$A_m$ = cross-sectional area of mortar

$A$ = total cross-section per unit width of lamina

A characteristic of ferro cement when considered as a composite material is the unusually low proportion of filament reinforcing to matrix material so that the elastic properties of the latter become of significance. Mortar is known to have a non-linear stress-strain relationship, as shown in Fig. 2.5, so that the modulus of a ferro cement lamina will also be non-linear with increasing stress. It is therefore necessary to use a secant modulus in evaluating the stiffness matrix C, (Eq.(3.9)) and this may be deduced for any lamina by considering the proportion of load carried by the steel and the corresponding strain of the steel, together with the proportion of load carried by the mortar which is now straining with, and prevented from cracking by, the steel fibres. The sum of the loadings when divided by the strain on the steel fibre yields the secant modulus. The strain curves for the component materials of ferro cement are shown in Fig. 4.5; the steel is following the normal linear relationship, however, the cement, which would have cracked at a low strain without the presence of the wire, is now following the steel without increase in stress.

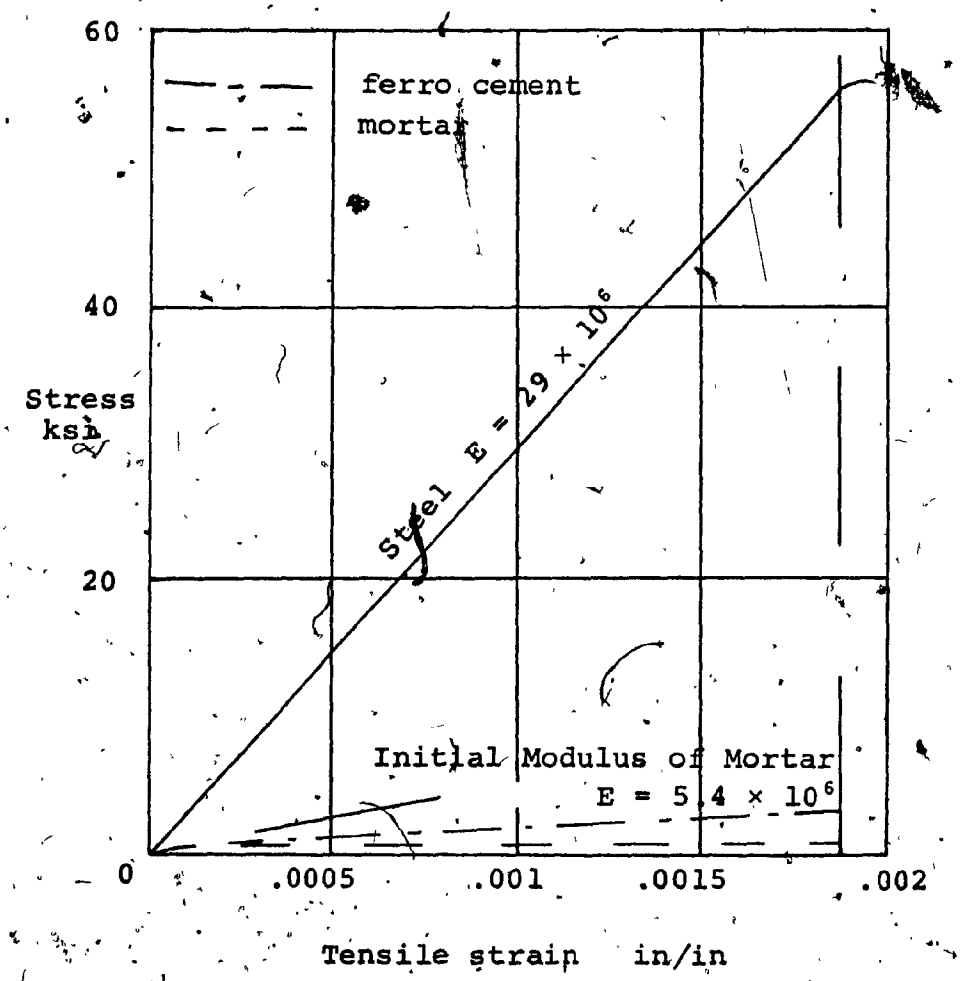


FIG. 4.5 STRESS STRAIN CURVES FOR THE COMPONENT MATERIALS OF FERRO CEMENT

Consider a strip of ferro cement comprising one layer of mesh with overall dimensions shown in Fig. 4.6.

Area of steel mesh in tension

$$A_s = 16 \times .000471 = .0075 \text{ sq.in.}$$

Area of cement

$$A_c = 4(.083 - .0245) = .234 \text{ sq.in.}$$

Area of cement less area of steel in tension = .2265 sq.in.

Hence, the areas of the constituents as a fraction of the whole,

$$\text{Steel} = \frac{.0075}{.234} = .032$$

$$\text{Cement} = \frac{.2265}{.234} = .968$$

and the

$$\text{Initial Modulus } E = (29 \times .032 + 5.4 \times .968) \times 10^6$$

$$= 6.15 \times 10^6 \text{ psi}$$

The E at failure is obtained from the load carried at failure and the yield strain of the wires.

Failing load = $26.4 \times 16 + .2265 \times 600 = 558$ lbs

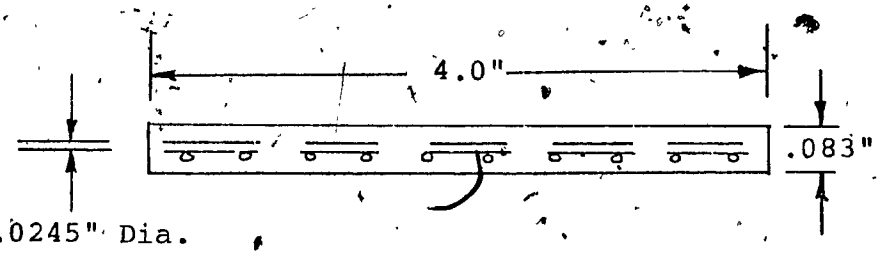


FIG. 4.6 THE STRIP OF FERRO CEMENT

$$\text{Average stress at failure} = \frac{558}{.083 \times 4.0} = 1680 \text{ psi}$$

$$E_f = \frac{1680}{.0019} = 0.88 \times 10^6 \text{ psi}$$

At halfway to ultimate load the modulus, $E_h$, is obtained by considering the wire at half load and the corresponding strain.

$$P = 0.5[26.4 \times 16] + .265 \times 600 = 347$$

$$\text{Average } \sigma t = \frac{347}{.332} = 1045 \text{ psi}$$

$$E_h = \frac{1045}{.00095} = 1.1 \times 10^6 \text{ psi}$$

## 4.6 PREDICTED FAILING LOAD USING LAMINA ANALYSIS

It has been shown that the end load on a composite plate is given by

$$\underline{N} = \underset{\sim}{A}\,\underline{\varepsilon} \qquad (4.1)$$

where

$$\underset{\sim}{A} = \sum_{i=1}^{I} C_i\, t_i$$

In the case of the specimen under consideration employing three layers of mesh, I = 3 and t = .25/3 = .083. The C matrix of the moduli of elasticity is obtained for the centre layer using the tangent modulus at failure,

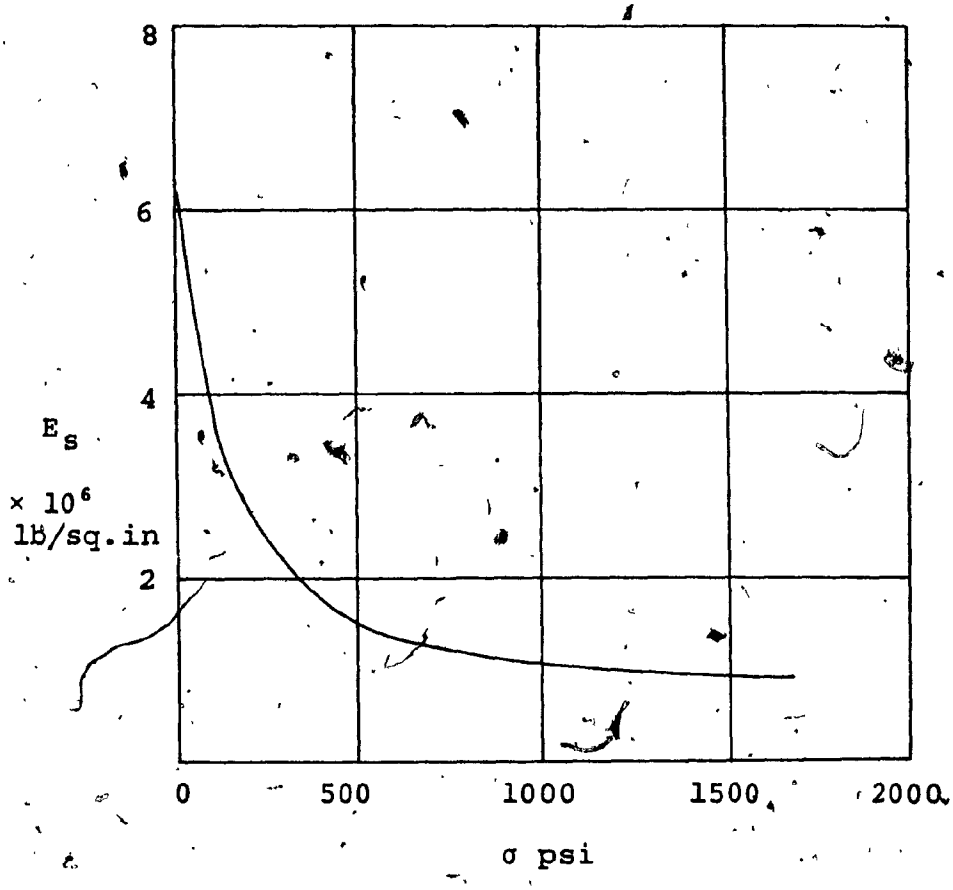


FIG. 4.7 SECANT MODULUS OF FERRO CEMENT REINFORCED WITH QUARTER INCH MESH AND LOADED LONGITUDINALLY

$E_s = 0.88 \times 10^6$ psi and Poisson's ratio $\nu = 0.13$, [12]. The shear modulus is taken as $0.3\ E_s$.

$$\frac{E_s}{1-\nu_p^2} = 0.895 \qquad \frac{\nu E_s}{1-\nu^2} = .1164$$

so that

$$C_2 = \begin{bmatrix} .895 & .1164 & 0 \\ .1164 & .895 & 0 \\ 0 & 0 & .26 \end{bmatrix}$$

and

$$C_2\ t_2 = \begin{bmatrix} .0743 & .00966 & 0 \\ .00966 & .0743 & 0 \\ 0 & 0 & .0216 \end{bmatrix}$$

The $C$ matrix for the two outer layers in which the lamina wire cloth has been placed at $45^\circ$ to the longitudinal axis is obtained by transforming the $C$ matrix of the central layer. The required transformation (see Eq. (3.29)) is

$$\underline{T}\ \underline{C}\ \underline{T}^{-1}$$

which, when multiplied out, yields the coefficients of the transformed $C$ matrix, $\bar{C}$.

$$\bar{C}_{11} = C_{11}\cos^4\theta + 2(C_{12}+2C_{66})\sin^2\theta\cos^2\theta + C_{22}\sin^4\theta$$

$$\bar{C}_{22} = C_{11}\sin^4\theta + 2(C_{12}+2C_{66})\sin^2\theta\cos^2\theta + C_{22}\cos^4\theta$$

$$\bar{C}_{12} = (C_{11}+C_{22}-4C_{66})\sin^2\theta\cos^2\theta + C_{12}(\sin^4\theta+\cos^4\theta)$$

$$\bar{C}_{66} = (C_{11}+C_{22}-2C_{12}-2C_{66})\sin^2\theta\cos^2\theta + C_{12}(\sin^4\theta+\cos^4\theta)$$

In this case

$$C_{16} = C_{26} + 0$$

The outer layers are at $45^\circ$ to the loading axis so that

$$\theta = 45^\circ \qquad \cos\theta = \sin\theta = .7071$$

$$\cos^4\theta = \sin^4\theta = \sin^2\theta\cos^2\theta = 0.25$$

Hence

$$\bar{C}_{11} = \bar{C}_{22} = .895 \times .25 + 2(.1164+2\times.26).25 + + .1164 \times .25 = .576$$

$$\bar{C}_{12} = \bar{C}_{21} = (.895+.895-4\times.26).25 + .1164(.25+.25) = .246$$

$$C_{66} = (.895+.895-2\times.1164-2\times.26).25 + .26(.25+.25) = .289$$

so that

$$C_1 = C_3 = \begin{bmatrix} .576 & .246 & 0 \\ .246 & .576 & 0 \\ 0 & 0 & .289 \end{bmatrix}$$

and

$$C_1 t_1 = C_3 t_3 = \begin{bmatrix} .0478 & .0204 & 0 \\ .0204 & .0478 & 0 \\ 0 & 0 & .024 \end{bmatrix}$$

Summing $C_i t_i$ from I = 1 to 3, yields the A matrix:

$$A = \begin{bmatrix} .1699 & .0504 & 0 \\ .0504 & .1699 & 0 \\ 0 & 0 & .0696 \end{bmatrix}$$

At the ultimate load

$$\varepsilon_x = .0019$$

$$\bar{\nu} = \frac{.0504}{.1699} = .29 \qquad \varepsilon_y = -\varepsilon_x \bar{\nu} = -.00056$$

From the strains at failure and the matrix of moduli of elasticity the failing load may be obtained:

$$\begin{bmatrix} N_x \\ N_y \\ N_{xy} \end{bmatrix} = \begin{bmatrix} .1699 & .0504 & 0 \\ .0504 & .1699 & 0 \\ 0 & 0 & .0609 \end{bmatrix} \times 10^6 \begin{bmatrix} .0019 \\ -.00056 \\ 0 \end{bmatrix} = \begin{bmatrix} 294 \\ 0 \\ 0 \end{bmatrix}$$

The test panel was four inches wide so that the predicted failing load would be

$$294 \times 4 = 1176 \text{ lbs}$$

The actual failing load was 1250 lbs

The load carried by the outer faces is

$$(.0478\times.0019-.0204\times.00056)4 = 318 \text{ lbs}$$

and on the inner layer

$$(.0743\times.0019-.00966\times.00056)4 = 543 \text{ lbs}$$

The load on each layer obtained in the analysis on pages 57 and 58 was

Outer faces $410/2 + 420/3 = 345$ lbs

Inner layer $422 + 420/3 = 562$ lbs

# CHAPTER 5

## ANALYSIS OF FERRO CEMENT IN BENDING

# CHAPTER 5

# ANALYSIS OF FERRO CEMENT IN BENDING

## 5.1 THE BENDING SPECIMEN

In order to investigate the behaviour of thin ferro cement panels in bending, it was decided to utilize a specimen sufficiently large to allow two-point loading. This enabled a constant bending moment without shear load to be applied to the part of the specimen under examination (see Fig. 5.1).

To fabricate the specimens, a split mold was constructed which enabled the reinforcing mesh to be gripped and held flat to receive the cement mortar which was applied from either side and trowelled to a smooth surface finish. When the cement had cured the mold was unbolted, so that the two halves separated and released the specimen which had finished dimensions of 34 inches by 6 inches (see Fig. 5.2).

A specimen was made having four layers of $\frac{1}{4}$ inch mesh welded steel wire fabric which had a wire diameter of .025 in. The mortar was made from one part of ordinary Portland cement to one and a half parts of sand by weight with a water cement ratio of 0.4. The finished panel was $\frac{1}{2}$ in. thick, a typical cross-section is shown in Fig. 5.3.

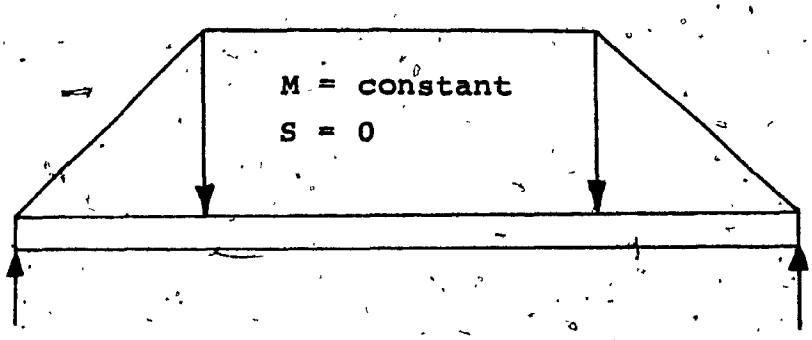


FIG. 5.1 TWO-POINT LOADING

FIG. 5.2 MOLD FOR THE BENDING SPECIMEN WITH WIRE IN PLACE

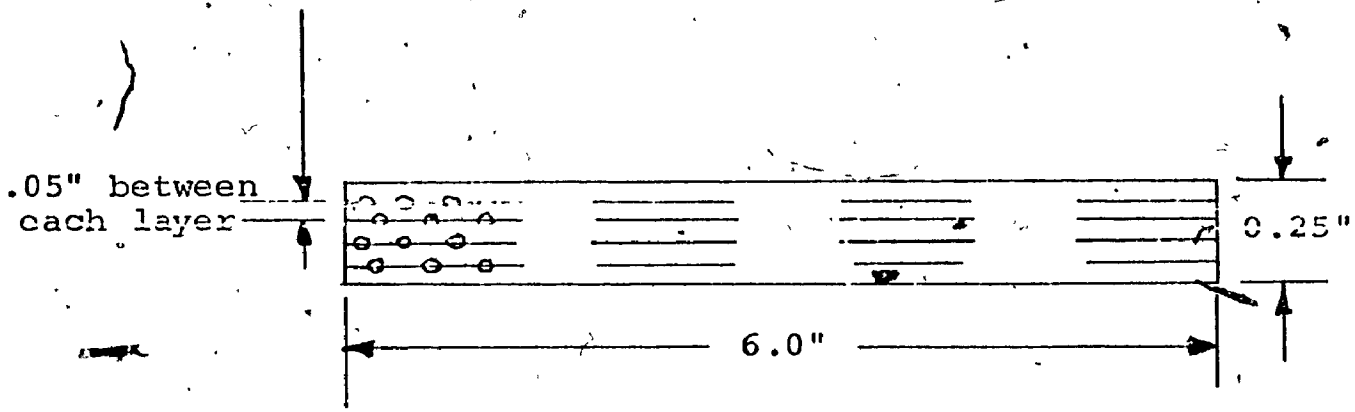


FIG. 5.3 CROSS-SECTION OF THE BENDING SPECIMEN

## 5.2 METHOD OF LOADING

The specimen was supported on bars representative of pin joints spaced 32 inches apart and the load was applied at the quarter points by means of weights. Five dial gauges were placed beneath the specimen, as shown in Fig. 5.4.

A load was applied and the dial gauges were read, the load was then increased by an increment and the procedure repeated so that a load deflection curve could be obtained. The results of this test are shown in Table 5.1. It was observed that at any load level deflection increased noticeably with time and at certain loads two sets of readings were taken at a short time interval apart.

## 5.3 TEST RESULTS

The test results of the deflection versus the load are shown in Table 5.1.

The deflections were increasing with time and were re-read after the following time intervals:

(a) 1 minute

(b) 2 minutes

(c) 3 minutes

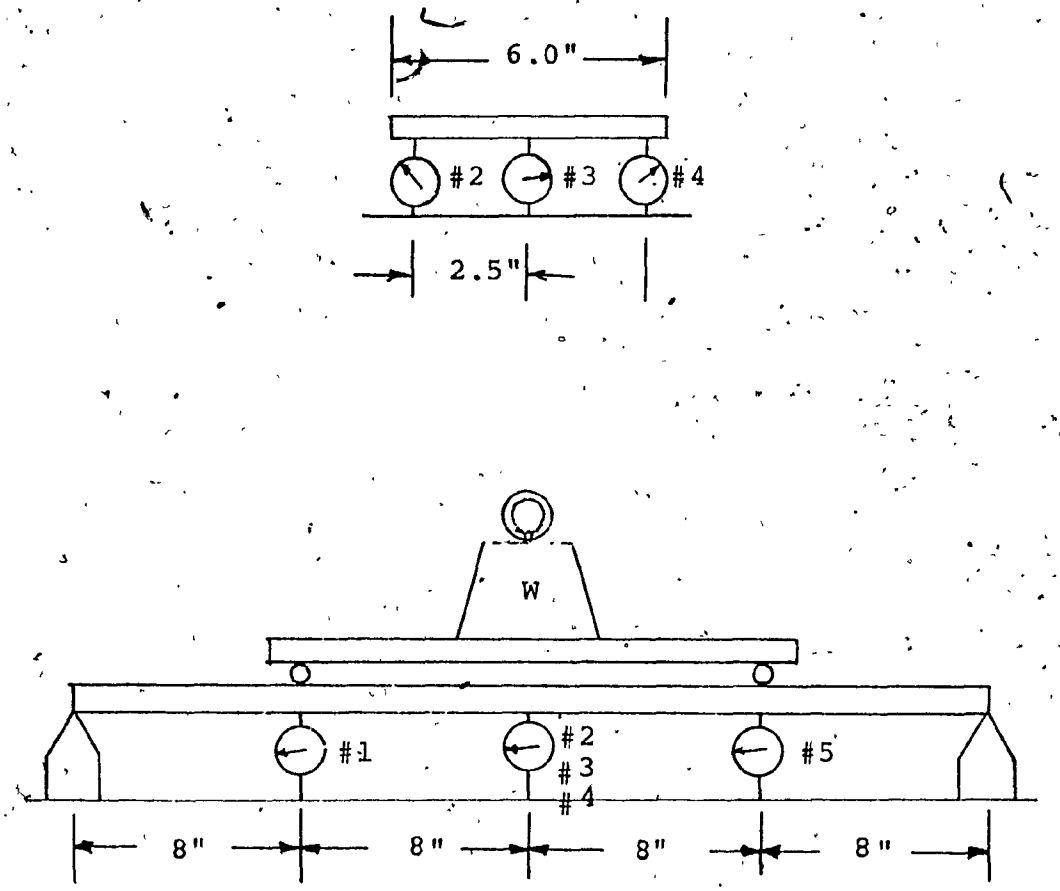


FIG. 5.4 THE SPECIMEN SHOWING THE METHOD OF LOADING AND THE POSITION OF THE DIAL GAUGES

TABLE 5.1 TEST RESULTS, DEFLECTION vs LOAD

| Load lb | Deflection inches at gauge No. | | | | |
|---|---|---|---|---|---|
| | #1 | #2 | #3 | #4 | #5 |
| 0 | 0 | 0 | 0 | 0 | 0 |
| 2.25 | .02 | .0275 | .0275 | .0275 | .007 |
| 3.25 | .046 | .064 | .064 | .064 | .03 |
| 3.25a | .047 | .067 | .067 | .067 | .032 |
| 4.25 | .074 | .100 | .100 | .099 | .054 |
| 5.25 | .105 | .138 | .138 | .137 | .082 |
| 6.25 | .155 | .207 | .207 | .205 | .130 |
| 6.75 | .178 | .237 | .240 | .237 | .152 |
| 6.75a | .185 | .248 | .246 | .245 | .160 |
| 7.25 | .210 | .278 | .282 | .277 | .181 |
| 7.75 | .232 | .308 | .312 | .307 | .204 |
| 7.75a | .240 | .318 | .320 | .318 | .210 |
| 8.25 | .262 | .345 | .350 | .347 | .230 |
| 8.75 | .307 | .397 | .399 | .396 | .262 |
| 8.75a | .317 | .406 | .409 | .406 | .268 |
| 9.25 | .338 | .431 | .435 | .431 | .294 |
| 9.25a | .343 | .443 | .448 | .443 | .296 |
| 9.75 | .370 | .471 | .476 | .471 | .310 |
| 9.75b | .373 | .476 | .480 | .476 | .320 |
| 10.25 | .395 | .504 | .508 | .504 | .340 |
| 10.75 | .427 | .541 | .547 | .541 | .364 |
| 10.75c | .432 | .547 | .552 | .547 | .368 |
| 11.25 | .448 | .570 | .577 | .572 | .382 |
| 11.65 | .484 | .605 | .610 | .605 | .403 |
| 11.65a | .490 | .610 | .613 | .610 | .406 |
| 12.65 | .550 | .683 | .689 | .681 | .455 |
| 12.65a | .560 | .696 | .700 | .693 | .462 |
| 13.65 | .603 | .750 | .759 | .751 | .504 |
| 14.65 | .643 | .790 | .823 | .793 | .534 |
| 15.65 | .663 | .840 | .869 | .840 | .574 |
| 15.65b | .695 | .853 | .887 | .849 | .584 |
| 16.65 | .748 | .910 | .944 | .911 | .624 |
| 17.65 | .823 | .985 | 1.027 | .986 | .684 |
| 17.65a | .836 | 1.016 | 1.051 | 1.017 | .694 |
| 18.65 | .883 | 1.073 | 1.113 | 1.074 | .744 |
| 19.65 | .933 | 1.139 | 1.179 | 1.144 | .796 |
| 19.65b | .945 | 1.170 | 1.193 | 1.164 | .804 |
| 21.65 | 1.045 | 1.268 | 1.319 | 1.281 | .894 |
| 21.65b | 1.053 | 1.280 | 1.339 | 1.301 | .906 |
| 24.15 | 1.111 | 1.400 | 1.463 | 1.419 | 1.009 |

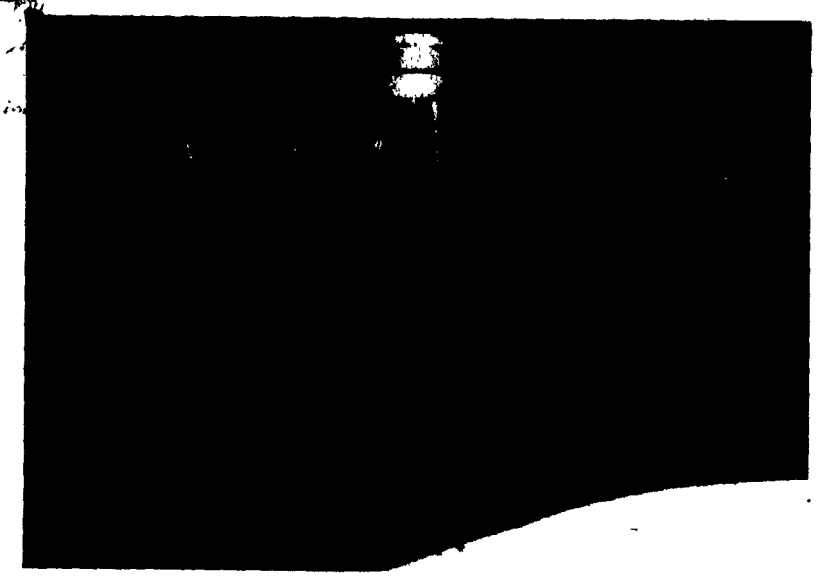

FIG. 5.5 SPECIMEN UNDER LOAD

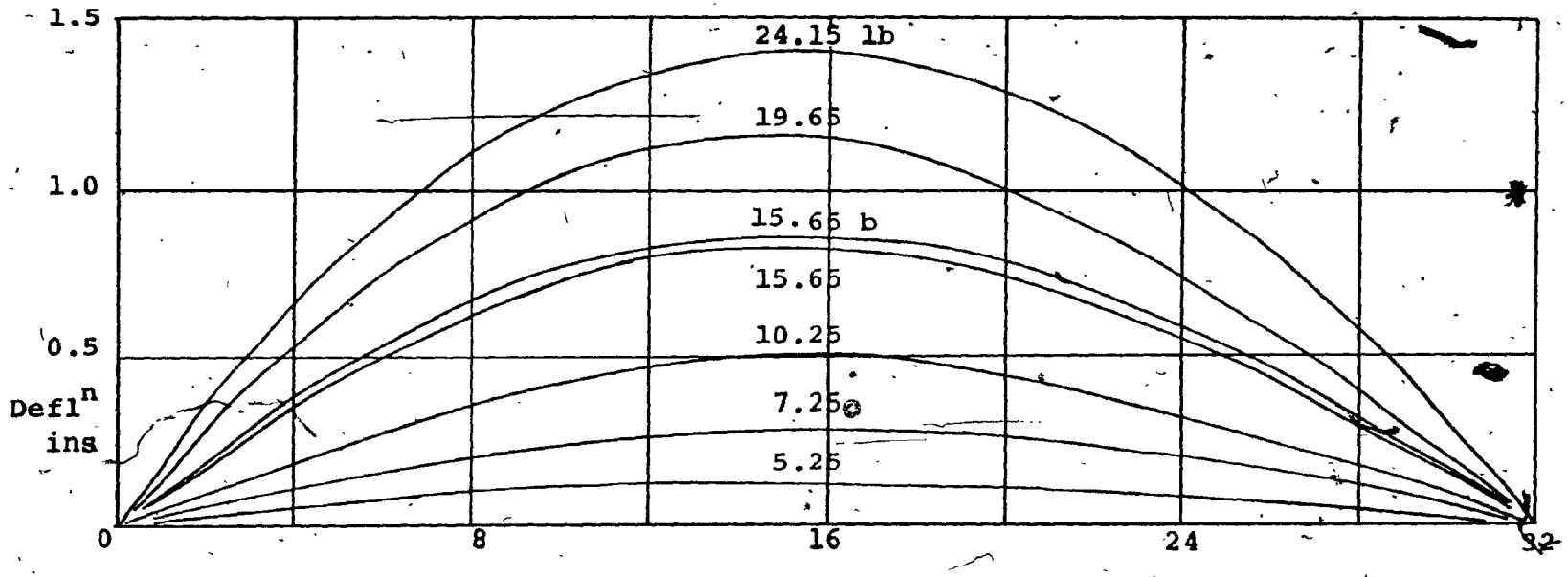


FIG. 5.6 DEFLECTION OF THE BENDING SPECIMEN

## 5.4 CURVATURE OF THE SPECIMEN

The radius of curvature of the loaded specimen may be obtained from the measured deflections by considering the circular arc passing through the points at which the dial gauges were located. The corresponding bending moment is given by the applied load and the geometry of the supports and loading points such that

$$\text{B.M.} = [\,4 \times \text{applied load}\,] \quad \text{lb in}$$

When the load of 24.15 lbs, which represented the maximum that could be applied by means of weights, had been reached and sustained, the loading was removed. The specimen returned to its original undeflected shape and revealed no signs of any cracking or other damage.

In order to determine the breaking strength of the beam, it was mounted in such a way that it could be loaded by the Tinius Olsen test machine. As a substantial deflection of the beam was anticipated, the support and loading points were moved to 7.5 in. centres with a mid-span length of 15.0 inches, (see Fig. 5.4), so that the specimen would not roll off the end supports. Dial gauges were omitted in this part of the test in order to avoid possible damage.

The load was applied in increments of 5 lbs, up to a total of 50 lbs, at which time, further attempts to load were marked by pronounced deflection and could not be maintained.

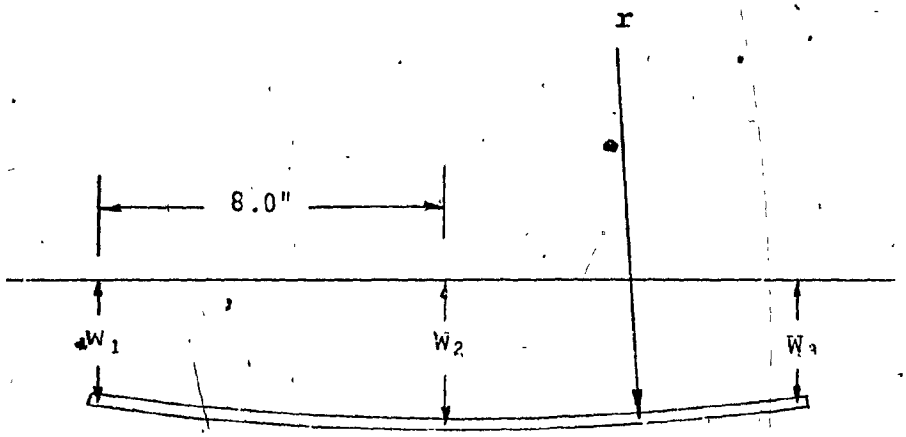


FIG. 5.7 RADIUS OF CURVATURE OF LOADED BEAM

TABLE 5.2 TRANSVERSE CURVATURE

| Load lb | B.M. lb/in | $w_m$ in | $2w_m - w_1 - w_3$ in | r in | transverse curvature $r_t$ in |
|---|---|---|---|---|---|
| 2.25 | 9. | .0275 | .028 | 2286 | |
| 3.25 | 13. | .064 | .052 | 1230 | |
| 4.25 | 17. | .0997 | .0713 | 897 | |
| 5.25 | 21. | .1375 | .088 | 727 | |
| 6.25 | 25. | .2063 | .1277 | 501 | |
| 6.75 | 27. | .238 | .146 | 438 | 1042 |
| 7.25 | 29. | .279 | .167 | 383 | 695 |
| 7.75 | 31. | .309 | .182 | 352 | 695 |
| 8.25 | 33. | .3473 | .2027 | 316 | 695 |
| 8.75 | 35. | .3973 | .2257 | 284 | 1041 |
| 9.25 | 37. | .4323 | .2327 | 275 | 625 |
| 9.75 | 39. | .4727 | .2653 | 241 | 625 |
| 10.25 | 41. | .5053 | .2757 | 232 | 781 |
| 10.75 | 43. | .543 | .295 | 217 | 521 |
| 11.25 | 45. | .573 | .315 | 202 | 480 |
| 12.65 | 50.6 | .684 | .3637 | 176 | 446 |
| 13.65 | 54.6 | .753 | .3997 | 160 | 386 |
| 14.65 | 58.6 | .802 | .427 | 150 | 99 |
| 15.65 | 62.6 | .8497 | .462 | 138 | 112 |
| 16.65 | 66.6 | .9217 | .4713 | 136 | 93 |
| 17.65 | 70.6 | .9993 | .4916 | 130 | 75 |
| 18.65 | 74.6 | 1.087 | .5463 | 117 | 79 |
| 19.65 | 78.6 | 1.154 | .579 | 110 | 83 |
| 21.65 | 86.6 | 1.289 | .6397 | 100 | 70 |
| 24.15 | 96.6 | 1.427 | .7346 | 87 | 58 |

The specimen was then removed and upon examination was found to contain hairline cracks on the tension face coincident with the transverse reinforcing wires. The specimen was then soaked in water, surface dried and strained to open the cracks. The resulting pattern is shown in Figure 5.8.

The ultimate bending moment sustained was:

$$M = \frac{50}{2} \times 7.5 = 187.5 \text{ lb ins}$$

Prior to the surface cracking which occurs at ultimate load, no cracking of a strained specimen could be observed when viewed through a microscope at 400x magnification.

## 5.5 INITIAL ANALYSIS

An initial analysis of the specimen may be accomplished by considering the central deflection of a homogeneous simply supported beam loaded symmetrically at two points, (see Fig. 5.9).

In this case

$$\delta = \frac{Pa}{24\ EI}(3L^2 - 4a^2)$$

and

$$EI\delta = 938.7P$$

The beam transverse moment of inertia

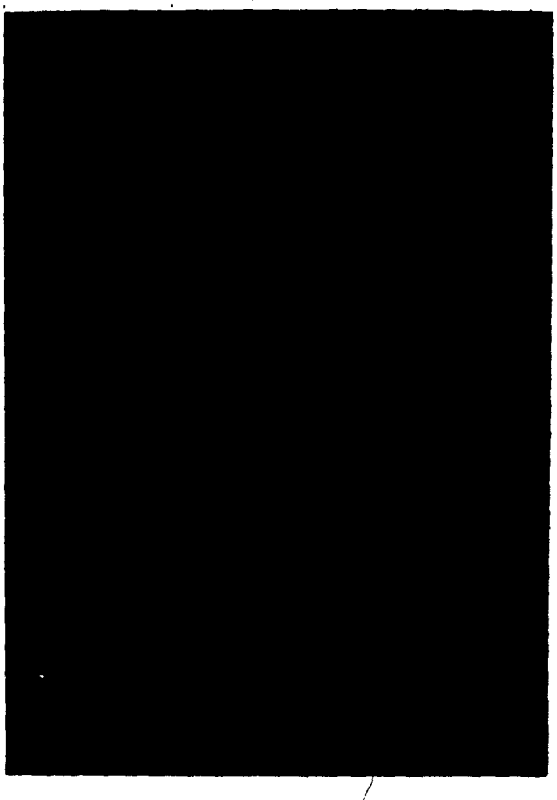

FIG. 5.8 THE CRACK PATTERN ON THE TENSION FACE OF THE BENDING SPECIMEN

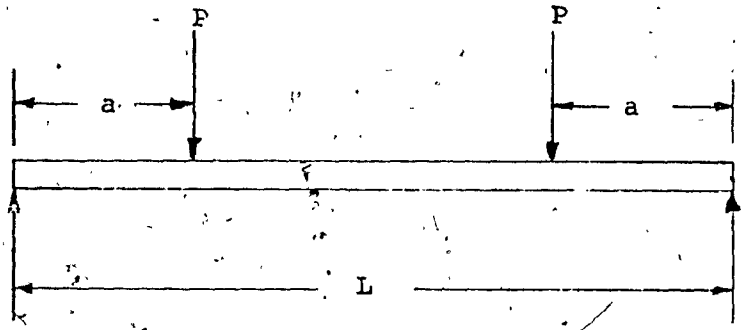


FIG. 5.9 SIMPLE BEAM DEFLECTION

$$I = \frac{6 \times .25^3}{12} = .0078125 \text{ in}^4$$

$$Z = \frac{.125}{.0078125} = 16 \text{ in}^3$$

The stress level at the extreme fibre of the equivalent homogeneous section is therefore given by

$$\sigma = 16 M$$

which, at the ultimate bending load represents

$$\sigma = 16 \times 187.5 = 3,000 \text{ psi}$$

Values of EI may be calculated for each load increment using classical theory and the specimen geometry. The mid-point deflection $\delta$, has been obtained experimentally and this, together with the value of the moment of inertia, I, obtained by considering the specimen to be homogeneous, allows an initial estimate to be made of the Elastic Modulus and of the extreme fibre stress level, $\sigma_{max}$. These values are shown in Table 5.3.

TABLE 5.3 INITIAL ESTIMATES OF ELASTIC MODULUS AND STRESS LEVEL

| Applied Load | $P_{lb}$ | $EI\delta$ | $\delta_{in}$ | $I\delta \times 10^{-3}$ | $E \times 10^{6}$ | $\sigma_{psi}$ |
|---|---|---|---|---|---|---|
| 2.25 | 1.125 | 1056 | .0275 | .2148 | 4.92 | 144 |
| 3.25 | 1.625 | 1525 | .064 | .5 | 3.05 | 208 |
| 4.25 | 2.125 | 1994 | .0997 | .779 | 2.56 | 272 |
| 5.25 | 2.625 | 2464 | .1375 | 1.074 | 2.29 | 336 |
| 6.25 | 3.125 | 2933 | .207 | 1.617 | 1.81 | 400 |
| 6.75 | 3.375 | 3168 | .238 | 1.86 | 1.71 | 432 |
| 7.75 | 3.875 | 3637 | .31 | 2.42 | 1.50 | 496 |
| 8.75 | 4.375 | 4106 | .397 | 3.10 | 1.32 | 560 |
| 9.75 | 4.875 | 4576 | .4727 | 3.69 | 1.24 | 624 |
| 10.75 | 5.375 | 5045 | .547 | 4.27 | 1.18 | 688 |
| 12.65 | 6.325 | 5937 | .684 | 5.34 | 1.11 | 810 |
| 14.65 | 7.325 | 6875 | .802 | 6.26 | 1.09 | 938 |
| 17.65 | 8.825 | 8284 | .9993 | 7.81 | 1.06 | 1130 |
| 19.65 | 9.825 | 9222 | 1.154 | 9.02 | 1.02 | 1258 |
| 24.15 | 12.07 | 11330 | 1.427 | 11.15 | 1.01 | 1546 |
| 50.0 | | | | | | 3000 |

## 5.6 LAMINA CONSTITUTIVE EQUATIONS AND THE GOVERNING DIFFERENTIAL EQUATIONS

Analysis of the bending specimen proceeds by considering the constitutive equations for lamina anisotropic materials which are shown on page 48.

$$\begin{bmatrix} N \\ \hline M \end{bmatrix} = \begin{bmatrix} A & | & B \\ \hline B & | & D \end{bmatrix} \begin{bmatrix} \varepsilon_0 \\ \hline \chi \end{bmatrix} \qquad (5.1)$$

solving equation (5.1) for the mid-plane strain yields

$$\varepsilon_0 = [A]^{-1} N - [A]^{-1}[B][\chi] \qquad (5.2)$$

Substituting Equation (5.2) back into (5.1) gives an expression for the bending moment in terms of direct load and rotation of the specimen cross-section.

$$M = [B][A]^{-1}[N] + (-[B][A^{-1}][B] + [D])[X]$$

or

$$M = [C^*][N] + [D^*][\chi] \qquad (5.3)$$

where $[C^*] = [B]\,[A^{-1}]$

and $[D^*] = [[D] - [B][A^{-1}][B]]$

Introducing the equations of equilibrium for a thin plate

$$\frac{\delta N_x}{\delta x} + \frac{\delta N_{xy}}{\delta y} = 0$$

$$\frac{\delta N_y}{\delta y} + \frac{\delta N_{xy}}{\delta x} = 0 \qquad (5.4)$$

$$\frac{\delta^2 M_x}{\delta x^2} + 2\frac{\delta^2 M_{xy}}{\delta x \delta y} + \frac{\delta^2 M_y}{\delta y^2} = -q_{(x,y)}$$

where $N_x$, $N_y$ and $N_{xy}$ are the stress resultants, $M_x$, $M_y$ and $M_{xy}$ are the moment resultants and $q_{(x,y)}$ is the distributed transverse load.

The equilibrium equations are satisfied identically by the Airy stress function $U$ such that

$$N_x = \frac{\partial^2 U}{\partial y^2}$$

$$N_y = \frac{\partial^2 U}{\partial x^2} \qquad (5.5)$$

$$N_{xy} = -\frac{\partial^2 U}{\partial x \partial y}$$

Hence

$$\begin{bmatrix} M_x \\ M_y \\ M_{xy} \end{bmatrix} = \begin{bmatrix} C^*_{11} & C^*_{12} & C^*_{16} \\ C^*_{21} & C^*_{22} & C^*_{26} \\ C^*_{61} & C^*_{62} & C^*_{66} \end{bmatrix} \begin{bmatrix} \frac{\partial^2 U}{\partial y^2} \\ \frac{\partial^2 U}{\partial x^2} \\ \frac{\partial^2 U}{\partial x \partial y} \end{bmatrix} + \begin{bmatrix} D^*_{11} & D^*_{12} & D^*_{16} \\ D^*_{21} & D^*_{22} & D^*_{26} \\ D^*_{61} & D^*_{62} & D^*_{66} \end{bmatrix} \begin{bmatrix} -\frac{\partial^2 w}{\partial x^2} \\ -\frac{\partial^2 w}{\partial y^2} \\ -2\frac{\partial^2 w}{\partial x \partial y} \end{bmatrix} \qquad (5.6)$$

Substituting Equation (5.6) into the equilibrium equation yields the governing equation for the bending of laminated plates.

$$C^*_{12}\frac{\partial^4 U}{\partial x^4} + (2C^*_{66} - C^*_{16})\frac{\partial^2 U}{\partial x^3 \partial y} + (C^*_{11} + C^*_{22} - 2C^*_{66})\frac{\partial^4 U}{\partial x^2 \partial y^2}$$

$$+ (2C^*_{61} - C^*_{26})\frac{\partial^4 U}{\partial x \partial y^3} + C^*_{21}\frac{\partial^4 U}{\partial y^4} - D^*_{11}\frac{\partial^4 w}{\partial x^4} - 4D^*_{16}\frac{\partial^4 w}{\partial x^3 \partial y} -$$

$$- 2(D^*_{12} - D^*_{66})\frac{\partial^4 w}{\partial x^2 \partial y^2} - 4D^*_{26}\frac{\partial^4 w}{\partial x \partial y^3} - D^*_{22}\frac{\partial^4 w}{\partial y^4} = -q_{x,y} \qquad (5.7)$$

Equation (5.7) contains two unknowns, the Airy stress function U, and the deflection w. In the case of a symmetrically reinforced specimen such as that under consideration, there is no coupling between bending and direct load. Consequently, $[B] = [0]$ and hence $[B^*] = [C^*] = [0]$ so that $[D^*] = [D]$, Equation (5.7) may then be reduced to:

$$D_{11}\frac{\partial^4 w}{\partial x^4} + 4D_{16}\frac{\partial^4 w}{\partial x^3 \partial y} + 2(D_{12} + 2D_{66})\frac{\partial^4 w}{\partial x^2 \partial y^2} +$$

$$+ 4D_{26}\frac{\partial^4 w}{\partial x \partial y^3} + D_{22}\frac{\partial^4 w}{\partial y^4} = q_{x,y} \qquad (5.8)$$

Reverting to Equation (5.6) and with $[C^*] = [0]$ yields.

$$\begin{bmatrix} M_x \\ M_y \\ M_{xy} \end{bmatrix} = \begin{bmatrix} D_{11} & D_{12} & D_{16} \\ D_{21} & D_{22} & D_{26} \\ D_{61} & D_{62} & D_{66} \end{bmatrix} \begin{bmatrix} -\frac{\partial^2 w}{\partial x^2} \\ -\frac{\partial^2 w}{\partial y^2} \\ -2\frac{\partial^2 w}{\partial x \partial y} \end{bmatrix} \qquad (5.9)$$

which may be further reduced for the specimen under consideration since $M_y = M_{xy} = 0$ and owing to the manner of supporting and loading the specimen torsional deflection was inhibited so that $2\frac{\partial^2 w}{\partial x \partial y} = 0$. The symmetrical manner in which the reinforcing layers were placed prevented coupling between bending and twist so that $D_{16} = D_{26} = D_{61} = D_{62} = 0$.

$$\begin{bmatrix} M_x \\ 0 \\ 0 \end{bmatrix} = \begin{bmatrix} D_{11} & D_{12} & 0 \\ D_{21} & D_{22} & 0 \\ 0 & 0 & D_{66} \end{bmatrix} \begin{bmatrix} \chi_1 \\ \chi_2 \\ 0 \end{bmatrix} \qquad (5.10)$$

## 5.7 MODULUS OF ELASTICITY

Now the longitudinal and transverse curvatures $\chi_1$ and $\chi_2$ at various values of bending moment $M_x$ have been obtained so that it is possible to evaluate the moduli of elasticity in bending at various loads.

Solving Equation (5.10) for $M_x$ yields

$$M_x = D_{11}\chi_1 + D_{12}\chi_2 \qquad (5.11)$$

But

$$D_{11} = \Sigma\, Z_i^2\, C_{11i}\, t_i b$$

and

$$D_{12} = \Sigma\, Z_i^2\, C_{12i}\, t_i b$$

so that

$$M_x = \Sigma\, Z_i^2\, t_i b \frac{E}{1-\nu^2}\chi_1 + \frac{\nu E}{1-\nu^2}\chi_2 \qquad (5.12)$$

where $b$ is the width of the specimen.

In this case

$$\nu = 0.13$$

so that

$$1 - \nu^2 = 0.9831$$

and

$$\frac{\nu}{1-\nu^2} = 0.1322$$

Values of radius of curvature which were measured on the test specimen and are presented in Table 5.2, are plotted in Fig. 5.10. The transverse curvature was measured over a shorter distance than the longitudinal curvature so that the smaller differences being measured made the resulting values more prone to scatter than in the case of the longitudinal curvature. A slippage of the curve was noticed after the

gauges had been reset and was corrected in the plot.

Putting Equation (5.12) in the form

$$\frac{M_x}{\frac{X_1}{1-\nu^2} + \frac{\nu X_2}{1-\nu^2}} = \Sigma\, Z_i^2\, t_i\, b\, E$$

enables the value of the elastic modulus E to be obtained in terms of the laminar section moment of inertia.

The bending section comprised four laminates so that the moment of inertia of the section may be obtained, (see Fig. 5.11).

$$I = \Sigma\, Z_i^2\, t_i\, b$$

$$= 2(.03125^2 + .09375^2).0625 \times 6.0$$

$$= 0.00732 \text{ in}^4$$

## 5.8 PREDICTED STRESS LEVELS USING LAMINA ANALYSIS

With the elastic constants determined, it is possible to calculate the stress level in each laminate using Equation (3.9), (see page 36).

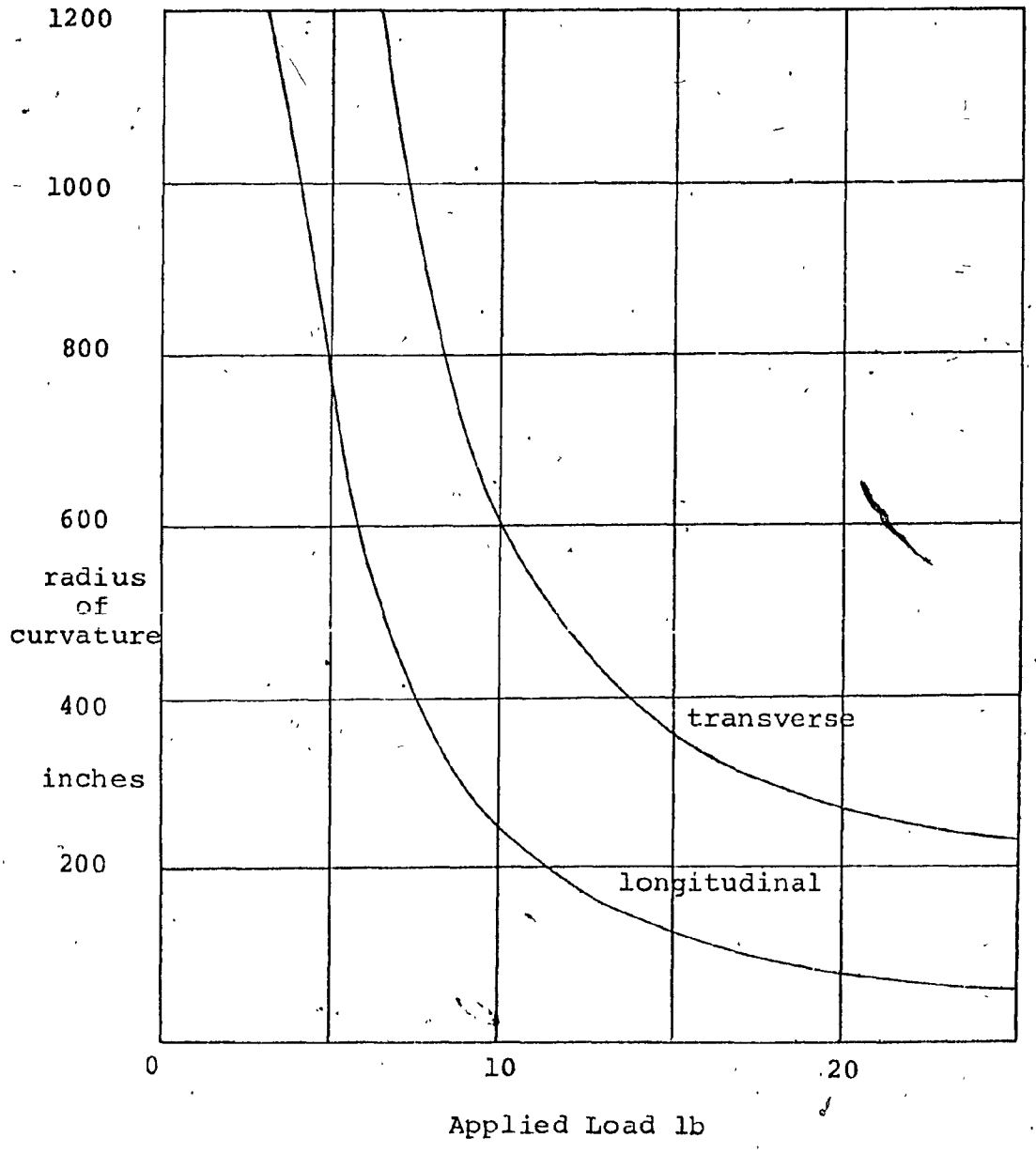


FIG. 5.10 LONGITUDINAL AND TRANSVERSE CURVATURE OF THE SPECIMEN UNDER LOAD

TABLE 5.4 - ELASTIC MODULUS OBTAINED FROM THE COMPOSITE SECTION

| Applied Load | B.M | $\chi_L \times 10^{-3}$ | $\chi_T \times 10^{-3}$ | $\frac{1}{1-\nu^2}\chi_L \times 10^{-3}$ | $\frac{\nu}{1-\nu^2}\chi_T \times 10^{-3}$ | $\Sigma\chi \times 10^{-3}$ | $\phi E \times 10^{-3}$ | $E \times 10^{-6}$ |
|---|---|---|---|---|---|---|---|---|
| 2.25 | 9 | .44 | 0 | .43 | 0 | .43 | 20.93 | 2.86 |
| 3.25 | 13 | .81 | 0 | .80 | 0 | .80 | 16.25 | 2.22 |
| 4.25 | 17 | 1.12 | 0 | 1.09 | 0 | 1.09 | 15.59 | 2.13 |
| 5.25 | 21 | 1.37 | 0 | 1.35 | 0 | 1.35 | 15.50 | 2.11 |
| 6.25 | 25 | 1.99 | 0 | 1.96 | 0 | 1.96 | 12.75 | 1.74 |
| 6.75 | 27 | 2.28 | .96 | 2.24 | .13 | 2.37 | 11.39 | 1.56 |
| 7.75 | 31 | 2.84 | 1.33 | 2.79 | .18 | 2.97 | 10.43 | 1.42 |
| 8.75 | 35 | 3.52 | 1.49 | 3.46 | .20 | 3.66 | 9.56 | 1.31 |
| 9.75 | 39 | 4.14 | 1.71 | 4.07 | .23 | 4.30 | 9.07 | 1.24 |
| 10.75 | 43 | 4.61 | 1.89 | 4.53 | .25 | 4.78 | 8.99 | 1.23 |
| 12.65 | 50.6 | 5.68 | 2.35 | 5.58 | .31 | 5.89 | 8.59 | 1.17 |
| 14.65 | 58.6 | 6.67 | 2.70 | 6.56 | .36 | 6.92 | 8.46 | 1.16 |
| 17.65 | 70.6 | 7.64 | 3.33 | 7.51 | .44 | 7.95 | 8.88 | 1.21 |
| 19.65 | 78.6 | 9.10 | 3.70 | 8.95 | .49 | 9.44 | 8.32 | 1.14 |
| 24.15 | 96.6 | 11.50 | 4.17 | 11.30 | .55 | 11.85 | 8.15 | 1.11 |

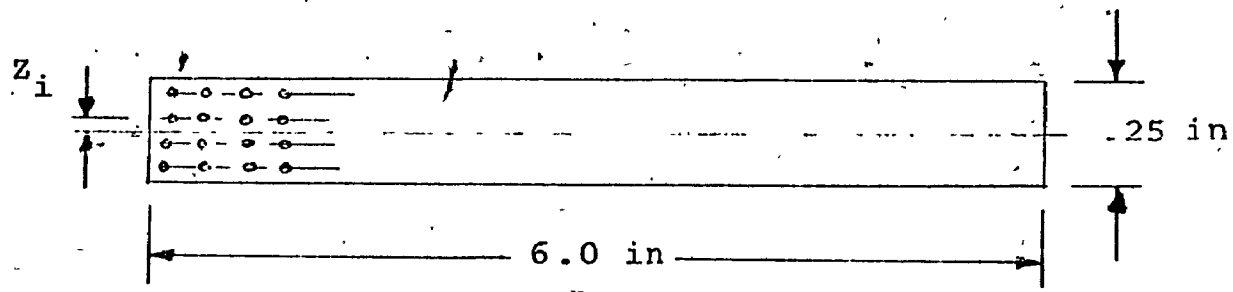


FIG. 5.11 BENDING CROSS-SECTION OF THE SPECIMEN

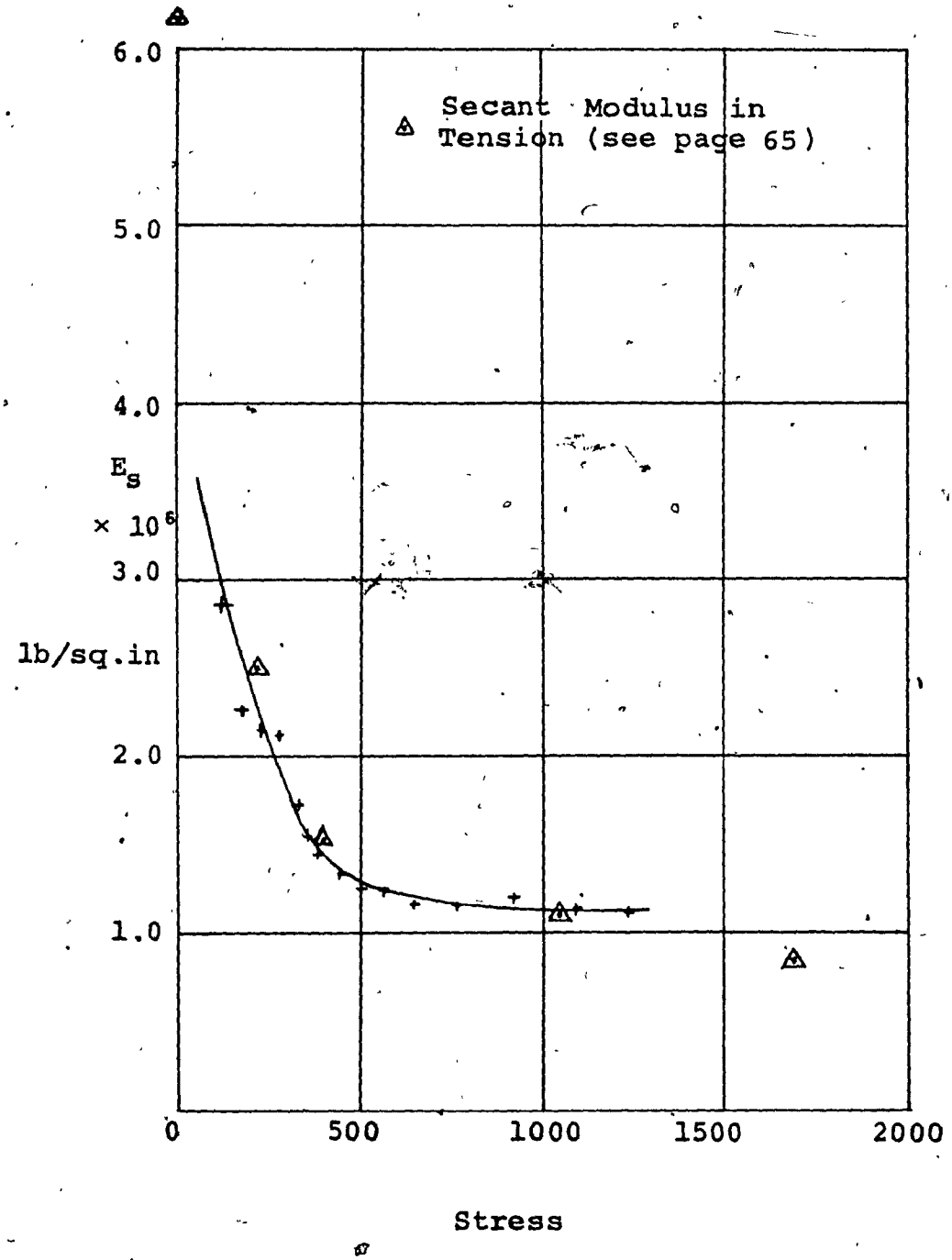


FIG. 5.12 SECANT MODULUS OF FERRO CEMENT IN BENDING

$$\begin{bmatrix} \sigma_x \\ \sigma_y \\ 0 \end{bmatrix} = \begin{bmatrix} C_{11} & C_{12} & 0 \\ C_{21} & C_{22} & 0 \\ 0 & 0 & C_{66} \end{bmatrix} \begin{bmatrix} \varepsilon_L \\ \varepsilon_T \\ 0 \end{bmatrix}$$

which, in this case, reduces to

$$\begin{bmatrix} \sigma_x \\ \sigma_y \end{bmatrix} = Z_i \begin{bmatrix} \frac{E}{1-\nu^2} & \frac{\nu E}{1-\nu^2} \\ \frac{\nu E}{1-\nu^2} & \frac{E}{1-\nu^2} \end{bmatrix} \begin{bmatrix} \chi_L \\ \chi_T \end{bmatrix}$$

so that

$$\sigma_x = Z_i \, E\left(\frac{\chi_L}{1-\nu^2} + \frac{\nu\chi_T}{1-\nu^2}\right)$$

The values of the elastic modulus, E, which are presented in Table 5.4, are used with the corresponding curvatures to establish the stress levels shown in Table 5.5.

The load carried by the outer laminate at failure may be calculated from the strength of its constituent material as was demonstrated in the case of the tensile specimen.

The total cross-sectional area of the laminate

$$A_{total} = .0625 \times 6 = 0.375 \text{ sq.in}$$

TABLE 5.5 STRESS LEVELS IN THE OUTER LAMINATE

| Applied Load lb | $\frac{\chi_L}{1-\nu^2}$ | $\frac{\nu\chi_T}{1-\nu^2}$ | E | $\Sigma\chi$ | $\sigma_x$ |
|---|---|---|---|---|---|
| 2.25 | .43 | 0 | 2.86 | .43 | 115 |
| 3.25 | .80 | 0 | 2.22 | .80 | 166 |
| 4.25 | 1.09 | 0 | 2.13 | 1.09 | 218 |
| 5.25 | 1.35 | 0 | 2.11 | 1.35 | 267 |
| 6.25 | 1.96 | 0 | 1.74 | 1.96 | 320 |
| 6.75 | 2.24 | .13 | 1.56 | 2.37 | 347 |
| 7.75 | 2.79 | .18 | 1.42 | 2.97 | 395 |
| 8.75 | 3.46 | .20 | 1.31 | 3.66 | 450 |
| 9.75 | 4.07 | .23 | 1.24 | 4.30 | 500 |
| 10.75 | 4.53 | .25 | 1.23 | 4.78 | 551 |
| 12.65 | 5.58 | .31 | 1.17 | 5.89 | 646 |
| 14.65 | 6.56 | .36 | 1.16 | 6.92 | 753 |
| 17.65 | 7.51 | .44 | 1.21 | 7.95 | 902 |
| 19.65 | 8.95 | .49 | 1.14 | 9.44 | 1008 |
| 24.15 | 11.30 | .55 | 1.11 | 11.85 | 1233 |

The wire cross-sectional area (see page 50) is

$$A_{wire} = .000471 \times 24 = 0.0113 \text{ sq.in}$$

Hence the area of the cement

$$A_{cement} = .375 - .0113 = 0.3637 \text{ sq.in}$$

The failing load of the lamina is given by the failing stress of the cement multiplied by the cement area added to the failing strength of the wires, so that

$$P_f = 600 \times .3637 + 24 \times 29.5$$
$$= 926 \text{ lb}$$

Consequently, the failing stress of the laminate

$$\sigma = \frac{926}{.375} = 2,469 \text{ psi}$$

and the yield stress is given by

$$\sigma = \frac{600 \times .3637 + 24 \times 26.4}{.375} = 2270 \text{ psi}$$

At this stress level, the strain is

$$\frac{2270}{1.1 \times 10^6} = .0021 \text{ in}$$

which is the yield strain of the wire.

The stress in the outer laminate at failure of the specimen may be approximated by ratioing the stress level of Table 5.5 in the proportion of the applied bending moments.

$$\sigma = 1233 \times \frac{187.5}{96.6} = 2393 \text{ psi}$$

which is comparable to the predicted values.

# CHAPTER 6

# FRACTURE TOUGHNESS OF FERRO CEMENT

# CHAPTER 6

# FRACTURE TOUGHNESS OF FERRO CEMENT

## 6.1 CRACK PROPAGATION

It has been postulated that cracking of the cement matrix in ferro cement is inhibited by the presence of fine wire reinforcing which serves to reduce the stress concentrations at the tips of the natural flaws in the material to below the critical value for crack propagation. In order to determine the spacing of the wire reinforcing necessary to produce ferro cement rather than reinforced concrete experiments were conducted to determine the size of these stress concentration areas, or intense energy zones surrounding the flaws.

Concrete is a very complex multi-phase material comprising aggregates and cement paste. Hardened cement paste comprises cement gel, hydrated cement particles and capillary pores. Cement gel consists of gel particles, gel pores and non-colloidal crystals. The average size of the gel pores has been estimated at 18 Å which is approximately five times the diameter of a water molecule. [26] The capillary pores form an interconnecting network throughout the cement, which at the optimum water/cement ratio will be completely filled with gel. At other than optimum ratios, a network of voids will be left throughout the cement, of varying size and

shape, but an order of magnitude larger than the gel pores.[27] It is these gel and capillary pores, as well as grains of unhydrated cement present in the cured cement matrix which form the natural flaws or crack nuclei.

Griffith [28] proposed that an existing crack would propagate if this resulted in a lowering of the total energy of the system. Accordingly, crack growth under plane stress conditions will occur if

$$\frac{d}{da}\left( - \frac{\sigma^2 \pi a^2}{E} + 4aT\right) = 0 \qquad (6.1)$$

Where the first term in the bracket represents the elastic energy loss of a plate of unit thickness under a stress $\sigma$ measured far away from the crack, if a crack of length 2a were suddenly cut into the plate at right-angles to the direction of the stress. The second term represents the energy gain of the plate due to the creation of a new surface having a surface tension T. [29] The principal argument against accepting this proposal is the difficulty of evaluating T, the surface tension, which figures prominently in the equation.

Both Irwin [30] and Orowan [31] pointed out that the Griffith type energy balance must be between the strain energy stored in the specimen and the surface energy plus the work done in plastic deformation. Irwin also pointed out

that the energy approach is equivalent to a stress intensity approach according to which fracture occurs when a critical stress distribution, characteristic of the material, is reached. Since the linear theory of elasticity provides unique and single valued relationships among stress, strain and energy, it follows that a fracture criterion expressed in terms of an energy concept has its equivalent stress criterion.

The critical stress at which fracture will occur can be obtained by differentiating Equation (6.1) to determine the instability condition, thus

$$\frac{2\sigma^2 \pi a}{E} + 4T = 0$$

$$\sigma_{crit} = \sqrt{2ET/\pi a} \qquad (6.2)$$

or

$$\sigma\sqrt{a} = \text{constant} - \text{psi } \sqrt{\text{in}}$$

If a term representing the plastic work done at the tip of the crack, 'p', is added to the surface tension T, then the constant term takes the form

$$K = \sqrt{2E(T + P)/\pi} \qquad (6.3)$$

or

$$K = \sigma\sqrt{\pi a} = \sqrt{2E(T+P)}$$

where K is the stress intensity factor. Fracture of the material will occur when K is equal to a limiting value $K_c$. This value $K_c$, is the fracture toughness of the material and is one of the basic physical properties of a material.

## 6.2 METHOD OF TESTING

In order to examine the effect of wire reinforcing on the fracture toughness of the cement matrix tests were carried out on samples of ferro cement using the method of Waddoups. [32] This makes use of the first mode fracture toughness equation

$$K_1 = \sigma\sqrt{\pi a} \qquad (6.4)$$

in this case the half crack width, a, represents the intense energy region at the tip of a natural crack or flaw.

Now, if a crack of length 2L is introduced into a specimen, this crack will, when loaded, have at its tip an intense energy region, a. The equivalent crack length will then be (L + a).

Thus

$$K_1 = \sigma\sqrt{\pi(L + a)} \qquad (6.5)$$

The procedure for determining $K_{1c}$ is to test two similar specimens, one with a crack and the other without.

The stress on the uncracked specimen at failure [33]

$$\sigma_0 = \frac{K_{1c}}{\sqrt{\pi a}} \qquad (6.6)$$

and on the cracked specimen

$$\sigma_c = \frac{K_{1c}}{\sqrt{\pi(L+a)}} \qquad (6.7)$$

hence

$$\frac{\sigma_0}{\sigma_c} = \sqrt{L+a/a} = \sqrt{L/a + 1}$$

and

$$a = \frac{L}{(\frac{\sigma_0}{\sigma_c})^2 - 1}$$

So that knowing $\sigma_0$, $\sigma_c$, and $L$ from the test specimen results the characteristic dimension of the intense energy region, a, may be calculated. This value of a may be substituted into Equation (6.6) to obtain the value of the fracture toughness $K_{1c}$ psi $\sqrt{in.}$

## 6.3 EVALUATION OF FRACTURE TOUGHNESS

In order to evaluate the fracture toughness, $K_{1c}$, of ferro cement specimens were made to the dimensions shown in Fig. 6.2. Each was 1/4 inch thick and contained one, two or three layers of 1/4 in. mesh reinforcing wire with a mortar made from one part of ordinary Portland cement to one-and-a-

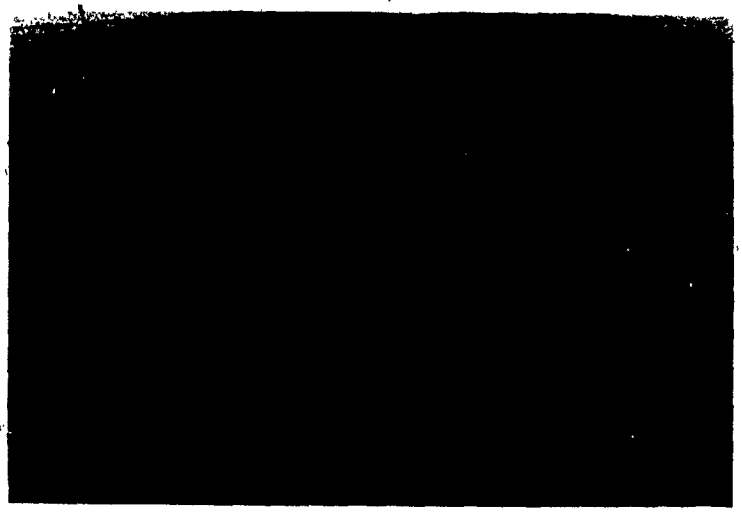

FIG.6.1 FRACTURE TOUGHNESS SPECIMENS. A CRACK HAS BEEN INTRODUCED INTO THE LEFT-HAND SPECIMEN WHEREAS THE RIGHT-HAND SPECIMEN IS UNCRACKED

half parts of sand by weight with a water cement ratio of 0.4.

Unreinforced specimens were also tested, as well as a specimen in which the cement was reinforced by the addition of chopped polypropylene fibres oriented in a random fashion.

The ends of the specimens which were to be gripped in the Tinius Olsen test machine were reinforced with fiberglas cloth. Polyester resin was used initially as the bonding agent but it was found that the resin would not harden in contact with the cement but remained sticky and allowed the fiberglas cloth to slip. In subsequent specimens, a water soluble plastic resin glue was used to effect this bond.

The tests were carried out by first loading an uncut specimen incrementally to its breaking point using an extensometer to record the stress-strain diagram. A second specimen incorporating a simulated crack was then tested to ultimate load at which time the crack progressed across the width of the specimen. The cross-sectional area of each specimen was a half square inch so that values of $\sigma_0$ and $\sigma_c$ could be obtained, and hence $K_{1c}$. The results of these tests are summarized in Table 6.1.

It will be noted that the intense energy region, a, decreases with increasing reinforcement and also that the addition of polypropylene fibre has little effect on the physical properties of the cement.

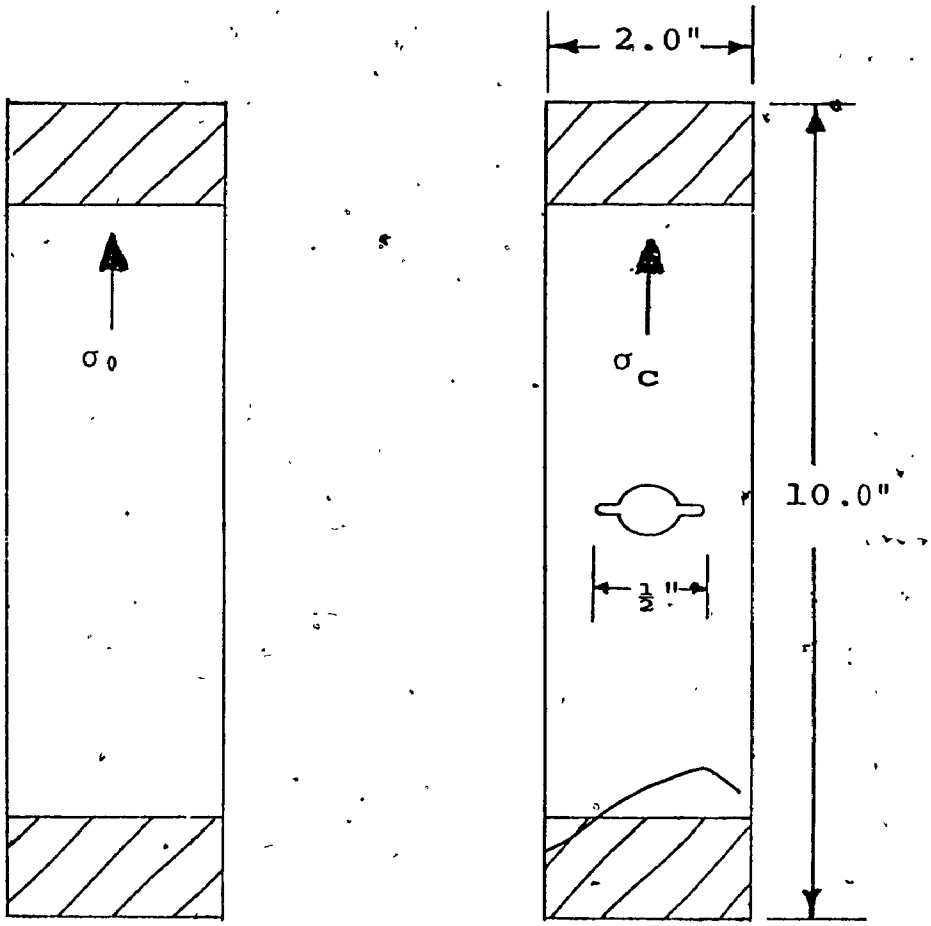


FIG. 6.2 DIMENSIONS OF THE TEST SPECIMENS

TABLE 6.1 THE FRACTURE TOUGHNESS OF FERRO CEMENT

| Laminates | Breaking Load | | $\sigma_0$ | $\sigma_c$ | a | $K_{1c}$ |
|---|---|---|---|---|---|---|
| | No Hole | Hole | | | | |
| 3 | 903 | 677 | 1870 | 1358 | 0.324 | 1823 |
| 2 | 669 | 510 | 1338 | 1020 | 0.347 | 1065 |
| 1 | 434 | 337 | 869 | 674 | 0.377 | 946 |
| Cement | 200 | 160 | 400 | 320 | 0.446 | 473 |
| Fibre | 185 | 140 | 370 | 280 | 0.35 | 380 |

The stress-strain curves for the test specimens which were recorded by the extensiometer are shown in Fig. 6.3. The unreinforced specimen exhibited a very small extension at failure and a relationship which appeared almost linear since the extensometer was not sufficiently sensitive in this load range. The specimen with one layer of reinforcing initially followed a line similar to the unreinforced specimen but showed a pronounced nonlinearity at a stress level just beyond the breaking strength of pure cement. Specimens with two or three layers of reinforcing show a pronounced curve throughout the loading regime.

In order to assess the fracture toughness of ferro cement when the reinforcing wire is laid diagonally to the loading line, a series of specimens was made. The first simulated the lay-up examined in the tensile specimen comprising a central layer parallel to the load line and each outer layer at 45°, (see page 50). Other specimens had two and three layers of 1/4 in. mesh, respectively.

The final specimen contained four layers of half-inch hexagonal mesh chicken wire. The results of these tests are summarized in Table 6.2.

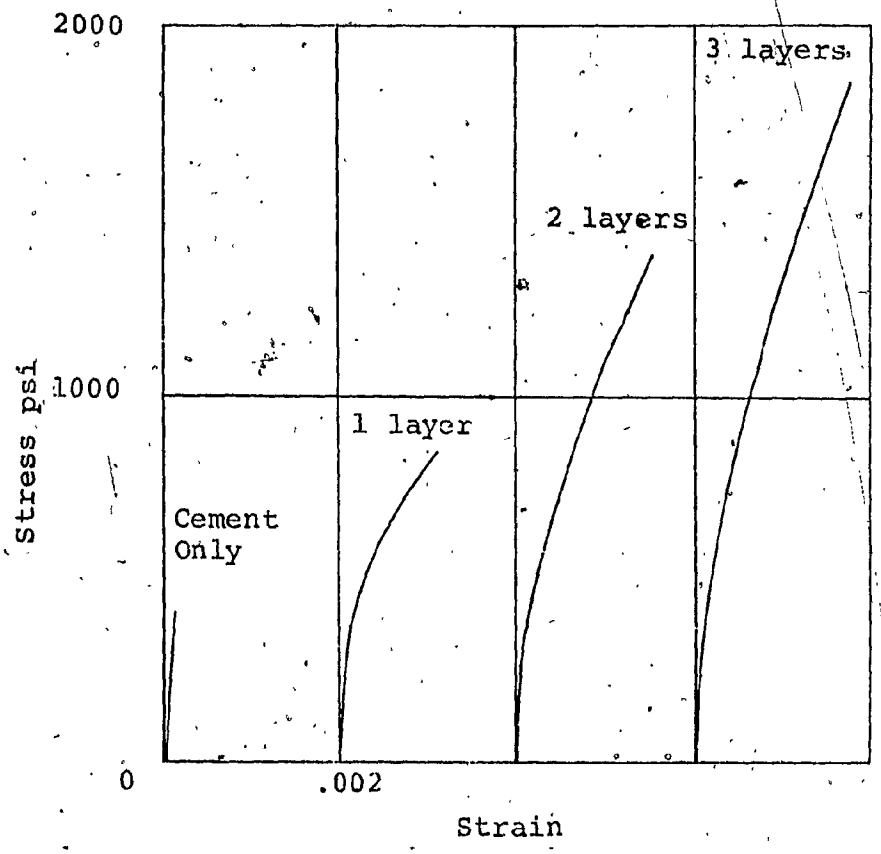


FIG. 6.3 STRESS STRAIN CURVES FOR VARIOUS REINFORCING

TABLE 6.2 FRACTURE TOUGHNESS OF FERRO CEMENT WITH DIAGONAL REINFORCING

| Laminates | Breaking Load | | $\sigma_0$ | $\sigma_c$ | a | $K_{1c}$ |
|---|---|---|---|---|---|---|
| | No Hole | Hole | | | | |
| 45,0,45 | 780 | 570 | 1560 | 1140 | .35 | 1640 |
| 45,45,45 | 620 | 487 | 1240 | 974 | .38 | 1350 |
| 45,45 | 375 | 295 | 750 | 590 | .41 | 850 |
| Hexagonal | 280 | 225 | 560 | 450 | .45 | 660 |

## 6.4 REINFORCING WIRE SPACING

The feature which distinguishes ferro cement is the ability of the cement matrix to follow the strain of the reinforcing wire without cracking. In order for this to happen it is necessary for these wires to traverse the intense energy regions at the tips of the natural flaws in the cement and reduce the stress level there, below the critical value.

It is therefore postulated that the spacing between the reinforcing wire should not exceed (a), the dimension of this region at each end of the flaw. This dimension is in the region of 0.6 to 0.8 inches, so that a half inch square mesh wire fabric would represent a prime choice of reinforcement for many applications.

# CHAPTER 7

# CONSTRUCTION OF FERRO CEMENT CANOES

# CHAPTER 7

# CONSTRUCTION OF FERRO CEMENT CANOES

## 7.1 THE CONCRETE CANOE RACE

During the course of the investigation which forms the subject of this thesis, an opportunity arose to provide a practical demonstration of a thin shell structure made from ferro cement. This occurred when the Department of Civil Engineering agreed to sponsor an entry into the first Canadian Concrete Canoe Race, organized by the University of Toronto, in accordance with the rules laid down by the American Concrete Institute. [34]

A canoe had been selected as a demonstrational vehicle since it requires to be both light and strong in order to function. Failure to achieve either objective would result in an unseaworthy and hence unsuccessful craft.

The exact location of the race and the weather and water conditions to be anticipated were not known at the time the canoes were being designed. It was therefore decided to make two craft. One of these would have rounded sections for a minimum wetted surface, whereas the other would have flatter sections for stability. They are referred to as 'canoe 1' and 'canoe 2', respectively, and their lines are shown in Figures 7.1, 7.2, and 7.3.

The structure and proportions of the canoes were then established in accordance with the principles described in the preceding Chapters.

## 7.2 THE REINFORCING MESH

The canoes were designed to be made from three laminates of quarter-inch mesh, welded steel wire fabric, having a wire diameter of .025 inch. The inner and outer laminates were placed diagonally over the canoe and the central laminate was parallel to the fore and aft line, but extending to within two feet of each end only. A single 3/16 in. diameter rod was used to reinforce each gunwale and the keel. Three layers of mesh were selected as this was considered to be the minimum which would retain the wet cement paste during construction.

## 7.3 DESIGN STRESS LEVELS

In order to check the strength of the canoes in bending, the cross-section area and moments of inertia at each section were obtained by summing the properties of the elements comprising the section, (see Fig. 7.4).

$$I_{xx} = A_i \, Y^2_{\text{mean } i} + \frac{t \, L \, D^2}{12}$$

$$I_{yy} \pm A_i \, X^2_{\text{mean } i} + \frac{t \, L \, C^2}{12}$$

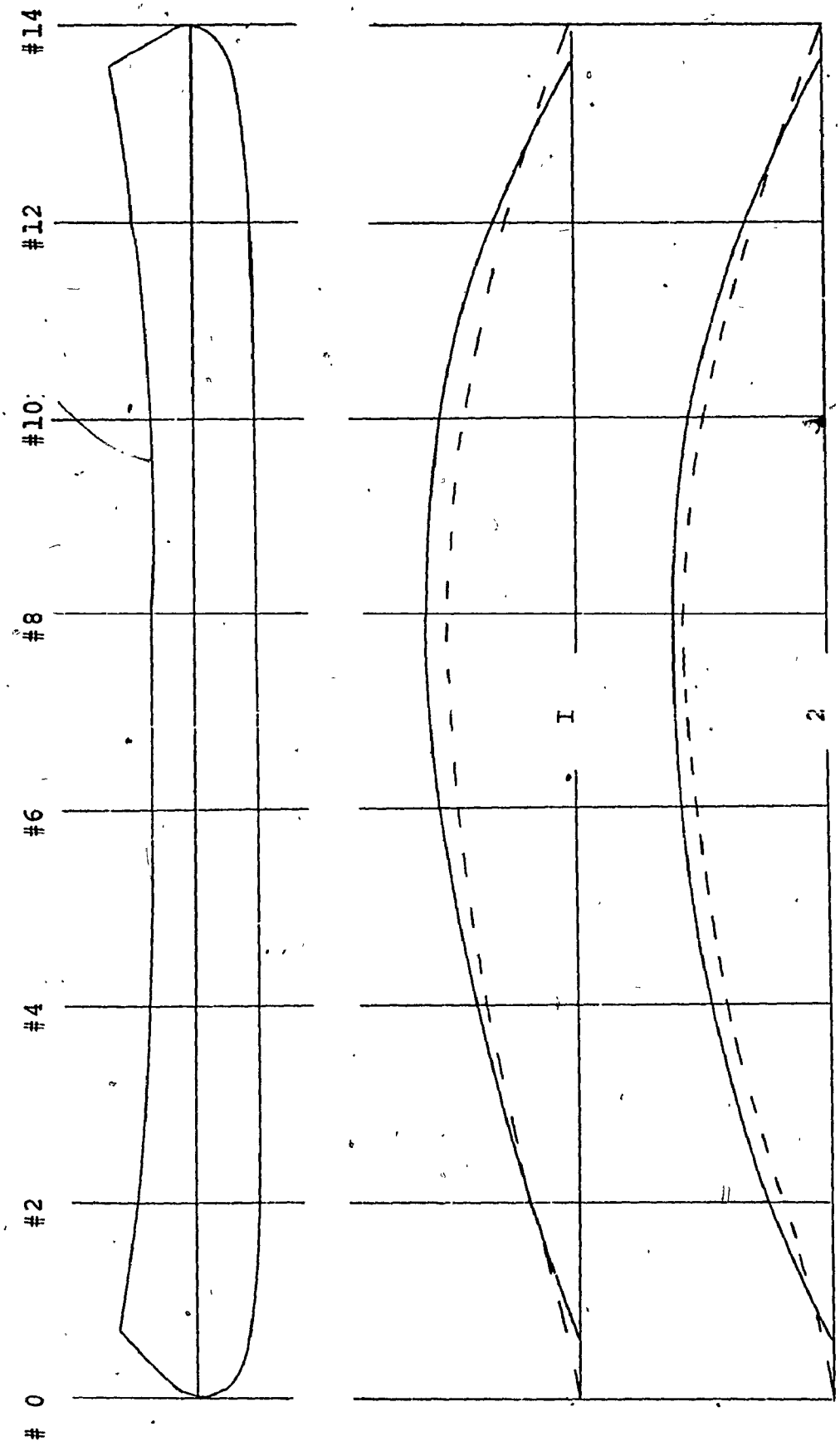


FIG. 7.1 PROFILE AND WATER LINES

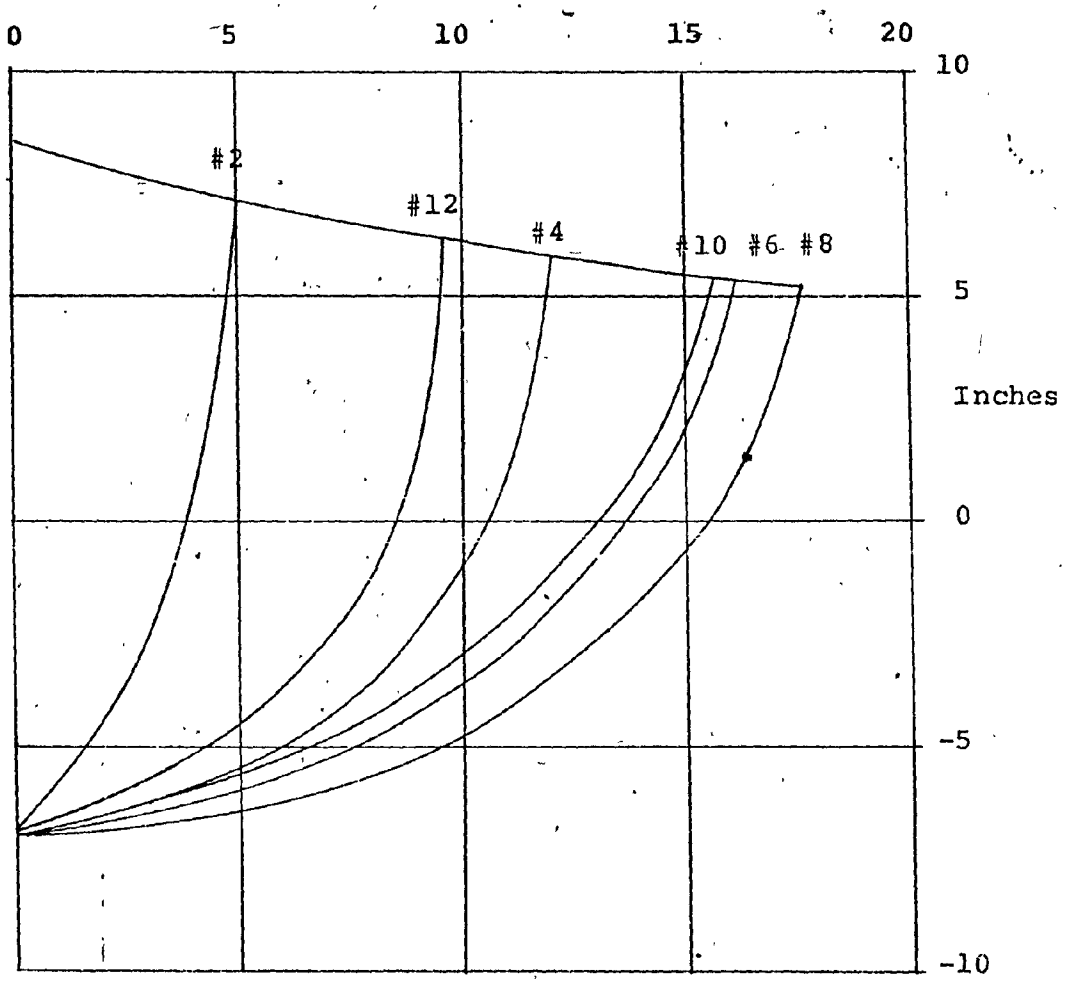


FIG. 7.2 LINES OF CANOE NO. 1, TO SCALE

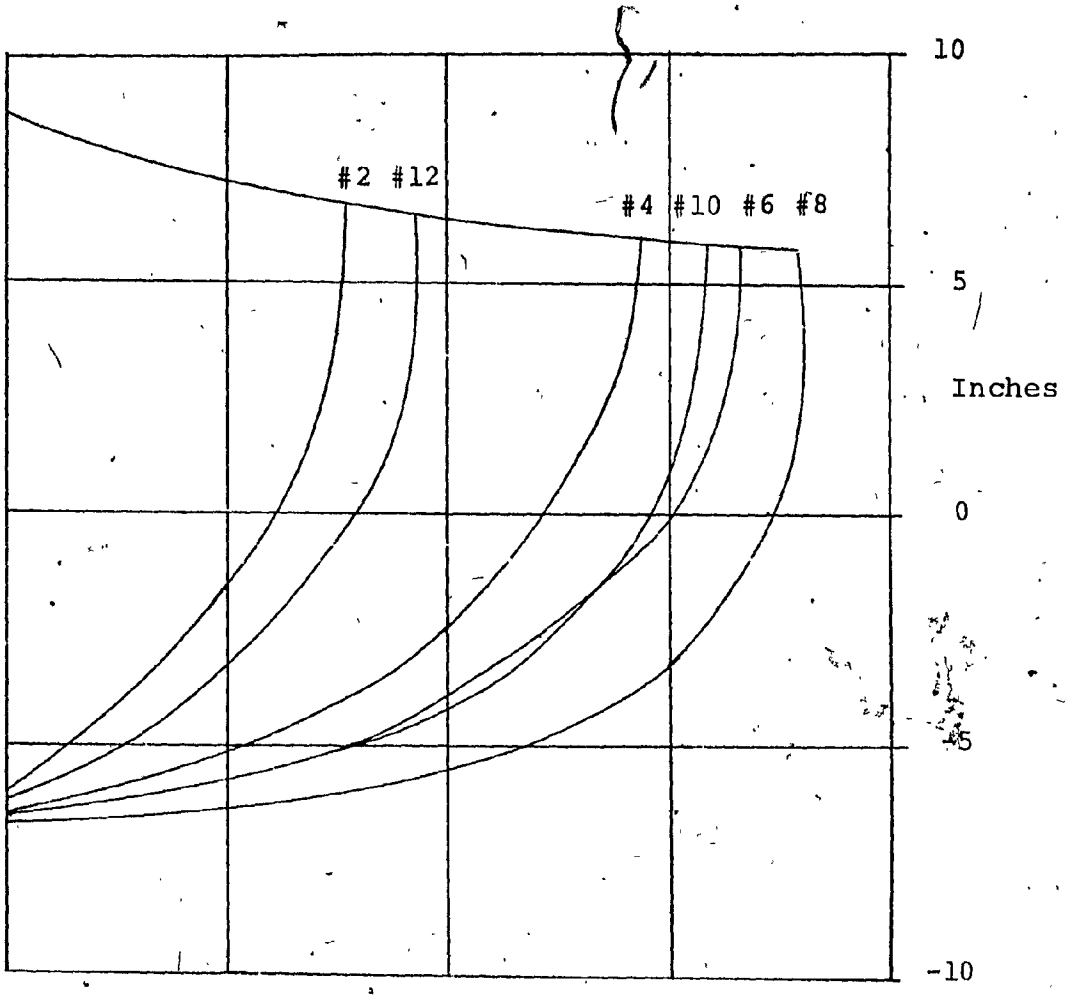


FIG. 7.3 LINES OF CANOE NO. 2, TO SCALE

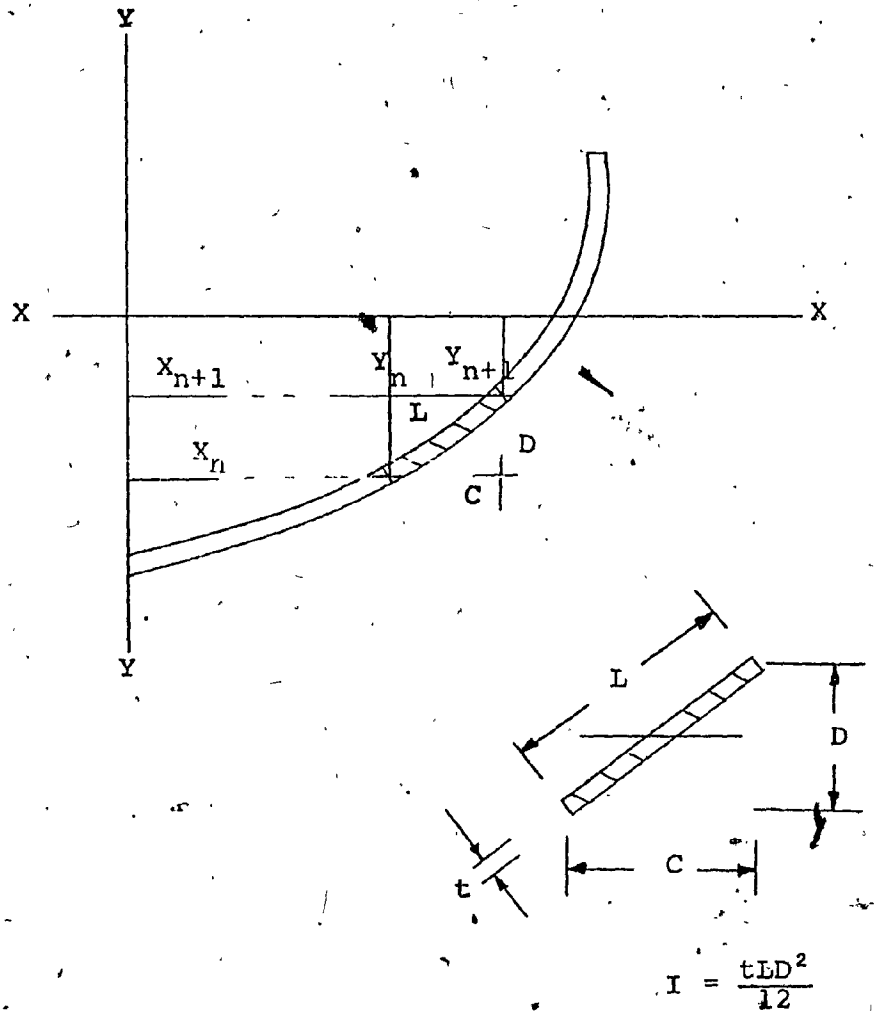


FIG. 7.4 MOMENTS OF INERTIA OF THE CANOE SECTIONS

This method has been programmed and a listing is presented in Appendix A. The geometric input data for the program is shown in Figures 7.2 and 7.3, and values of the cross-sectional area and the moments of inertia are presented in Fig. 7.5.

The structural design case was found to arise in handling the canoe out of the water when point loads were applied rather than the continuous supporting load provided by the water when the canoe was afloat. With a canoe weight of 200 lbs and a support provided at each end of the 14 ft length, the maximum bending moment occurring at the centre was:

$$M_{max} = \frac{200 \times 168}{8} = 4,200 \text{ lb.in.}$$

and the maximum stress

$$max = \frac{4,200 \times 7.6}{240} = 133 \text{ psi}$$

Allowing a factor of safety of 3.0 gives an ultimate stress level of 400 psi, so that the canoes had ample reserve strength.

## 7.4 METHOD OF CONSTRUCTION

The canoes were constructed on wooden molds which were made by first drawing the lines of the canoes to full-scale and obtaining the required cross-sections at two-foot intervals

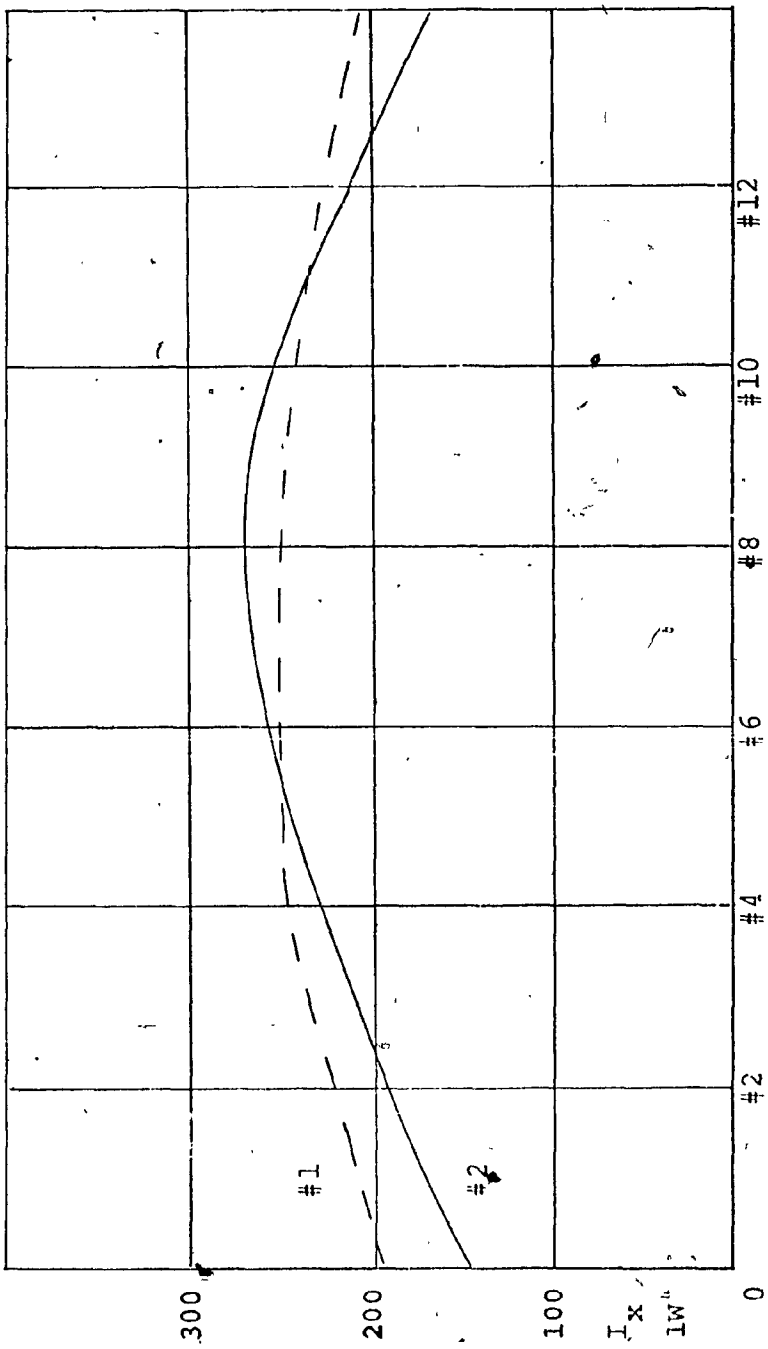


FIG. 7.5 MOMENTS OF INERTIA OF THE CANOES

along the hull. These sections were then cut out of half-inch plywood and mounted on a piece of 4 × 2 in. lumber at the correct locations.

With the cross-sections and stem and stern profiles in place, a series of 1 × 1/2 in. lathes were positioned longitudinally to give the required inside shape of the canoe. Strips of mesh were laid diagonally across the wooden mold to form the first layer of reinforcing. The longitudinal layer was laid next, followed by a third and final layer which was laid with the length of the wire mesh on the opposite diagonal to the first layer.

The 3/16 in. diameter bars forming the keel and the gunwales were installed next and the whole reinforcement was wired together and faired to the required canoe shape. At this stage of construction, particular attention must be paid to the wiring together of the laminates in order to prevent them from parting as the cement mortar is applied. If they should open out an excessive amount of mortar will lodge between them causing an overweight structure. The finishing reinforcing on the wooden mold is shown in Fig. 7.6.

The mortar mix comprised one part of ordinary Portland cement to one-and-a-half parts of sand by weight, with a water/cement ratio of 0.4. In order to place the cement mortar in the mesh, the lathes forming the mold were cut away between the plywood sections, thus exposing the inside of

the mesh reinforcing. The mortar was then forced through the mesh from the inside of the canoe to the outside. All excess mortar was removed and the outside surface was smoothed to a high surface finish (Fig. 7.7).

The schedule for building the canoes was such that there was insufficient time to allow a conventional twenty-eight day cure. The cement was therefore steam cured by enveloping the canoes in a polyethylene tent and introducing steam which was generated, using an automobile steam-cleaning machine. By this, means a cure was effected in two days.

After the cement had cured, the remainder of the mold was removed from the canoes and a block of styrofoam was positioned inside the canoe at the bow and stern, and secured in place. This was sufficient to provide positive buoyancy, even when the canoe was filled with water, so that it was unsinkable. [35]

FIG. 7.6 A FINISHED REINFORCING ON THE WOODEN MOLD

FIG.7.7 A CANOE WITH THE CEMENT MORTAR IN PLACE

FIG. 7.8 A CANOE IN THE WATER PRIOR TO A RACE

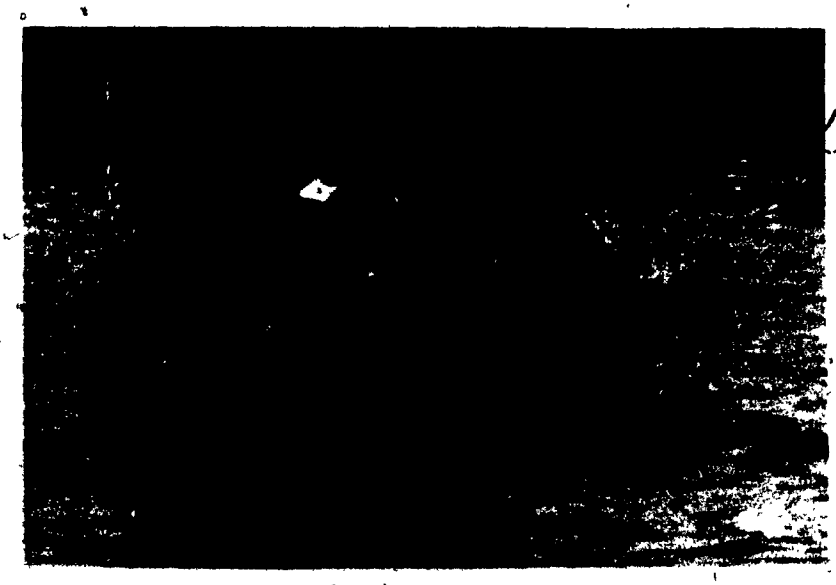

FIG. 7.9 A CANOE DURING A RACE

# CHAPTER 8

# HYDRODYNAMIC CHARACTERISTICS OF THE CANOES

# CHAPTER 8

# HYDRODYNAMIC CHARACTERISTICS OF THE CANOES

## 8.1 GENERAL

The canoe race was held over a triangular course six hundred yards long. Twenty crews participated in a series of heats and a final race in which the Sir George Williams entries finished fifth and sixth, respectively. In order to appraise the performance of the canoes and find ways of improving the designs, an analysis of their hydrodynamic characteristics was undertaken. The nature and causes of the resistances to be overcome have been assessed, as well as the magnitude of the power available to overcome them, and are presented in this Chapter. Towing tests have been carried out to determine the drag of a canoe experimentally and a stability curve is presented.

The lines of the canoes are shown in Figs. 7.1,7.2, and 7.3.

## 8.2 BUOYANCY

The position of the loaded water-line is found by obtaining the areas of the immersed portion of the cross-sections for varying depth of immersion. These areas are subsequently plotted against water-line length to obtain the displaced volume. Multiplying the displaced volume by the

density of water yields the curve of loaded weight vs depth of immersion.

The cross-sectional areas listed in Tables 8.1 and 8.2, are plotted against water-line length in Fig. 8.2. The areas under these curves were integrated by means of a planimeter, and when multiplied by the scale factor, yield the displacement for each depth of immersion.

$$\text{Scale Factor} \quad 1 \text{ sq in} = \frac{40 \times 24}{1728} \times 62.4 = 34.67 \text{ lbs}$$

The canoes were weighed in the finished condition prior to shipment to Toronto. Canoe 1 weighed 220 lbs and Canoe 2, 240 lbs. The estimated weight of the crew was 170 lbs each man, so that the all-up weight for each canoe was:

| | | | |
|---|---|---|---|
| Canoe 1 | 560 lbs | Depth of immersion | 7.25 in. |
| Canoe 2 | 580 lbs | Depth of immersion | 6.5 in |

## 8.3 WETTED SURFACE

The wetted surface, or area of the canoe hull which is in contact with the water, is obtained by measuring the perimeter of the sections, plotting them against water-line length and integrating. The perimeter lengths for both canoes are listed in Table 8.4 and plotted in Fig. 8.4.

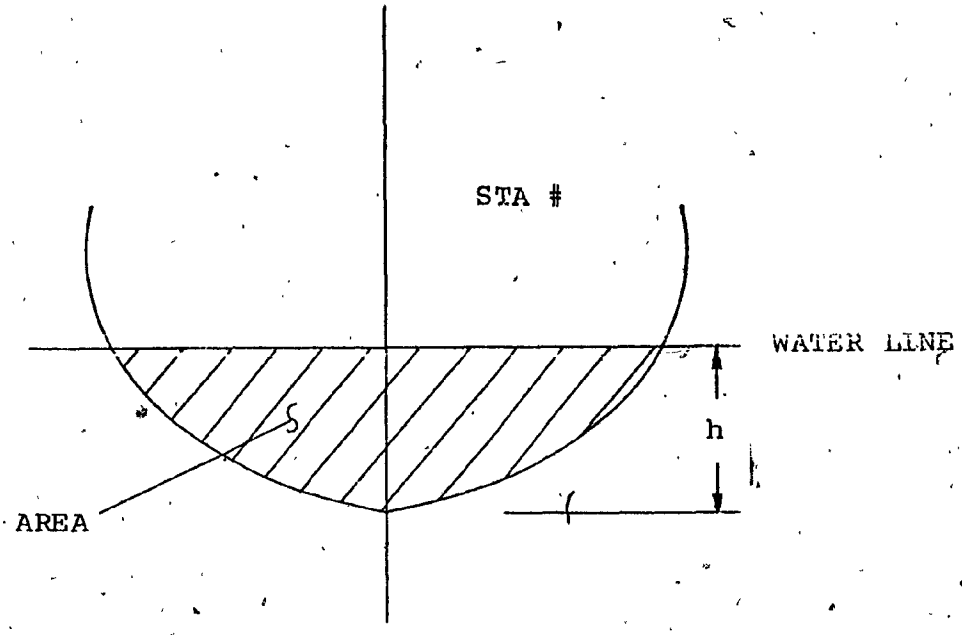


FIG. 8.1 IMMERSED AREA

TABLE 8.1 CROSS-SECTIONAL AREAS vs DEPTH OF IMMERSION

CANOE 1

| h | 2 in | 4 in | 6 in | 8 in |
|---|---|---|---|---|
| Sta # 0 | 2 sq.in | 4 sq.in | 6 sq.in | 8 sq.in |
| # 2 | 4.8 | 14.4 | 27.8 | 44.8 |
| # 4 | 17.6 | 48.0 | 83.8 | 128.0 |
| # 6 | 20.8 | 60.8 | 100.8 | 156.8 |
| # 8 | 22.4 | 70.4 | 123.2 | 187.2 |
| #10 | 19.2 | 60.8 | 108.8 | 182.4 |
| #12 | 8.0 | 28.8 | 62.4 | 92.8 |
| #14 | 2.0 | 4.0 | 6.0 | 8.0 |

TABLE 8.2 CROSS-SECTIONAL AREAS vs DEPTH OF IMMERSION

CANOE 2

| h | 2 in | 4 in | 6 in | 8 in |
|---|---|---|---|---|
| Sta # 0 | 2 sq.in | 4 sq.in | 6 sq.in | 8 sq.in |
| # 2 | 4.8 | 16.0 | 35.2 | 64.0 |
| # 4 | 14.4 | 48.0 | 92.8 | 140.8 |
| # 6 | 22.4 | 64.0 | 115.2 | 179.2 |
| # 8 | 35.2 | 92.8 | 155.2 | 227.2 |
| #10 | 25.6 | 68.8 | 120.0 | 179.2 |
| #12 | 8.0 | 30.4 | 52.8 | 84.8 |
| #14 | 2.0 | 4.0 | 6.0 | 8.0 |

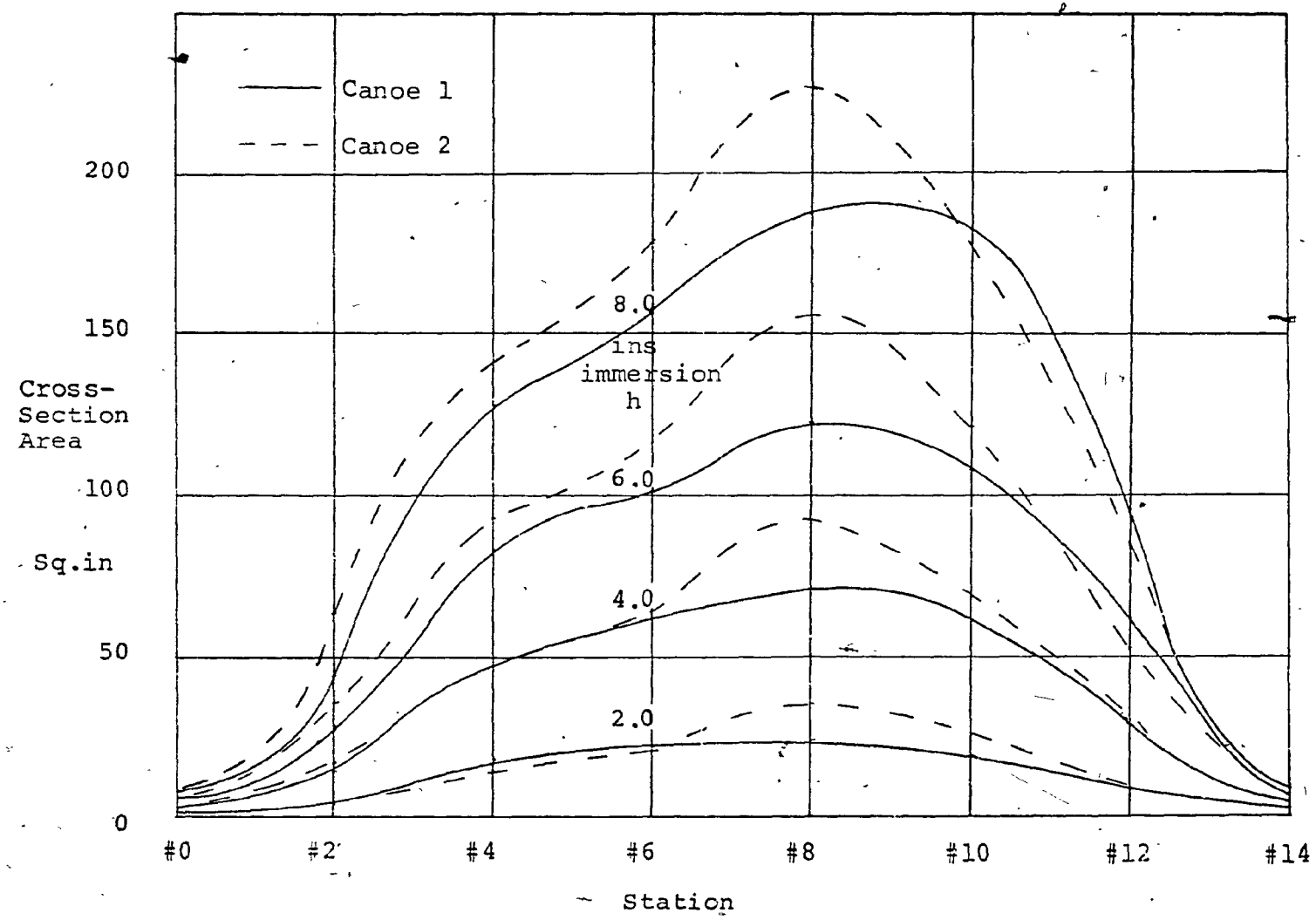


FIG. 8.2 CROSS-SECTIONAL AREAS vs WATERLINE LENGTH

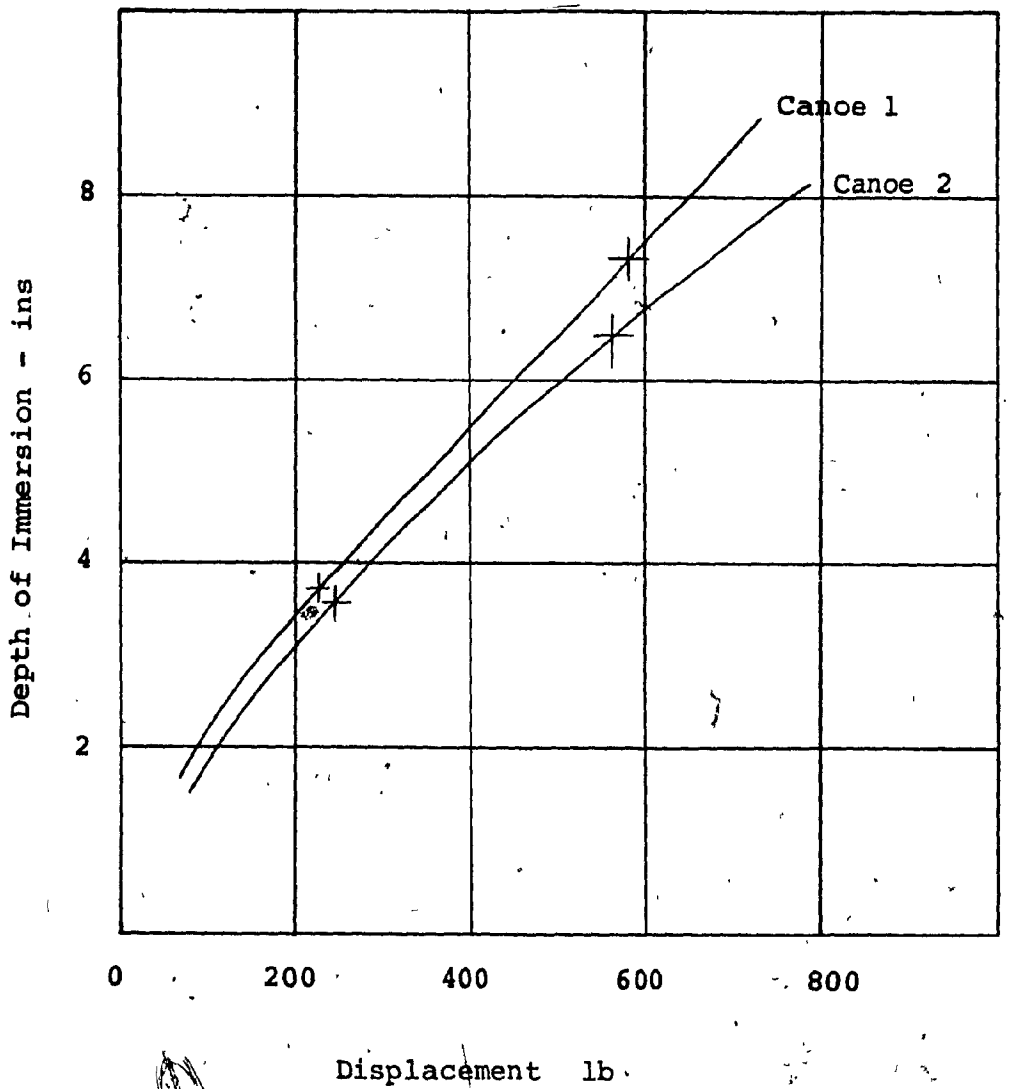


FIG. 8.3 DEPTH OF IMMERSION vs DISPLACEMENT

TABLE 8.3 DISPLACEMENT vs DEPTH OF IMMERSION

| h in | Canoe 1 | | Canoe 2 | |
|---|---|---|---|---|
| | A sq.in | Disp[1] lb | A sq.in | Disp[1] lb |
| 2.0 | 2.55 | 88.4 | 3.15 | 109.2 |
| 4.0 | 7.45 | 258.3 | 8.15 | 282.5 |
| 6.0 | 14.15 | 455.8 | 14.85 | 514.8 |
| 8.0 | 18.6 | 644.8 | 22.4 | 776.5 |

TABLE 8.4 PERIMETER OF IMMERSED SECTIONS

| Sta. | Canoe 1 | Canoe 2 |
|---|---|---|
| # 0 | 13.0 in. | 12.0 in. |
| # 2 | 16.4 | 17.2 |
| # 4 | 27.0 | 28.4 |
| # 6 | 31.2 | 33.6 |
| # 8 | 34.0 | 39.0 |
| #10 | 30.0 | 33.2 |
| #12 | 20.4 | 21.0 |
| #14 | 12.0 | 12.0 |

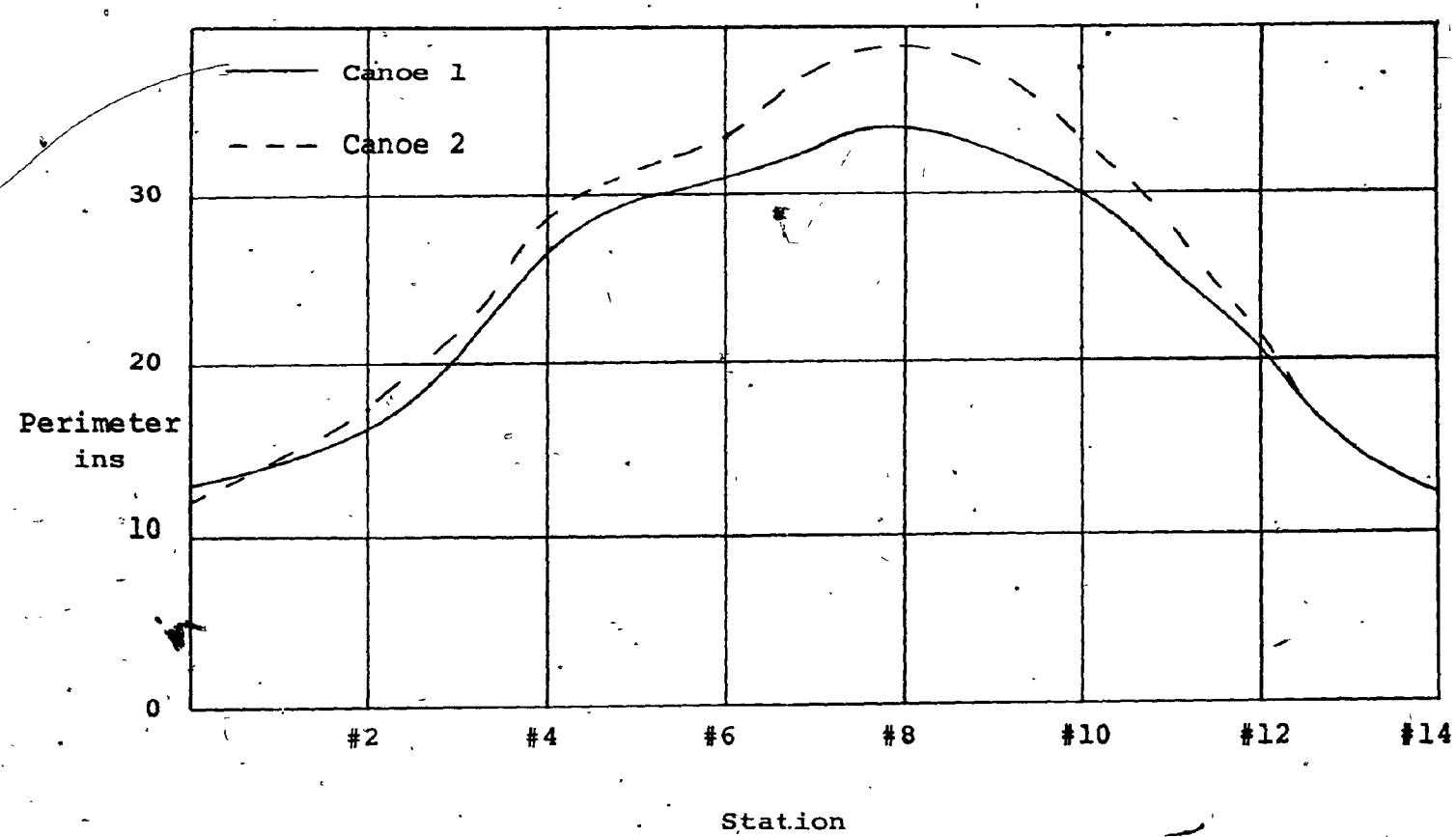


FIG. 8.4 WETTED SURFACE

Integrating the curves of Figure 8.4 by means of a planimeter yields the following values for wetted surface.

| | |
|---|---|
| Canoe 1 | 29.07 sq.ft. |
| Canoe 2 | 31.5 sq.ft. |

## 8.4 FRICTIONAL RESISTANCE

A ship in motion experiences a frictional resistance from the flow of water past the hull. This resistance is a function of the dynamic pressure, q, the wetted surface, S, and the drag coefficient, $C_d$.

$$R = C_d \, q \, S$$

where

$q = 0.5\rho \, v^2 = 0.97 \, v^2$

v = Speed ft/sec

$\rho$ = density of fresh water = 1.94 slug/cu.ft.

A typical value of $C_d$ is .0035 in turbulent flow and .00035 in laminar flow. The flow will be laminar at Reynolds Numbers, Rn, below $10^5$, and turbulent above $10^7$. It will be transitional between these two values. [36,37]

$$Rn = \frac{\rho \, L \, v}{M}$$

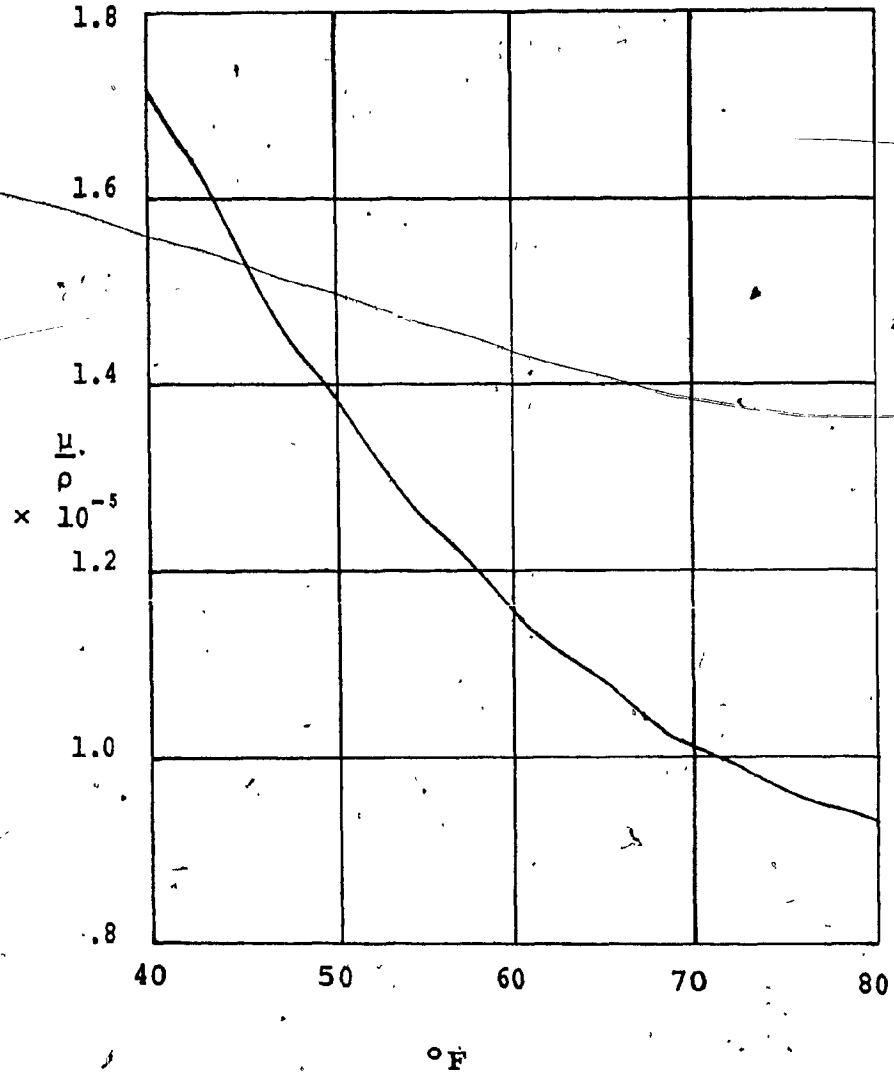


FIG. 8.5 VARIATION OF KINEMATIC VISCOSITY OF WATER WITH TEMPERATURE

TABLE 8.5 FRICTIONAL RESISTANCE

| V Knots | V Ft/sec | q | $Rn \times 10^6$ | $C_d$ | $R_{1b}$ Canoe 1 | $R_{1b}$ Canoe 2 |
|---|---|---|---|---|---|---|
| 1.0 | 1.69 | 2.77 | 1.9 | .005 | 0.4 | 0.4 |
| 1.5 | 2.53 | 6.21 | 2.8 | .0048 | 0.9 | 1.0 |
| 2.0 | 3.38 | 11.08 | 3.8 | .0045 | 1.7 | 1.8 |
| 2.5 | 4.22 | 17.30 | 4.7 | .0042 | 2.1 | 2.3 |
| 3.0 | 5.07 | 24.93 | 5.7 | .0041 | 3.0 | 3.2 |
| 3.5 | 5.91 | 33.88 | 6.6 | .0040 | 4.0 | 4.3 |
| 4.0 | 6.76 | 44.33 | 7.6 | .0039 | 5.0 | 5.4 |
| 4.5 | 7.60 | 56.03 | 8.5 | .0038 | 6.2 | 6.7 |
| 5.0 | 8.40 | 68.44 | 9.4 | .0037 | 7.4 | 8.0 |
| 5.5 | 9.29 | 83.45 | 10.4 | .0036 | 8.7 | 9.4 |

where

L = Length in ft.

$\frac{\mu}{\rho}$ = Kinematic viscosity

and is dependent on temperature (see Fig. 8.5).

The predicted values of frictional resistance for the two canoes are listed for a range of speeds in Table 8.5.

The values of $C_d$ [38] are taken for a typical hull and the wetted surface areas of the canoes, S, is given on page 134.)

## 8.5 WAVE-MAKING RESISTANCE

A canoe floats on and is propelled through water. The relative motion between the canoe and the water causes a variation of dynamic pressure along the hull and consequently, changes in the level at the free surface in the neighbourhood. Wave motion at the free surface is accordingly set up and these waves possess energy which is carried away and dissipated. This energy has been provided by paddling the canoe against the wave resistance.

Since the speed of propagation of waves is $\sqrt{gL}$, it follows that this will be a limiting speed for displacement type hulls. To exceed this speed, the hull must rise over its bow wave and start to plane.

An indication of the wave pattern is given by the Froude Number $\frac{V}{\sqrt{gL}}$ a dimensionless parameter. Since g, the acceleration due to gravity, is a constant, the Froude Number is generally used in the form $\frac{V}{\sqrt{L}}$ KTS the speed length ratio. Hydrodynamic resistance depends on the wave pattern formed around the hull, and consequently, on the speed length ratio.

Wave making resistance increases rapidly with speed, but the increase is not of a simple regular type which could be represented by a power law. Humps of wave drag occur at Froude numbers of $\frac{0.4}{\sqrt{n}}$ where $n = 2,4,6,8$. There is a last hump at $Fn = 0.45$.

This phenomena may be described in terms of critical speeds for wave-making resistance

$$V_{crit}(\text{knots}) = (.75,1.0,1.5)\ \sqrt{L}\ \text{ft}$$

It is apparent that these humps, or critical speeds coincide with the production of an integer number of waves along the hull. [39]

The canoes were timed at 5 minutes to cover the 600 yd course, whereas, the winning canoe took 4.5 minutes. Their speeds were averaging 6.0 and 6.7 ft/sec. respectively, so that they were operating in the region of the fourth hump or second critical speed.

TABLE 8.6 FROUDE NUMBER AND SPEED/LENGTH RATIO

| V Knots | V Ft/sec | Froude Number Fn | $\frac{V}{\sqrt{L}}$ | Drag Hump Fn | $V_{crit}$ Knots | $\frac{V_{crit}}{\sqrt{L}}$ |
|---|---|---|---|---|---|---|
| 1.0 | 1.69 | .079 | .267 | | | |
| 1.5 | 2.53 | .119 | .400 | | | |
| 1.77 | 2.99 | | .473 | .141 | | |
| 2.0 | 3.38 | .159 | .534 | | | |
| 2.04 | 3.46 | | .545 | .163 | | |
| 2.5 | 4.22 | .199 | .668 | | | |
| 2.51 | 4.25 | | .67 | .20 | 2.8 | .748 |
| 3.0 | 5.07 | .239 | .802 | | | |
| 3.5 | 5.91 | .278 | .935 | | | |
| 3.55 | 6.01 | | .95 | .283 | 3.74 | .999 |
| 4.0 | 6.76 | .318 | 1.07 | | | |
| 4.5 | 7.60 | .358 | 1.20 | | | |
| 5.0 | 8.40 | .396 | 1.34 | | | |
| 5.5 | 9.29 | .437 | 1.47 | | | |
| 5.65 | 9.55 | | 1.5 | .45 | 5.6 | 1.5 |

The wave system generated by a moving hull comprises a transverse and divergent part, each contributing approximately half of the total drag.

There are two primary sources of disturbance creating waves, one situated near the bow and the other near the stern. The transverse waves determine the interference between the bow and the stern systems. Depending on whether the bow and stern transverse wave systems are in phase or not, they can add or partially subtract from each other. This is the reason for the humps in the drag curve.

The hump at a Froude Number in the region of 0.3 is the most important and careful hull design is directed towards raising this critical number as high as possible.

The bow and stern transverse wave systems do not interfere.

## 8.6 PRISMATIC COEFFICIENT

The prismatic coefficient is the ratio between the volume of displacement and the volume of a solid having a constant section the shape of the largest cross-section multiplied by the water-line length. [40]

Canoe 1

Displacement $\frac{560}{62.3}$ = 8.96 cu ft

Cross-Section 1.145 sq ft

$$Pc = \frac{8.96}{14. \times 1.145} = 0.56$$

Canoe 2

Displacement $\frac{580}{62.5}$ 9.28 cu ft

Cross-Section 1.25 sq ft

$$Pc = \frac{9.28}{14. \times 1.25} = 0.53$$

This parameter is important in determining the drag of a hull. There is an optimum value of Pc for any speed-length ratio $v/\sqrt{L}$. This value is plotted in Figure 8.6.

## 8.7 EDDY MAKING RESISTANCE

As the hull passes through the water eddies are set up at blunt bow and stern sections and also at any projections that may be present. It is very difficult to determine the magnitude of this drag, however by providing sharpness at the bow and stern and by keeping the hull fair eddies can be kept to a minimum.

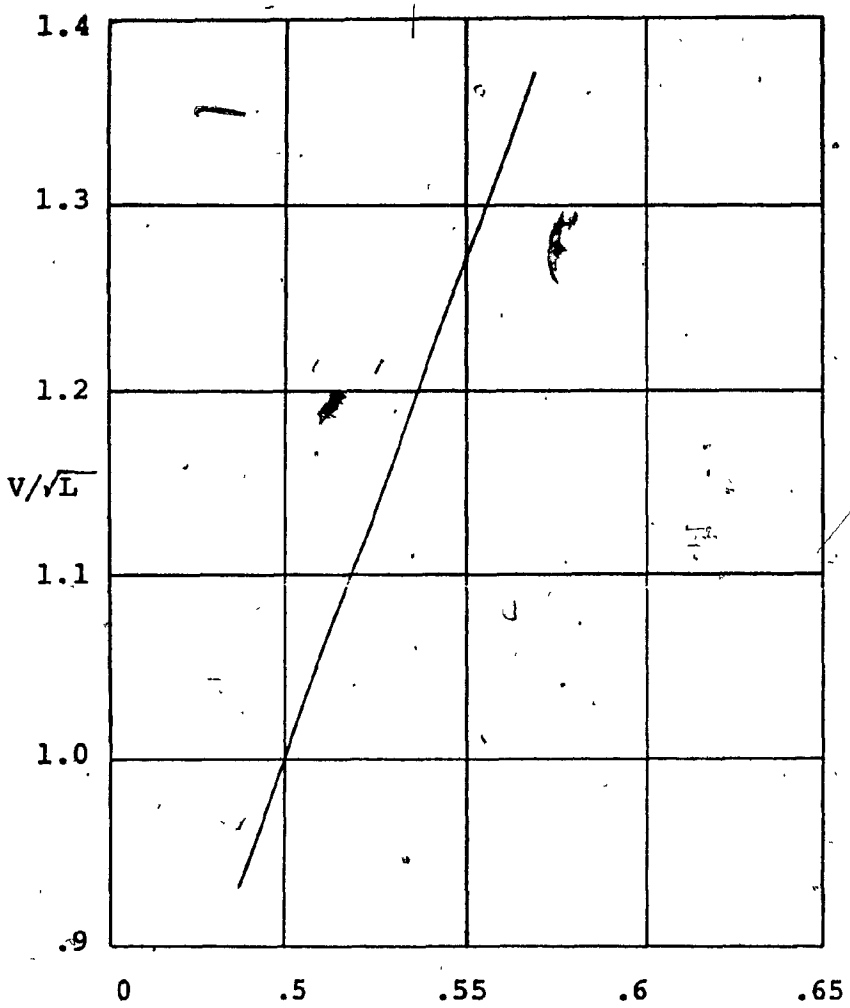


FIG. 8.6 OPTIMUM PRISMATIC COEFFICIENT

## 8.8 PROPULSION

A canoe is propelled by two men using eight inch paddles, one of these men has the additional task of steering. The power available to drive the canoe is therefore dependent upon human muscle-power and the power output of the body is limited in the following manner and for the reasons stated. [41]

(1) In brief bouts of exercise (0.1 to 5 min) to 2.0 - 0.5 hp; by the availability in the muscles of stores of chemical substances that can yield energy by hydrolysis.

(2) In steady-state work (5 min to 150 min or more) to 0.5 - 0.4 hp; by the ability of the body to absorb and transport oxygen.

The above figures refer to champion athletes using both arms and legs. Ordinary healthy individuals would produce less than 70 to 80 percent as much power.

Since canoe paddling is primarily an arm action the power available would be in the region of a quarter of a horsepower for each man. Depending upon the experience of the crew and the effort required to steer, the power available to propel the canoe would be 0.3 to 0.5 horsepower.

## 8.9 METACENTRIC HEIGHT

The metacentre is a point on the geometric centre line of a vessel where it is intersected by a line through the centre of buoyancy and normal to the water surface, in a slightly heeled position. The metacentric height is the distance between the metacentre and the centre of gravity and it must be positive for positive stability. [36]

$$\text{Metacentric height} = \frac{I}{V} - a$$

where

I is the moment of inertia of the water-line cross-section

V is the volume of displaced water

a is the distance between the centre of buoyancy and the centre of gravity.

The moments of inertia were obtained from the water-line sections shown in Figure 7.1, by considering two-inch wide strips and summating the values obtained.

Canoe 1

$$\frac{I}{V} = \frac{7.54}{8.96} = .841 \text{ ft} \quad \text{or} \quad 10.1 \text{ in.}$$

Canoe 2

$$\frac{I}{V} = \frac{10.66}{9.28} = 1.15 \text{ ft} \quad \text{or} \quad 13.8 \text{ in.}$$

## 8.10 THE MEASURED RESISTANCE

The total resistance of canoe No. 2 was established by towing tests carried out on deep open water. The canoe, which is shown floating empty in Fig. 8.8, was balasted to simulate the two occupants, The tow load was measured by means of a spring balance to which the tow line was attached.

The first run was made at 2.8 ft/sec and the tow load was 0.65 lb. At this speed, the waves produced were negligible, Fig. 8.9, and the resistance was due to skin friction so that the coefficient of frictional resistance, Cd, may be obtained.

$$Cd = \frac{R}{q\,S} = \frac{0.65}{7.6 \times 31.5} = 0.00272$$

The second run was made at 4.2 ft/sec with a tow load of 3.9 lb. A pronounced bow wave was visible, Fig. 8.10, and transverse stern waves were discernable. At this speed, the wave-making drag was approximately equal to the frictional resistance.

The third run, at 6.25 ft/sec, coincided with the second critical speed. In this case, the drag was 15.5 lb and pronounced bow and stern waves were visible, Fig. 8.11.

The fourth run was at 8.3 ft/sec, approaching the third critical speed, with a drag of 30 lb. The front of the canoe was begining to ride up onto the bow wave whilst the body settled into the trough between bow and stern waves, Fig. 8.12. The canoe was in danger of swamping during this run and no higher speeds were attempted.

A curve of total resistance plotted against speed for canoe No. 2, is shown in Fig. 8.7. A curve of frictional resistance based upon the value of Cd obtained at 2.8 ft/sec is also shown. The difference between these two curves represents the resistance due to wave-making and eddies.

## 8.11 STABILITY CURVE

A curve of righting moments at various angles of heel was obtained experimentally for canoe No. 2. A beam was lashed to the thwart of the canoe and a weight was moved outboard along this beam. The angle of heel was measured at the corresponding applied moment, the canoe having been balasted to simulate its running condition.

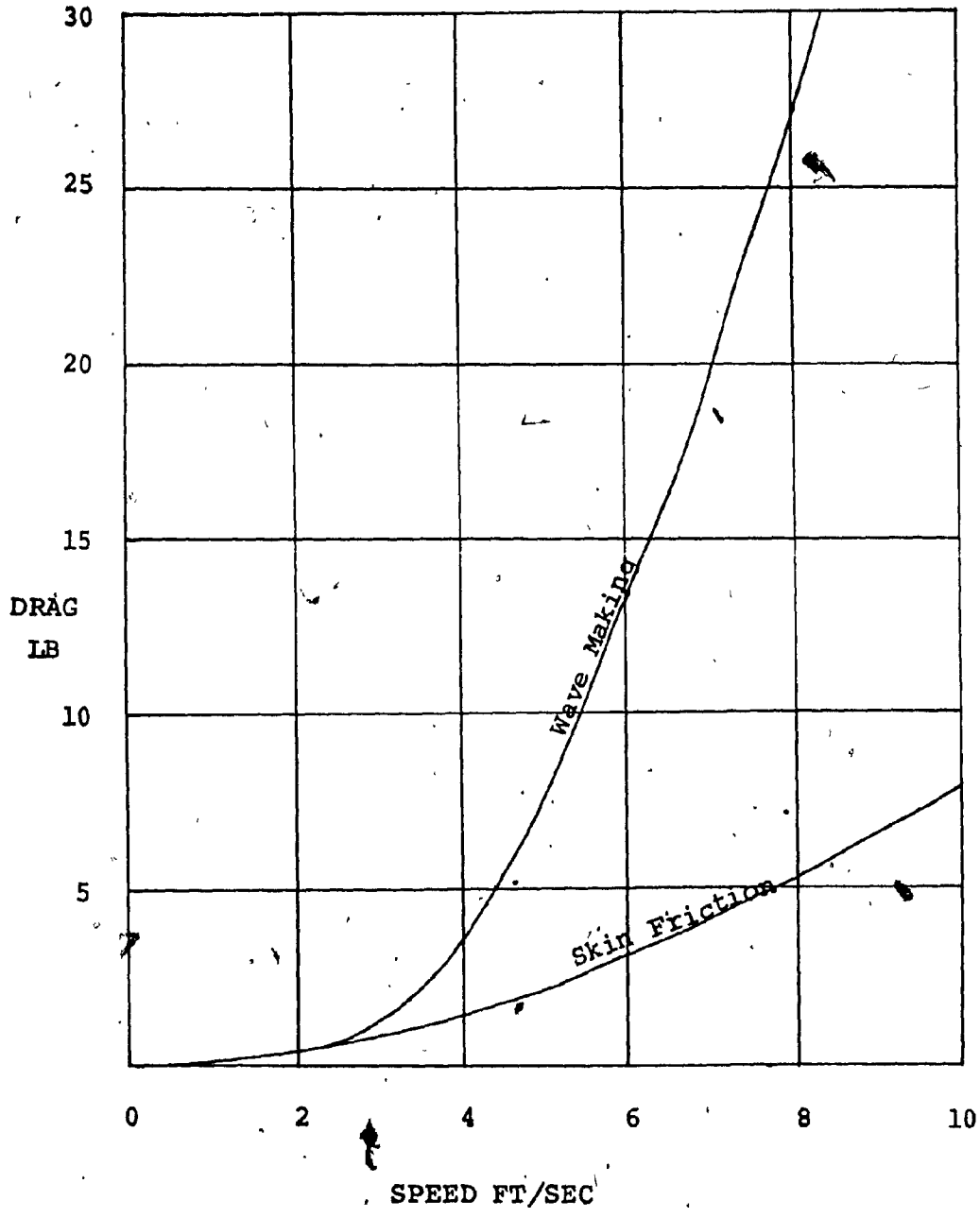


FIG. 8.7 THE VARIATION OF TOTAL RESISTANCE WITH SPEED

FIG. 8.8 CANOE NO. 2 FLOATING EMPTY

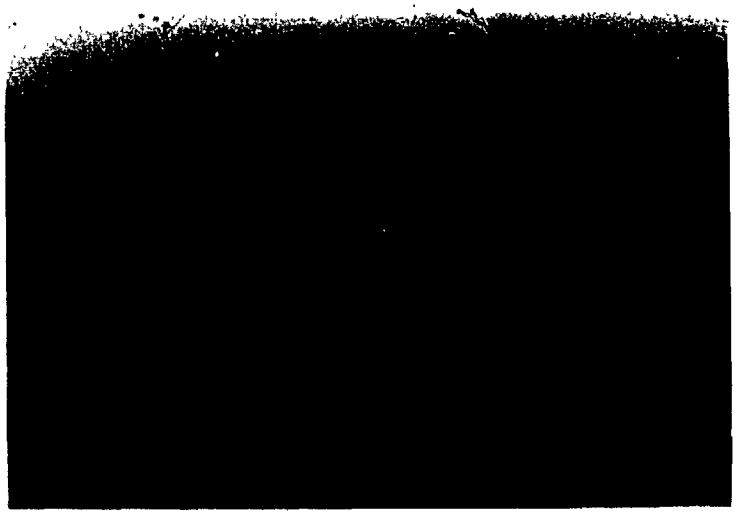

FIG. 8.9 THE CANOE BEING TOWED AT 2.8 ft/sec BALASTED TO SIMULATE THE CREW WEIGHT

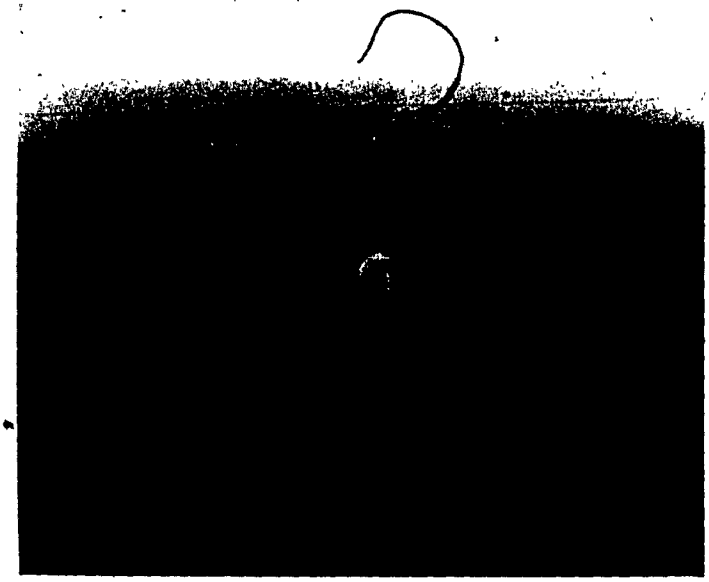

FIG. 8.10 THE CANOE AT 4.2 ft/sec, THE BOW WAVE IS DISTINCTLY VISIBLE

FIG. 8.11 THE CANOE AT 6.25 ft/sec, THE STERN WAVE AND TRANSVERSE WAVE PATTERN MAY BE SEEN

FIG. 8.12 THE CANOE AT 8.3 ft/sec, SETTLING INTO THE TROUGH BETWEEN THE BOW AND STERN WAVES

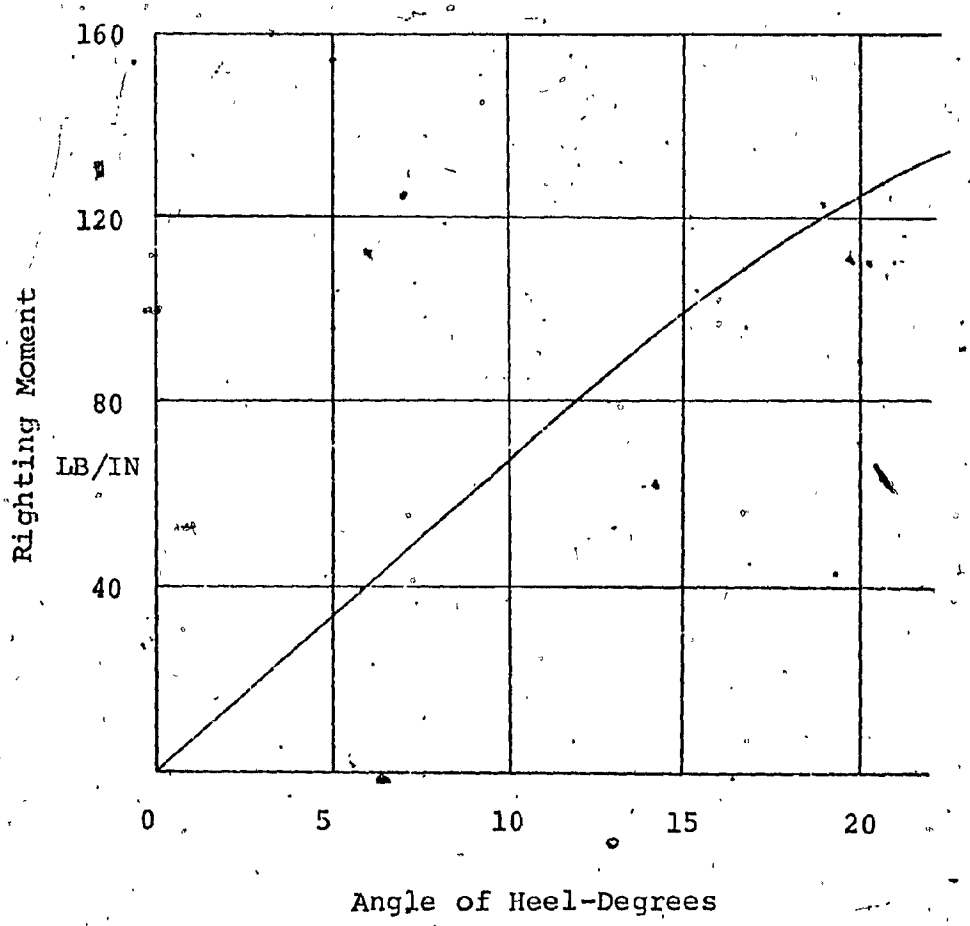


FIG. 8.13 STABILITY CURVE OF CANOE NO. 2

# CHAPTER 9

# SUMMARY AND CONCLUSIONS

# CHAPTER 9

# SUMMARY AND CONCLUSIONS

## 9.1 SUMMARY

The properties of the constituent materials of ferro-cement are discussed and it is shown that there is an order of magnitude difference between the failing strain of cement and of steel when each is acting independently. When the two are combined into ferro cement then the failing strain of the cement becomes compatible with that of steel. Specimens of ferro cement which have been strained to the yield strength of the steel exhibit no cracking of the cement when viewed through a microscope at 400 × magnification.

It is postulated that the natural flaws and voids in cement provide the stress concentrations sufficient to cause the cohesive strength to be exceeded at comparatively low mean tensile stress levels in unreinforced cement. The presence of fine wire reinforcing reduces the stress levels in these high energy zones and enables the cement matrix to strain at the same rate as the wire reinforcing. Ferro cement is therefore acting as a composite material in which the major loading is carried by the reinforcing wire and the cement acts as a shear carrying matrix.

The equations required for the stress analysis of ferro cement are derived together with the requisite transformation matrices. These equations are used to analyse test specimens in both tension and bending, and it is shown that laminate analysis is applicable to ferro cement. Compliance matrices are derived both analytically and by test.

To demonstrate the use of ferro cement as a material suitable for the construction of thin shell structures, two canoes were made and tested.

## 9.2 CONCLUSIONS

Based on the investigations carried out in this research, the following conclusions are formulated:

(1) Ferro cement is obtained when a large number of fine steel reinforcing wires are spread throughout a matrix made from Portland cement and fine sand. These wires will then reduce the stress concentrations at the tips of natural flaws and voids below the critical fracture stress.

(2) Ferro cement acts as a composite material in which the major loading is carried by the reinforcing wires and the cement matrix follows a non-linear stress strain curve so that it is only effective at low stress levels and carries a constant load

at higher levels.

(3) The non-linearity of cement combined with the linear behaviour of steel result in a non-linear stress strain curve for ferro cement. Consequently, there exists a tangent modulus curve which may be predicted for any combination of reinforcing and cement. The values of tangent modulus may then be used in the stress analysis of ferro cement using lamina composite theory.

(4) Values of the fracture toughness of ferro cement have been obtained and the dimension of the high energy regions at the tips of natural flaws has been estimated. This data has been used to predict a wire spacing in ferro cement of one-half inch.

(5) Specimens of ferro cement which have been strained up to the yield strain of the steel reinforcing wire have been viewed under a 400 × magnification microscope. No cracking of the cement matrix has been observed.

(6) The practicability of making small thin shell structures using ferro cement has been demonstrated in the construction of two canoes.

(7) An analysis of the design of the canoes shows that

the shape of the hull below the water-line is as important as the weight of the canoe in determining its limiting speed.

# REFERENCES

## REFERENCES


[1] Jackson,G.W., and Sutherland, M., Concrete Boat-building Its Technique and Its Future, John De Graffe, Tuckahoe, N.Y., (1969).

[2] Samson,J., and Wellens, G., The Ferro Cement Boat, Samson Marine Design, Vancouver, (1972).

[3] Kelly, A.M., and Mouat, T.W., "Ferro Cement as a Fishing Vessel Construction Material", Conference on Fishing Vessel Construction Material, Montreal, (1969).

[4] Fyson, J.P., "Ferro Cement Construction for Fishing Vessels", United Nations Food and Agricultural Organization Regional Office, Bangkok, Thailand, (1969).

[5] Håviland, J., "American Concrete Steamers in the First and Second World Wars", Neptune Magazine, Vol. 22, No. 3, (1962).

[6] Sutherland, M., "Ferro Cement Boats", Sea Spray Annual, Aukland, New Zealand, (1966).

[7] Nervi, P.L., "Il Ferro-Cemento sue Caratteristiche e Possibilita", L'Ingegnere, Rome, (1951).

[8] Bezukladov, V.F., et al, "Ship Hulls Made of Reinforced Concrete", Clearing House for Federal Scientific and Technical Information, Springfield, Va., AD680042,(1968).

[9] Gunn, B.M., Letter to the Editor of Yachting Monthly, London, (1971).

[10] Lachance, L., and Fugere, P., "Construction of a Ferro Shotcrete Motor Sailer Hull", L'Ingenieur, Quebec,(1971).

[11] Waitsman, I.M., "An Investigation of Concrete for Submarine Structures", General Dynamics Report P 413-69-079, Groton, Conn., U.S.A. (1969).

[12] Turner, D.R., "An Investigation into the Tensile Strength of Ferro Cement", M.Eng. Dissertation, Sir George Williams University, Montreal, (1971).

[13] Neville, A.M., Properties of Concrete, Sir Isaac Pitman and Sons, London, (1963).

[14] McClintock, F.A., and Argon, A.S., Mechanical Behaviour of Materials, Addison Wesley Publishing Co., Reading, Mass., (1966).

[15] Mattar, S.G., "Ferro Cement in Tension and Compression", M.Sc. Thesis, University of Calgary, Alberta, (1971).

[16] A.S.T.M. Standards, Part 4: "Cement Concrete and Mortars", American Society for Testing Materials, Philadelphia, Pa., (1958).

[17] Design and Control of Concrete Mixes, Canada Cement Lafarge, Montreal, (1968).

[18] Catalogue, Drummond McCall Ltd., Montreal, (1966).

[19] Bresler, B., and Lin, T.Y., Design of Steel Structures, John Wiley and Sons, New York, (1963).

[20] A.S.T.M. Standards, Part 4: "Structural and Boiler Steel, Reinforcing Steel and Ferrous Filler Material", American Society for Testing Materials, Philadelphia, Pa., (1968).

[21] Catalogue, Pedlar's Steelcrete Expanded Metal, Oshawa, Ontario, (1966).

[22] Urquhart, L., O'Rourke, C.E., and Winter, G., Design of Concrete Structures, McGraw-Hill, New York, (1958).

[23] Calcote, L.R., The Analysis of Laminated Composite Structures, Van Nostrand Reinhold Co., New York, N.Y., (1969).

[24] Ashton, J.E., Halpin, J.C., and Petit, P.H., Primer on Composite Materials, Technomic Publishing Co., Stanford, Conn., (1969).

[25] Kaminski, B.E., and Lantz, R.B., "Composite Materials Testing and Design", American Society for Testing Materials, Special Technical Publication #460, Baltimore, Md., (1969).

[26] Powers, T.C., "Physical Properties of Cement Paste", Proceedings of the Fourth International Symposium on the Chemistry of Cement, National Bureau of Standards, Washington, D.C., (1962).

[27] Kaplan, M.F., "The Application of Fracture Mechanics to Concrete", International Conference on the Structure of Concrete, Paper D1, Cement and Concrete Association, London, England, (1965).

[28] Griffith, A.A., "The Phenomena of Rupture and Flow in Solids", Philosophical Transactions of the Royal Society, A221, (1920).

[29] Weiss, V., and Yukawa, S., "Critical Appraisal of Fracture Mechanics", American Society for Testing Materials, Special Technical Publication #381, Baltimore, Md., (1965).

[30] Irwin, G.R., "Fracture Dynamics", Fracturing of Metals, American Society of Metals, Cleveland, (1948).

[31] Orowan, E., "Energy Criteria of Fracture", Welding Research Supplement, Vol. 20, (1955).

[32] Waddoups, M.E., Eisenmann, J.R., and Kaminski, B.E., "Macroscopic Fracture Mechanics of Advanced Composite Materials", Journal of Composite Materials, Vol.5, (October 1971).

[33] Paris, P.C., and Sih, G.C., "Stress Analysis of Cracks", American Society for Testing Materials, Special Technical Publication #381, Baltimore, Md., (1965).

[34] "Concrete Canoe Races, Rules and Regulations", American Concrete Institute, Detroit, Michigan.

[35] Troitsky, M.S., and Turner, D.R., "The Design and Construction of Two Ferro Cement Canoes", Journal of Structural Engineering, Roorkee, India, (January, 1975).

[36] Prandtl, L., and Tietjens, O.G., "Fundamentals of Hydro and Aeromechanics", Dover Publications Inc., New York, (1957).

[37] Milne-Thomson, L.M., Theoretical Hydrodynamics, Macmillan and Co., London, (1962).

[38] Hoerner, S.F., Fluid-Dynamic Drag, Published by the Author, 148 Busteed Drive, Midland Park, New Jersey, (1958).

[39] Marchaj, C.A., Sailing Theory and Practice, Dodd Mead and Company, New York, N.Y. (1964).

[40] Kinney, F.S., Skene's Elements of Yacht Design, Dodd Mead and Company, New York, N.Y. (1973).

[41] Wilkie, D.R., "Man as an Aero Engine", Journal of the Royal Aeronautical Society, London, (August 1960).

# APPENDIX A

## SECTION PROPERTIES

# APPENDIX A

## SECTION PROPERTIES

This Appendix contains a list of the computer program used to calculate the section properties of the canoes. The input data is obtained from Chapter 7, Figures 7.2 and 7.3.

The output data presented herein is plotted in Figure 7.5.

## A.1.1 Program to Derive Section Properties

```
      DIMENSION X(30),Y(30),T(30),XMEAN(30),YMEAN(30),C(30),D(30),
     1C2(30),D2(30),HYP(30),A(30),AX2M(30),AY2M(30),DIX(30),DIY(30),
     2AY(30),YTR(30)
    1 FORMAT (3I5)
    2 FORMAT(3F10.2)
    3 FORMAT (5F10.2)
  100 FORMAT (1H ,10X,I5,3F10.2)
  101 FORMAT(1H1)
  102 FORMAT(1H ,//,10X,'NUMBER',I2,'   STATION',I3)
  103 FORMAT(1H ,/,10X,'AREA',F8.2,'  IBAR',F8.3,/,10X,'  IX',F8.2,'   IY
     1',F8.2)
  104 FORMAT(//10X,' NODE      X          Y          T')
   10 READ (5,1) CAN,STA,NNODE
      IF ( CAN) 11,12,11
   11 NN = NNODE - 1
      WRITE (6,101)
      READ(5,2)(X(I),Y(I),T(I), I=1,NNODE)
      READ (5,3)  AG,XG,YG,HAK,YK
      DO 50 J=1,NN
      J1 = J+1
      XMEAN(J) = (X(J) + X(J1)) / 2.0
      YMEAN(J) = (Y(J) + Y(J1)) / 2.0
      C(J) = X(J) - X(J1)
      D(J) = Y(J1) - Y(J)
      C2(J) = C(J)**2
      D2(J) = D(J)**2
      HYP(J) = SQRT(C2(J) + D2(J))
      A(J) = HYP(J) * T(J)
      AY(J) = A(J)*YMEAN(J)
      AX2M(J) = A(J) * XMEAN(J)**2
      AY2M(J) = A(J) * YMEAN(J)**2
      DIX(J) = (A(J) * D2(J))/12.0
   50 DIY(J) = (A(J) * C2(J))/12.0
      SAY = 0.0
      SIX = 0.0
      SIY = 0.0
      ARE = 0.0
      DO 51 K=1,NN
      SAY = SAY + AY(K)
      SIX = SIY + AY2M(K) + DIX(K)
      SIY = SIY + AX2M(K) + DIY(K)
   51 ARE = ARE + A(K)
      AXG = AG * XG
      AX2G = AXG * XG
      AYG = AG * YG
      AY2G = AYG * YG
      HAYK = HAK * YK
      HA2YK = HAYK * YK
      SAY = SAY + AYG + HAYK
      ARE = ARE + AG + HAK
      YBAR = SAY/ARE
      SI2Y = 2.0 * (SIY + AX2G)
      SI2X = 2.0 * (SIX + AY2G + HA2YK - ARE*YBAR*YBAR)
```

```
      AREA = 2.0 * ARE
      DO 52 I=1,NN
   52 YTR(I) = YMEAN(I) + YBAR
      YKTR = YK - YBAR
      YGTR = YG - YBAR
      WRITE (6,102) CAN,STA
      WRITE (6,104)
      WRITE(6,100) (I,X(I),Y(I),T(I),   I=1,NNODE)
      WRITE(6,103) AREA,YBAR,S2IX,S2IY
      GO TO 10
   12 CONTINUE
      STOP
      END
```

## A.1.2 Input and Output Data - Canoe No. 1

### Station 2

| NODE | X | Y | T |
|---|---|---|---|
| 1 | 0.0 | -6.80 | 0.25 |
| 2 | 2.00 | -4.50 | 0.25 |
| 3 | 3.20 | -2.00 | 0.25 |
| 4 | 3.90 | 0.0 | 0.25 |
| 5 | 4.30 | 2.00 | 0.25 |
| 6 | 4.70 | 4.00 | 0.25 |
| 7 | 4.90 | 6.00 | 0.25 |
| 8 | 5.00 | 7.00 | 0.25 |

AREA 9.60 |BAR 0.197
IX 217.43 IY 129.47

### Station 4

| NODE | X | Y | T |
|---|---|---|---|
| 1 | 0.0 | -7.20 | 0.25 |
| 2 | 2.00 | -6.60 | 0.25 |
| 3 | 4.00 | -6.00 | 0.25 |
| 4 | 6.00 | -5.00 | 0.25 |
| 5 | 8.00 | -3.60 | 0.25 |
| 6 | 9.40 | -2.00 | 0.25 |
| 7 | 10.60 | 0.0 | 0.25 |
| 8 | 11.30 | 2.00 | 0.25 |
| 9 | 11.90 | 4.00 | 0.25 |
| 10 | 12.10 | 5.90 | 0.25 |

AREA 11.79 |BAR -1.564
IX 244.45 IY 886.32

## Station 6

| NODE | X | Y | T |
|---|---|---|---|
| 1 | 0.0 | -7.20 | 0.25 |
| 2 | 2.00 | -6.70 | 0.25 |
| 3 | 4.00 | -6.40 | 0.25 |
| 4 | 6.00 | -5.80 | 0.25 |
| 5 | 8.00 | -4.90 | 0.25 |
| 6 | 10.00 | -3.70 | 0.25 |
| 7 | 12.00 | -2.10 | 0.25 |
| 8 | 13.80 | 0.0 | 0.25 |
| 9 | 15.00 | 1.90 | 0.25 |
| 10 | 15.90 | 4.00 | 0.25 |
| 11 | 16.10 | 5.30 | 0.25 |

AREA 13.02 IBAR -2.10E
IX 240.01 IY 1579.14

## Station 8

| NODE | X | Y | T |
|---|---|---|---|
| 1 | 0.0 | -7.20 | 0.25 |
| 2 | 2.00 | -7.00 | 0.25 |
| 3 | 4.00 | -6.70 | 0.25 |
| 4 | 6.00 | -6.30 | 0.25 |
| 5 | 8.00 | -5.70 | 0.25 |
| 6 | 10.00 | -4.80 | 0.25 |
| 7 | 12.00 | -3.50 | 0.25 |
| 8 | 14.00 | -1.80 | 0.25 |
| 9 | 15.50 | 0.0 | 0.25 |
| 10 | 16.60 | 2.00 | 0.25 |
| 11 | 17.30 | 4.00 | 0.25 |
| 12 | 17.70 | 5.10 | 0.25 |

AREA 13.72 IBAR -2.491
IX 249.83 IY 1575.26

Station 10

| NODE | X | Y | T |
|---|---|---|---|
| 1 | 0.0 | -7.20 | 0.25 |
| 2 | 2.00 | -6.70 | 0.25 |
| 3 | 4.00 | -6.00 | 0.25 |
| 4 | 6.00 | -5.30 | 0.25 |
| 5 | 8.00 | -4.30 | 0.25 |
| 6 | 10.00 | -3.00 | 0.25 |
| 7 | 12.00 | -1.30 | 0.25 |
| 8 | 13.90 | 1.00 | 0.25 |
| 9 | 15.00 | 2.10 | 0.25 |
| 10 | 15.70 | 5.40 | 0.25 |

AREA 12.81 |BAR -1.859
IX 231.73 IY 1472.42

Station 12

| NODE | X | Y | T |
|---|---|---|---|
| 1 | 0.0 | -6.80 | 0.25 |
| 2 | 2.00 | -6.20 | 0.25 |
| 3 | 4.00 | -5.20 | 0.25 |
| 4 | 6.00 | -3.70 | 0.25 |
| 5 | 7.50 | -2.00 | 0.25 |
| 6 | 8.50 | 0.0 | 0.25 |
| 7 | 9.20 | 2.00 | 0.25 |
| 8 | 9.50 | 4.00 | 0.25 |
| 9 | 9.70 | 6.10 | 0.25 |

AREA 10.87 |BAR -1.024
IX 222.49 IY 552.97

## A.1.3 Input and Output Data - Canoe No. 2

### Station 2

| NODE | X | Y | T |
|---|---|---|---|
| 1 | 0.0 | -6.00 | 0.25 |
| 2 | 2.00 | -4.60 | 0.25 |
| 3 | 4.00 | -2.70 | 0.25 |
| 4 | 6.00 | -0.10 | 0.25 |
| 5 | 7.00 | 2.00 | 0.25 |
| 6 | 7.50 | 4.00 | 0.25 |
| 7 | 7.60 | 6.00 | 0.25 |
| 8 | 7.60 | 6. | 0.25 |

AREA 9.87 IBAR 0.149
IX 189.80 IY 307.96

### Station 4

| NODE | X | Y | T |
|---|---|---|---|
| 1 | 0.0 | -6.50 | 0.25 |
| 2 | 2.00 | -6.10 | 0.25 |
| 3 | 4.00 | -5.50 | 0.25 |
| 4 | 6.00 | -4.80 | 0.25 |
| 5 | 8.00 | -3.90 | 0.25 |
| 6 | 10.00 | -2.50 | 0.25 |
| 7 | 11.20 | -1.00 | 0.25 |
| 8 | 12.80 | 1.00 | 0.25 |
| 9 | 13.80 | 3.00 | 0.25 |
| 10 | 14.20 | 4.50 | 0.25 |
| 11 | 14.30 | 5.90 | 0.25 |

AREA 12.36 IBAR -1.378
IX 229.08 IY 1242.39

## Station 6

| NODE | X | Y | T |
|---|---|---|---|
| 1 | 0.0 | -6.50 | 0.25 |
| 2 | 2.00 | -6.30 | 0.25 |
| 3 | 4.00 | -6.00 | 0.25 |
| 4 | 6.00 | -5.60 | 0.25 |
| 5 | 8.00 | -4.80 | 0.25 |
| 6 | 10.00 | -4.00 | 0.25 |
| 7 | 12.00 | -2.70 | 0.25 |
| 8 | 14.00 | -1.10 | 0.25 |
| 9 | 15.56 | 1.00 | 0.25 |
| 10 | 16.35 | 3.00 | 0.25 |
| 11 | 16.60 | 4.30 | 0.25 |
| 12 | 16.50 | 5.80 | 0.25 |

AREA 13.54 IBAR -1.818
IX 245.07 IY 1833.86

## Station 8

| NODE | X | Y | T |
|---|---|---|---|
| 1 | 0.0 | -6.60 | 0.25 |
| 2 | 2.00 | -6.60 | 0.25 |
| 3 | 4.00 | -6.40 | 0.25 |
| 4 | 6.00 | -6.10 | 0.25 |
| 5 | 8.00 | -5.80 | 0.25 |
| 6 | 10.00 | -5.40 | 0.25 |
| 7 | 12.00 | -4.88 | 0.25 |
| 8 | 14.00 | -3.88 | 0.25 |
| 9 | 16.00 | -2.18 | 0.25 |
| 10 | 17.40 | 0.08 | 0.25 |
| 11 | 17.80 | 2.08 | 0.25 |
| 12 | 17.80 | 3.98 | 0.25 |
| 13 | 17.50 | 5.70 | 0.25 |

AREA 14.76 IBAR -2.462
IX 272.04 IY 2432.96

Station 10

| NODE | X | Y | T |
|---|---|---|---|
| 1 | 0.0 | -6.50 | 0.25 |
| 2 | 2.00 | -6.30 | 0.25 |
| 3 | 4.00 | -6.00 | 0.25 |
| 4 | 6.00 | -5.60 | 0.25 |
| 5 | 8.00 | -5.00 | 0.25 |
| 6 | 10.00 | -4.40 | 0.25 |
| 7 | 12.00 | -2.90 | 0.25 |
| 8 | 13.80 | -1.00 | 0.25 |
| 9 | 15.00 | 1.00 | 0.25 |
| 10 | 15.60 | 3.00 | 0.25 |
| 11 | 15.80 | 4.30 | 0.25 |
| 12 | 15.80 | 5.80 | 0.25 |

AREA 13.38 YBAR -1.900
IX 247.35 IY 1694.91

Station 12

| NODE | X | Y | T |
|---|---|---|---|
| 1 | 0.0 | -6.30 | 0.25 |
| 2 | 2.00 | -5.50 | 0.25 |
| 3 | 4.00 | -4.20 | 0.25 |
| 4 | 6.00 | -2.50 | 0.25 |
| 5 | 7.90 | 0.0 | 0.25 |
| 6 | 8.90 | 2.00 | 0.25 |
| 7 | 9.20 | 4.00 | 0.25 |
| 8 | 9.20 | 6.50 | 0.25 |

AREA 10.61 YBAR -0.417
IX 209.85 IY 447.39